Expression and Function of Kir2.1 and Kv1.3 Channels in Cytokine-induced Activation of Rat and Mouse Microglia: A Tale of Two Rodents

by

Doris Lam

A thesis submitted in conformity with the requirements

for the degree of Doctor of Philosophy

Graduate Department of Physiology

University of Toronto

Abstract

Expression and Function of Kir2.1 and Kv1.3 Channels in Cytokine-induced Activation of Rat and Mouse Microglia: A Tale of Two Rodents

Ph. D. 2017
Doris Lam
Graduate Department of Physiology
University of Toronto

After acute CNS damage, microglia undergo complex molecular and functional changes. Pro-inflammatory (M1) activation can exacerbate tissue damage, while multiple anti-inflammatory (M2) states can help resolve inflammation and promote tissue repair. Potassium (K^+) channels are potential targets for modulating inflammation, but their expression and roles in activated microglia are poorly understood. Also, whether rat and mouse microglia respond the same is unclear. This thesis presents two studies: 1) expression and roles of Kir2.1 in rat microglial migration and proliferation in unstimulated (CTL) and two M2 states, M2a and M2c; and 2) a comparative analysis of the molecular (gene expression) and functional (K^+ channel activity, migration) responses between rat and mouse microglia in M1, M2a and M2c states. *Study 1:* Kir2.1 channels are necessary for microglial Ca^{2+} signaling and migration but weakly inhibit proliferation under CTL, M2a and M2c states. Microglial Kir2.1 expression (transcript, currents) were comparable in CTL, M2a and M2c states. Kir2.1 blockers (Ba^{2+} or ML133) increased proliferation slightly in CTL or M2a (but not M2c) microglia. While M2 states increased migration and chemotaxis, blocking Kir2.1 reduced both. In all three states, ML133 reduced Ca^{2+} influx through Ca^{2+}-release-activated Ca^{2+} channels. *Study 2:* This collaborative project showed that pro-inflammatory genes increased only in the M1 state, but genes associated with the M2a state were not consistent between species and/or were induced in multiple activation states. Gene

expression for several Kir2 and Kv1 family members was detected in both species, but the currents were mainly Kir2.1 and Kv1.3, and depended on the activation state and species. Migration was affected similarly in both species by the activation state (reduced in M1, increased in M2a or M2c), and by channel blockers (reduced by Kir2.1 block, increased by Kv1.3 block). Thus, caution is recommended in generalizing microglial responses to activating stimuli between species.

Acknowledgments

First and foremost, I would like to express my gratitude to my supervisor, Dr. Lyanne Schlichter, whose expertise, guidance, and patience, has stimulated and enhanced my PhD work and graduate experience. I am also thankful for her continuous support in my research career (i.e., attendance at several national and international conferences to network, and choosing a career path outside of academia). I would also like to thank my PhD committee members, Dr. Robert Tsushima, Dr. Peter Backx, and Dr. Shannon Dunn for their time, for asking the hard questions, and the helpful comments; e.g. ML133 (suggested by Dr. Tsushima), and the detection of other Kir2 family members (Dr. Backx). And thank you to Dr. Xi Huang for being apart of my final supervisory PhD committee.

Appreciation also goes out to previous and current members of the Schlichter lab, who have been a collaborator, a support system, a source of knowledge, and an outlet to vent my frustrations and during my PhD studies; Dr. Starlee Lively, Dr. Tamjeed Siddiqui, Raymond Wong, Michael Joseph, Dr. Roger Ferreira, Dr. Jayalakshmi Caliaperumal, and Sarah Hutchings. A very special thanks goes out to Dr. Xiaoping Zhu, who has taken the time to teach me cellular (e.g., cell culture) and molecular techniques (e.g., qRT-PCR and Western blot).

Lastly, I would like to thank my family and Nemanja, my better half, for all their love, encouragement, and support during my PhD and all my other pursuits.

Table of Contents

List of Tables

List of Figures

List of Appendices

Abbreviations

4-AP	4-aminopyridine
AgTx-2	Agitoxin-2
ADP	Adenosine diphosphate
ANOVA	Analysis of variance
ARG1	Arginase 1
ATP	Adenosine triphosphate
Ba^{2+}	Barium ion
BSA	Bovine serum albumin
Ca^{2+}	Calcium ion
CCL	Chemokine (C-C motif) ligand
CD	Cluster of differentiation
Cm	Membrane capacitance
CNS	Central nervous system
CO_2	Carbon dioxide
COX	Cyclooxygenase
CRAC	Calcium release-activated calcium channels
CT	Threshold cycle
CTL	Control
CXCL	Chemokine (C-X-C motif) ligand
Cs^{+}	Cesium ion
CTL	Control group
DAMP	Damage-associated molecular pattern
DAPI	4′,6-diamidino-2-phenylindole
DIC	Days in culture
ECM	Extracellular matrix
EGTA	Ethylene glycol bis(2-aminoethyl ether)-N,N,N’N’-tetracetic acid
FBS	Fetal bovine serum
FIZZ1	Found in inflammatory zone 1
HEPES	4-(2-hydroxyethyl)-1-piperazineethanesulfonic acid
KCa	Calcium activated potassium channel

Kd	Dissociation constant
Kir	Inward rectifier potassium channel
Kv	Voltage-gated potassium channel
I	Current
IC_{50}	Half maximal inhibitory concentration
ICE	Interleukin-1 converting enzyme
IFN-γ	Interferon-gamma
IL-x	Interleukin-number
iNOS	Inducible nitric oxide synthase
LPS	Lipopolysaccharide
MgTx	Margatoxin
ML133	N-(4-methoxybenzyl)-1-(naphthalen-1-yl)methanamine
MRC1	Mannose receptor, C Type 1
mRNA	Messenger ribonucleic acid
M-CSF	Macrophage colony-stimulating factor
MEM	Minimum essential medium
Na^+	Sodium ion
NCF1	Neutrophil cytosolic factor 1
NOX	Nicotinamide adenine dinucleotide phosphate-oxidase
NO	Nitric oxide
OGD	Oxygen glucose deprivation
P2X	Ionotripic purinergic receptor
PAP-1	5-(4-phenoxybutoxy)psoralens
PBS	Phosphate buffered saline
PPAR-γ	Peroxisome proliferator-activated receptor gamma
PTK	Protein tyrosine kinase
PTP	Protein tyrosine phosphatase
PYK2	Protein tyrosine kinase 2 beta
ROS	Reactive oxygen species
RNA	Ribonucleic acid
qRT-PCR	Quantitative reverse transcription polymerase chain reaction
SEM	Standard error of the mean

SHP-1	Src homology region 2 domain-containing phosphatase-1
SOCE	Store-operated calcium entry
SOCS	Suppressor of cytokine signaling
SR-A	Scavenger receptor-A
TEA	Tetraethylammonium
TGF-β	Transforming growth factor-beta
TLR	Toll-like receptor
TNF-α	Tumor necrosis factor-alpha
TREM2	Triggering receptor expressed on myeloid cells 2
TSPO	Translocator protein
V	Volts
Vm	Membrane potential

Publications

Peer reviewed publications:

Lam, D., Lively, S., and Schlichter, L.C. A rat versus mouse comparison of microglia in different activation states: Molecular profiles, K^+ channels and migration. (Journal of Neuroinflammation. Under revision, October 2016)

Lam, D., and Schlichter, L.C. (2015) Expression and contributions of the Kir2.1 inward-rectifier K^+ channel to proliferation, migration and chemotaxis of microglia in unstimulated and anti-inflammatory states. Frontiers Cellular Neuroscience, 9:185.

Schlichter, L.C., Jiang, J., Wang, J., Newell, E.W., Tsui, F.W., and **Lam, D**. (2014) Regulation of hERG and hEAG channels by Src and by SHP-1 tyrosine phosphatase via an ITIM region in the cyclic nucleotide binding domain. PLoS One, 9(2): e90024.

Published conference proceedings:

Lam, D. *, Lively, S., and Schlichter, L.C. (2016) Microglial activation: a tale of two rodent species. 46th Annual meeting for Society of Neuroscience, San Diego, USA.

Lam, D. *, and Schlichter, L.C. (2016) Expression and roles of K^+ channels (Kir2.1, Kv1.3) in microglial anti-inflammatory states: Proliferation and migration. 10th Annual meeting for the Canadian Association for Neuroscience, Montreal, Canada.

Lam, D. *, and Schlichter, L.C. (2016) Expression and contributions of the inward-rectifier K^+ channel, Kir2.1, to proliferation, migration and chemotaxis of microglia in unstimulated and anti-inflammatory states. 2016 Biophysical Society, Los Angeles, USA.

Lam, D. *, and Schlichter, L.C. (2016) Expression and contributions of the inward-rectifier K^+ channel, Kir2.1, to proliferation, migration and chemotaxis of microglia in

unstimulated and anti-inflammatory states. 45th Annual meeting for Society of Neuroscience, Chicago, USA.

Lam, D. *, and Schlichter, L.C. (2015) Expression and contributions of the inward-rectifier K^+ channel, Kir2.1, to proliferation, migration and chemotaxis of microglia in unstimulated and anti-inflammatory states. 2015 CPIN Research Day, Toronto, Canada.

Lam, D. *, and Schlichter, L.C. (2015) Expression and contributions of the inward-rectifier K^+ channel, Kir2.1, to proliferation, and migration of microglia in unstimulated and anti-inflammatory states. 2015 Brain Research and Integrated Neurophysiology (B.R.A.I.N) Neuroscience Research Day, Toronto, Canada.

Schlichter, L.C., Jiang, J., Wang, J., Newell, E.W., Tsui, F.W., **Lam, D***. (2014) Regulation of hERG and hEAG channels by Src and by SHP-1 via an ITIM region in the cyclic nucleotide binding domain. 8th Annual meeting for the Canadian Association for Neuroscience, Montreal, Canada.

Lam, D.*, and Schlichter, L.C. (2013) Comparison of K^+ channels in rat and mouse microglia. 2013 CPIN Research Day, Toronto, Canada.

* indicates presenter

1 General Introduction

1.1 OVERVIEW

In this thesis, I will present the relevant background information on microglia, which includes a brief overview of their origin and role in the developing central nervous system (CNS) (§1.2). In the context of acute CNS injury in the mature brain (§1.3), I will introduce the current view of 'microglial activation' (§1.3.1), and studying microglial activation *in vitro* (§1.3.1.1). Ion channels (§1.4), transmembrane proteins that regulate the cell's electrical activity, have been targeted for several diseases and disorders, especially those of the cardiovascular system and the CNS. Before an ion channel can be successfully targeted in microglia, we must understand its fundamental roles in microglia physiology. Microglia express a variety of ion channels, and my work focuses on two subsets of potassium (K^+) channels: the inward rectifier Kir2.1 (§1.4.1) and outward rectifying Kv1.3 (§1.4.2). The expression pattern of both channels has been described in activated microglia (§1.4.3). Functionally, Kir2.1 and Kv1.3 channels are proposed to affect cellular activity by regulating the membrane potential (§1.5.1), and in turn affecting intracellular calcium homeostasis (§1.5.2). However, when I began my thesis work, very little was known about whether and how Kir2.1 and Kv1.3 channels contribute to microglial functions (§1.5.3). Both rat and mouse models have been used to study microglial responses, but not enough is known about whether these two rodent models behave the same (§1.6). Finally, I present the rationale and hypothesis (§1.7), which sets up the focus for the two studies, one published (Lam & Schlichter, 2015) and the other is currently under revision (Lam et al., under revision), presented in this thesis as almost verbatim to the manuscripts (Chapter 3 and Chapter 4, respectively).

1.2 MICROGLIA: ORIGINS AND DEVELOPMENT OF THE BRAIN

The origin of microglia was a subject of debate until recently. It was initially proposed that microglia are of myeloid origin, having shared cell-surface markers with mononuclear phagocytes (e.g. monocytes, macrophages, dendritic cells) (discussed in §1.3, Chan et al., 2007). In recent years, genetic fate mapping studies in mice have provided compelling evidence that microglia are ontogenetically distinct from the mononuclear phagocyte system (Ginhoux et al., 2013; Tay et al., 2016). Unlike other mononuclear phagocytes, microglia are derived from primitive myeloid progenitors in the extra-embryonic yolk sac (between embryonic day 7 and 8), which arise after the first wave of hematopoiesis (called primitive hematopoiesis). Microglial progenitors enter the circulatory system (E8.5 and E10), and colonize the CNS (by migration and proliferation) during late gestation and into postnatal development (Schulz et al., 2012; Arnoux et al., 2013; Ginhoux et al., 2013; Kierdorf et al., 2013). Microglia are crucial to the development of the brain: secreting growth factors to promote neuronal survival; inducing programmed cell death in immature neurons; phagocytosing dying cells; and regulating synapse development (Nayak et al., 2014; Tay et al., 2016). Maturation of microglia during postnatal development is detected by morphology (e.g. transformation from an amoeboid to a ramified morphology), decreased expression of genes associated with adult macrophage differentiation factors and molecular markers of microglia/macrophage activation, and a decrease in cell proliferation (Zusso et al., 2012; Schulz et al., 2012; Crain et al., 2013; Arnoux et al., 2013; Kierdorf et al., 2013). By the third postnatal week, microglial cell numbers decline, with only 50% remaining by the

sixth week of age, and then they are maintained under a steady state condition in the adult brain through a process of self-renewal (Hashimoto et al., 2013; Nikodemova et al., 2015).

1.3 MICROGLIAL ACTIVATION: FROM SURVEILLANCE TO IMMUNE RESPONDERS

Microglia in the adult brain express some of the same cell-surface markers as mononuclear phagocytes (Tay et al., 2016), such as the fractalkine receptor, CX3CR1; the hematopoietic growth factor receptor, CSF-1R; the integrin, CD11b; surface glycoproteins, F4/80 and CD68 (macrosialin); and ionized calcium-binding adaptor molecule 1 (Iba1). This, combined with their comparable morphologies, poses a problem for distinguishing resident microglia from infiltrating macrophages in damaged brain tissue using immunohistochemical methods. Nonetheless, these cell-surface markers have been useful to visualize resting microglia in the healthy brain or activated microglia/macrophages in the damaged tissue.

In the healthy adult brain, microglia represent a small proportion of CNS cells (~5-15%) (Lawson et al., 1992), and are positioned in a grid-like fashion within the brain parenchyma. These cells display a highly ramified morphology, with fine branched protrusions extending from the small cell soma. Microglia are highly motile, dynamically extending and retracting their ramified processes, with no cell body displacement (Divalos et al., 2005; Nimmerjahn et al., 2005; Kim & Dustin, 2006). In this phenotype, microglia are in their so-called ‘resting’ or ‘surveillance’ state, and are actively scanning their extracellular space and interacting with neurons, astrocytes and blood vessels. Microglia rapidly respond to acute CNS injury. This is proposed to occur in two stages:

an acute phase (within minutes to hours), where microglia in the vicinity project their processes to the site of tissue damage; and a delayed phase (within one to several days), where neighbouring microglia migrate to the damaged site (Divalos et al., 2005; Nimmerjahn et al., 2005; Kim & Dustin, 2006). Activated microglia are mostly found in and around the lesion (Perry, Nicoll and Holmes, 2010). Activation alters various microglial effector functions, including migration, proliferation, phagocytosis, and production and secretion of pro-or anti-inflammatory mediators (Lynch, 2009; Kettenmann et al., 2011; Hanisch, 2013). Several different morphologies of activated microglia have been described (Boche et al., 2013; Ziebell et al., 2015): hyper-ramified and bushy microglia, hypertrophic microglia with a larger soma and fewer processes than the resting phenotype, amoeboid activated microglia that are indistinguishable from macrophages, multinucleated microglia, cells with a rod-like cell body and polarized processes, and dystrophic microglia with the appearance of 'beading' of the processes. Whether these diverse morphologies reflect different activation phenotypes is not known.

1.3.1 Concept of microglial activation

Following brain injury, cells release 'damage-associated molecular pattern' molecules (DAMPs or 'alarmins') and other soluble mediators, including high-mobility group box 1, purine metabolites, nucleic acids, and cytokines (Hanisch, 2013). In response, microglia 'activate', and this is accompanied by dramatic changes in morphology, gene expression, and effector functions. While microglia are the first responders to any perturbation to the brain parenchyma, it is important to be aware that other cell types, particularly infiltrating peripheral leukocytes (e.g. neutrophils, macrophages, T cells),

can influence the inflammatory milieu within hours to days following tissue damage (Russo & McGavern, 2015). Thus, microglial activation phenotypes can evolve.

The nomenclature of activated microglia has evolved over the years in an attempt to categorize the different phenotypes (Colton et al., 2009; Hanisch, 2013, Cherry et al., 2014; Michell-Robinson et al., 2015). Microglial activation is often modeled after the responses of tissue macrophages *in vitro* (Fig. 1.1). 'Classical' activation (M1) is a pro-inflammatory phenotype thought to exacerbate tissue damage. It is usually induced *in vitro* by bacterial lipopolysaccharide (LPS), with or without IFN-γ, which upregulates genes and proteins of various pro-inflammatory and cytotoxic mediators; e.g. tumor necrosis factor (TNF-α), interleukin (IL)-6, IL-1β, reactive oxygen species and nitric oxide (NO). The anti-inflammatory (M2) phenotype is divided into subclasses. 'Alternative activation' (M2a; induced by IL-4 and/or IL-13) and 'acquired deactivation' (M2c; induced by IL-10, TGF-β or glucocorticoids) are commonly investigated *in vitro*. The M2a state is characterized by upregulation of genes and proteins involved in tissue repair and matrix deposition; e.g. arginase 1 (ARG1), mannose receptor (MRC1; also known as CD206), found in inflammatory zone 1 (FIZZ1) and chitinase-like lectin (CHIL3; also known as Ym1). The M2c state, like M2a, contributes to the resolution of inflammation by downregulating pro-inflammatory cytokines (Colton, 2009; Michell-Robinson et al., 2015), but not enough is known about its inflammatory expression profile. Moreover, little is known about effector functions associated with the different activation phenotypes.

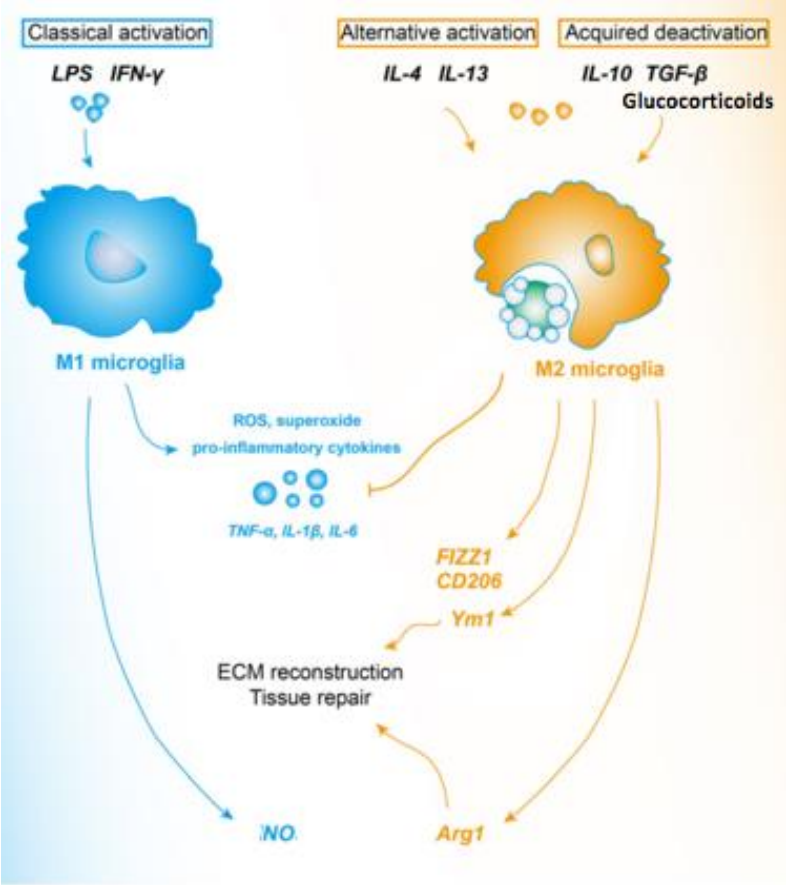

Figure 1.1. Nomenclature of activated microglia. Microglia possess states of "classical activation", "alternative activation," and "acquired deactivation," depending on the milieu in which they become activated and the factors they are stimulated. Microglia in classical activation state are also termed M1 microglia, which induce iNOS and NF-κB pathways and produce various pro-inflammatory cytokines such as TNF-α, IL-1β, and IL-6, as well as superoxide, ROS and NO. M2 states include the states of both alternative activation (M2a) and acquired deactivation (M2c), which are induced by IL-4 and/or IL-13 and IL-10, TGF-β or glucocorticoids, respectively. M2 microglia promote ECM reconstruction and tissue repair, and antagonize the M1 pro-inflammatory responses that finally results in immunosuppression and neuron protection. [Modified figure and figure legend from Tang and Le, 2016]

1.3.1.1 Microglial activation phenotypes *in vitro*

In a controlled environment, activation phenotypes of microglia are studied *in vitro* by stimulating cells with bacterial toxins or cytokines, which can alter cell morphology (Fig. 1.2), initiate different signaling pathways that alter gene expression patterns, and/or ion channel activity (Ransohoff and Perry, 2009; Skaper, 2011). But not enough is known about whether microglial functions are modulated by different activation phenotypes.

M1 phenotype. Lipopolysaccharide (LPS) is an endotoxin found on the outer cell wall of gram-negative bacteria. It is commonly used to polarize microglia into a M1 state, which is a good model for CNS infection but not for acute CNS injury (Cunningham et al., 2013). During my PhD studies, the Schlichter lab has begun to characterize microglia stimulated with cytokines relevant to acute CNS damage; e.g. IFN-γ and TNF-α to induce the M1 phenotype (Siddiqui et al., 2016). Unpublished work from the Schlichter lab has compared the pro-inflammatory response in M1-activated microglia induced by IFN-γ and TNF-α versus LPS (Lively and Schlichter, manuscript in preparation). Our findings suggest that LPS exaggerates the pro-inflammatory response, which is consistent with the literature (Cunningham et al., 2013; Lively and Schlichter, manuscript in preparation). Within a few hours following acute CNS injury, protein levels of IFN-γ and TNF-α are detected in the damaged tissue (Harting et al., 2008; Dalgard et al., 2012; Ansari, 2015). IFN-γ binds to the IFN receptor, comprised of IFN-γ receptor 1 (IFNGR1) and IFN-γ receptor 2 (IFNGR2) subunits, and signals mainly through the Janus kinases, JAK1 and JAK2, and signal transducer and activator of transcription (STAT) 1 (Schneider et al., 2014). TNF-α can bind to TNF-α receptor 1 (TNFR1) and/or TNF-α receptor 2 (TNFR2), which differ in binding affinity and signalling pathways that trigger apoptotic and/or inflammatory responses (Olmos and Lladó, 2014). The

cytoplasmic tail of TNFR1 contains a death domain that is not present in TNFR2. Activation of TNFR1 triggers caspase-dependent apoptotic cell death. However, both TNFR1 and TNFR2 receptor activation can trigger signalling pathways including extracellular signal-regulated kinase (ERK), c-Jun N-terminal kinase (JNK), p38 mitogen-activated protein kinase (p38 MAPK), and nuclear factor-kappa B (NFκB). Both cytokines synergistically promote the pro-inflammatory response in the brain, shown directly by injection or infusion, or indirectly by knocking out one or both cytokines in a rodent model of Parkinson's disease (Kong et al., 2000; Blais & Rivest, 2004; Barcia et al., 2011). However, very little is known about gene expression profiles, ion channel activity, and functional responses of microglia stimulated with both cytokines together.

M2 phenotypes. We are only beginning to understand the differences between the subclasses within the M2 phenotype, particularly M2a and M2c activation states.

M2a phenotype. IL-4 is often used to polarize microglia into a M2a state (Van Dyken and Locksley, 2013). IL-4 binds to the IL-4 receptor α chain (IL-4Rα) that is part of Type I and II receptor complexes, and initiates two signaling pathways involving insulin receptor substrate 2 (IRS2) and phosphoinositide 3-kinase (PI3K), and STAT6, resulting in upregulation of genes that encode for proteins described in §1.3.1. **M2c phenotype**. Like others, the Schlichter lab has used IL-10 to polarize microglia into a M2c state (Siddiqui et al., 2014). IL-10 binds to the IL-10Ra subunit of the IL-10 receptor complex and activates a signalling cascade involving JAK1 and STAT3, leading to an immunosuppressive phenotype in peripheral immune cells (Moore et al., 2001). Little is known about IL-10-induced changes in microglia, particularly microglial functions and ion channel activity. However, it has been suggested that they are similar in gene

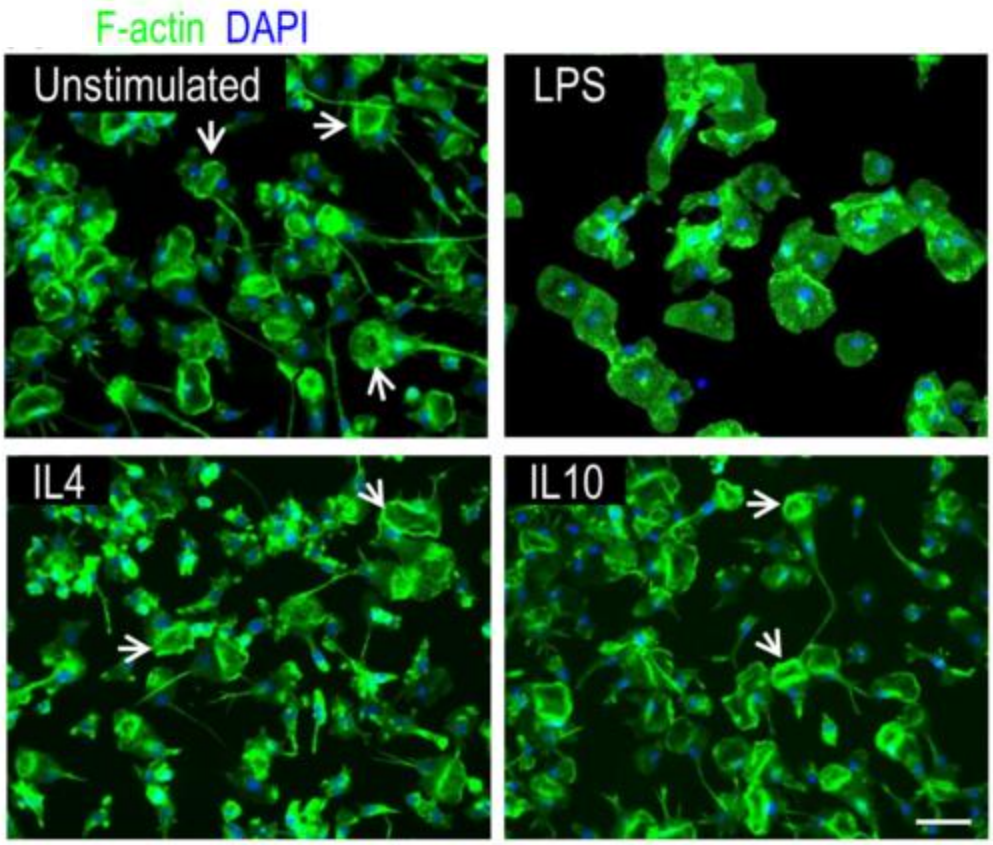

Figure 1.2. Microglia morphology in different activation states *in vitro.*

Representative fluorescence micrographs show unstimulated primary rat microglia or 24 h after treatment with LPS (10 ng/mL), IL4 (20 ng/ mL) or IL10 (20 ng/mL). LPS-treated cells were amoeboid, round or flat. While IL-4- or IL-10 treated microglia were predominantly unipolar cells. The arrows indicate examples of a single, large donut-shaped ring of podosomes, which we call a 'podonut' in the lamellum of unipolar microglia. Cells were stained for filamentous (F-) actin with phalloidin (green) and with the nuclear marker, DAPI (blue). Scale bar, 50 µm. [Reprinted figure and modified figure legend from Siddiqui et al., 2014]

expression profile to pro-inflammatory stimuli (e.g. LPS), but with smaller responses (Chhor et al., 2013).

During the course of my PhD studies, a major focus of the Schlichter lab has been to characterize and compare functions of activated rat microglia in M1, M2a and M2c states *in vitro*. Our lab has shown that microglial migration and invasion are activation-state dependent: M2a (induced by IL-4) or M2c (induced by IL-10) activation states enhance their ability to degrade the ECM, invade, and migrate; whereas, the M1 (induced by LPS) activation state reduced these functions (Lively & Schlichter, 2013; Siddiqui et al., 2014).

1.4 EXPRESSION AND FUNCTION OF ION CHANNELS

Microglia express a variety of ion channels, a few of which have been associated with microglial functions, such as migration, proliferation, cytokine and reactive oxygen species production, and phagocytosis (Eder, 2005; Kettenmann et al., 2011; Stebbing, et al., 2014). Ion channels are transmembrane proteins that form a pore with the ability to open and close in response to chemical, electrical and/or mechanical signals, allowing the passive movement of inorganic ions [e.g. potassium (K^+), calcium (Ca^{2+}), sodium (Na^+), chloride (Cl^-)] across the membrane. The movement of charged ions through their pores creates an electrical current and charge separation that contributes to the overall difference in voltage across the membrane. In microglia, ion channels are important modulators of cell functions that include cell volume, by modulating swelling and shrinking as the cell changes shape; and intracellular Ca^{2+} homeostasis, involved in cytoskeleton rearrangement (Eder, 2005; Kettenmann et al., 2011; Stebbing, et al., 2014).

In recent years, K^+ channels have been proposed as potential drug targets to modulate autoimmune diseases, such as multiple sclerosis, rheumatoid arthritis, type 1 diabetes, and psoriasis (Chandy et al., 2004; Wulff and Zhorov, 2008; Feske et al., 2015). Their expression and function have been extensively studied in the adaptive immune system, specifically in T lymphocytes (Chandy et al., 2004; Wulff and Zhorov, 2008; Feske et al., 2015). Kv1.3 and KCa3.1 channel expression patterns can be distinguished between the three types of T cells: naïve, central memory (T_{CM}) T cells, and effector memory (T_{EM}). However, Kv1.3 channels are upregulated only in T_{EM} cells (~1500 channels/cell) when activated during an immune response, but not in naïve and T_{CM} cells (~300 channels/ cell), which are in a quiescent state. This phenotypic change in Kv1.3 channel expression provided a possible therapeutic target for immunomodulatory actions in autoimmune diseases. Blocking Kv1.3 channels leads to membrane depolarization, and inhibition of Ca^{2+} influx, cytokine production and proliferation in activated T_{EM} cells but not naïve or T_{CM} cells (Chandy et al., 2004; Cahalan and Chandy, 2009; Wulff & Christophersen, 2015). However, whether these channels can be modulated in microglia involved in the innate immune system in the CNS is not clear. In this thesis, I will focus on prominent K^+ currents expressed in microglia: the inward rectifying and outward rectifying currents, mediated by Kir2.1 and Kv1.3, respectively. The biophysical properties of these channels have been well characterized in microglia, but whether their expression is regulated under different microglial activation states was not clear.

1.4.1 Inward rectifying (Kir) potassium (K^+) channels in microglia

The general architecture of K^+ channels is four identical or similar peptide subunits around a central pore to form a functional channel. Each peptide subunit in a Kir channel contains 2 transmembrane segments (TM1 and TM2) linked by a selectivity filter loop (called the p-loop), which contains the signature sequence (T-X-G-Y(F)-G) for K^+ selectivity that is conserved across other K^+ selective ion channels, as well as amino (NH2)- and carboxy (COOH)-terminal domains on the intracellular side of the membrane (Hibino et al., 2010). Unlike voltage-gated K^+ channels (see 1.4.2), Kir channels do not possess an S4 voltage sensor region, and are thus incapable of intrinsic voltage-dependent gating. Kir channels do, however, display extremely rapid, voltage-dependent block by intracellular Mg^{2+} and polyamines (Lu, 2004) that can make them appear to be voltage dependent. K^+ conductance for Kir (and other K^+ channels) is dependent on the electrochemical gradient for K^+ ions, which is the difference between the membrane potential (Vm) and the reversal potential for K^+ (E_K). A large inward current is observed when $Vm < E_K$, which moves K^+ inward, but when $Vm > E_K$, K^+ moves outward. However, when $Vm > E_K$, Mg^{2+} and polyamines enter the Kir channel and bind to specific regions within the inner vestibule, they block the K^+ conductance. These intracellular molecules cause the inward rectification of Kir channels.

While not directly proven to be Kir2.1, the electrophysiological profile of the current in microglia is consistent with Kir2.1, based on fast opening kinetics, Na^+-dependent relaxation at very hyperpolarized potentials, and a single channel conductance of 25-30 pS (Kettenmann et al., 1990; Nöremberg et al., 1994; Schilling et al., 2000). The Kir2.1 channel belongs to the Kir2 family, one of seven subfamilies in the

Kir family that are encoded by *Kcnj* genes (Hibino et al., 2010). While genes for Kir1.1 (*Kcnj1*) and Kir2.1 (*Kcnj2*) were detected in immortalized mouse (BV-2 and C8-B4) microglia (Schilling et al., 2000; Moussaud et al., 2009), the Kir current was insensitive to the Kir1.1 inhibitor ∂-dendrotoxin (Schilling et al., 2000) but sensitive to Ba^{2+} (Kettenmann et al., 1990& 1993; Schlichter et al., 1996; Schilling et al., 2000), a nonspecific Kir channel blocker (Hibino et al., 2010) that is commonly used to study Kir2.1 channels in cellular function, including microglia (see §1.5). While homo-tetrameric complexes of Kir2.1 channels are possible, hetero-tetramers of Kir2.1 co-assembled with other Kir2.x family members can occur (Hibino et al., 2010). Gene expression for other Kir2 members, Kir2.2 (*Kcnj12*), Kir2.3 (*Kcnj4*) and Kir2.4 (*Kcnj14*), have been detected in the brain (deBoer et al., 2010), but it is not known whether they are expressed specifically in microglia.

1.4.2 Outward rectifying voltage-gated (Kv) K^+ channels in microglia

Voltage-gated (Kv) K^+ channels are also tetrameric structures. However, unlike Kir channels, each peptide subunit contains six transmembrane segments (S1-S6) that make up key functional elements of the channel (Yellen, 2002). The voltage sensing domain (VSD) is formed by four transmembrane segments (S1-S4) where S4 contains positively charged amino acids that periodically align and act as a voltage sensor. A pore domain (S5-P-S6) is equivalent to TM1 and TM2 in Kir channels and contains the 'selectivity filter'. They also contain cytoplasmic NH2 and COOH terminal domains. Kv channels can also associate with auxillary β subunits, which can attach to the NH2

terminal domain of Kv channels and assist in trafficking or affect the gating properties of the channel (Coetzee et al., 1999).

Kv channels are the largest group of ion channels, containing 12 subfamilies (Kv1 to Kv12), encoded by about 40 genes (Gutman et al., 2005). In primary rodent microglia, members of the Kv1 (Shaker-related) subfamily have been detected. This includes mRNA and protein expression for Kv1.2, Kv1.3, and Kv1.5 (Fordyce et al., 2005; Kotecha & Schlichter, 1999; Pannasch et al., 2006; Li et al., 2008). Only one study reported Kv1.6 mRNA transcripts in primary rat cultures, but the level was low (Kotecha & Schlichter, 1999) and it is not known whether its protein is expressed. In addition, that study did not detect Kv1.1 or Kv1.4 mRNA transcripts in primary rat microglial cultures (Kotecha & Schlichter, 1999).

Electrophysiological and pharmacological characterization of the Kv current in resting and activated microglia *in vitro* and *in situ* (§1.4.3) strongly support the expression of Kv1.3 channels. Depolarizing voltages (above –50 mV) activate an outward K^+ current that displays C-type inactivation, seen as a slow decline in current with a time constant of hundreds of milliseconds following channel activation (Kotecha & Schlichter et al., 1999). This C-type inactivation is a hallmark of Kv1.3, more so than other members of the Kv1 subfamily, in addition to cumulative inactivation, a use-dependent phenomenon in which successive depolarizing pulses incrementally reduce current amplitude (Korotzer & Cotman, 1992; Grissmer et al., 1994; Nöremberg et al., 1994; Kotecha & Schlichter, 1999; Cayabyab et al., 2000). Also, the voltage dependence of activation and steady-state inactivation of Kv currents in cultured microglia closely resembles cloned Kv1.3 channels (Kotecha & Schlichter et al., 1999). Lastly, the Kv current is blocked by broad-spectrum Kv blockers (e.g.

tetraethylammonium (TEA), 4-AP), by potent and more selective Kv1.3 peptide toxins (e.g. margatoxin (MgTx), agitoxin-2 (AgTx-2)) and small molecule Kv1.3 blockers (e.g. PAP-1) in microglia *in vitro* (Schlichter et al., 1996; Draheim et al., 1999; Kotecha & Schlichter; 1999; Cayabyab et al., 2000; Fordyce et al., 2005; Chen et al., 2015) and *in situ* (Menteyne et al., 2009; Arnoux et al., 2013). To study Kv1.3 channels involved in microglial functions, our lab routinely uses AgTx-2, an extremely potent Kv1.3 blocker (Garcia et al., 1997), with a K_d of 177 pM in activated T lymphocytes (Kotecha & Schlichter 1996).

1.4.3 Membrane current patterns in microglial cells *in vitro* and *in situ*

The Kir current is prevalent in unstimulated rat (Kettenman et al., 1990; Korotzer and Cotman, 1992; Visentin et al., 1995; Schlichter et al., 1996) and mouse microglia (Draheim et al., 1999; Prinz et al., 1999). The literature suggests that there might be species dependent regulation of Kir currents in M1-activated primary microglia but this has not been directly investigated. Mouse microglia exposed to LPS or IFN-γ displayed reduced Kir current (Draheim et al., 1999; Prinz et al., 1999; Boucsein et al., 2003). However, rat microglia have shown variable responses from no change to an increase in the Kir current when stimulated LPS or IFN-γ (Nörenberg et al., 1992 & 1994; Visentin et al., 1995; Draheim et al., 1999). But very little is known about whether this current is regulated by stimuli that are anti-inflammatory. Only two studies showed that TGF-β1 and TGF-β2, both considered as resolving cytokines, like IL-10 (Suzumura et al., 1993; Pratt and McPherson, 1997), did not affect the Kir current in primary and

immortalized (BV-2 and C8-B4) mouse microglia (Schilling et al., 2000; Moussaud et al., 2009).

The appearance of a Kv current in microglia is generally believed to be an indicator of the M1 activation state. This is based on early studies that have reported very little to no Kv current at depolarized potentials (Kettenman et al., 1990 & 1993; Nörenberg et al., 1992; Walz et al., 1993), while LPS or IFN-γ stimulation upregulated Kv currents in both rat (Nörenberg et al., 1992 & 1994; Visentin et al., 1995; Fordyce et al., 2005), and mouse microglia (Draheim et al., 1999; Prinz et al., 1999; Pannasch et al., 2006). Also, Kv currents were detected in activated microglia/macrophages *in situ* in rodent models of ischemia, epilepsy, and facial nerve axotomy (Lyons et al., 2000; Boucsein et al., 2000; Menteyne et al., 2009). Two studies have reported that anti-inflammatory stimuli, specifically TGF-β1and TGF-β2 increased Kv currents in primary and immortalized (BV-2 and C8-B4) mouse microglia (Schilling et al., 2000; Moussaud et al., 2009). These findings suggest that expression of Kv currents might not be an indicator of the M1 state but instead, might be stimulus dependent.

The literature suggests that there might be species-dependent regulation of Kir currents in M1-activated microglia and stimulus-dependent upregulation of Kv currents. But it is not clear whether these currents are regulated by anti-inflammatory cytokines, like IL-4 or IL-10.

1.5 REGULATORY ROLES OF K^+ CHANNELS IN MICROGLIA

1.5.1 Membrane Potential

Microglia membranes have a very high electrical resistance (~8 GΩ) making these cells

susceptible to leak-induced depolarization (Newell & Schlichter, 2005). Conventional current clamp is commonly used to measure the membrane potential of cells, but it is an invasive technique that does not compensate for leak conductance caused by the electrode. So the measured membrane potentials could potentially be more depolarized than the actual resting membrane potential of the cell, a limitation of this technique. Keeping this in mind, studies using current clamp have reported a bi-stable distribution of resting membrane potentials sampled from a population of microglial cells, with peaks around –35 and –70 mV for unstimulated rat and mouse microglia (Nöremberg et al., 1994; Visentin et al., 1995; Bouscein et al., 2003) but shifted to –45 mV and –70 mV in LPS-activated rat microglia (Chung et al., 1999). This bi-stable distribution coincided with Kir and Kv current activity. Using a pharmacological approach, subsequent studies have shown that Ba^{2+}-sensitive Kir currents were important for stabilizing the resting membrane potential around –70 mV (Chung et al., 1999; Franchini et al., 2004), while 4-AP-sensitive Kv currents maintained the membrane potential at about –35 mV (Chung et al., 1998 & 1999). Also, the Schlichter lab has shown that membrane potential oscillations (between –60 mV and –30 mV) in rat microglia, induced by a depolarizing current, required a very negative initial resting membrane potential, and blocking Kv1.3 channels with AgTx-2 prevented the oscillatory response. Collectively, these studies show that Kir and Kv channels regulate the membrane potential of resting microglia: Kir channels are important for keeping the resting membrane potential very negative, while Kv1.3 channels are important for repolarization and membrane potential oscillations.

1.5.2 Intracellular calcium (Ca^{2+}) homeostasis

Intracellular Ca^{2+} ($[Ca^{2+}]_i$) concentrations in microglia are relatively low ~23 nM (Ohana et al., 2009), but external stimuli can activate signalling pathways that elevate $[Ca^{2+}]_i$ levels to hundreds of nM and even as high as several µM (Möller, 2002). Intracellular Ca^{2+} is a ubiquitous second messenger that regulates a number of cellular functions: migration, proliferation, phagocytosis, production of chemokines and cytokines (Stebbing et al., 2015). Various proteins (e.g. Ca^{2+}-permeable ion channels, exchangers, pumps) regulate $[Ca^{2+}]_i$ levels by controlling either Ca^{2+} transport across the cell membrane and its release/ uptake by intracellular organelles (e.g. mitrochondria and endoplasmic reticulum), or through chelation by Ca^{2+} buffers (Möller, 2002; Schwaller, 2010). In rat microglia, there are several candidates that can potentially increase Ca^{2+} transport across the plasma membrane: Ca^{2+}-release activated Ca^{2+} (CRAC/Orai1) channels, TRPM7 channels, ionotropic purinergic receptors, and the reverse mode of the Na^+/Ca^{2+} exchanger (Jiang et al. 2003; Newell et al. 2007; Inoue 2008; Ohana et al. 2009; Siddiqui et al. 2014).

Of these candidates, the CRAC channel is highly selective for Ca^{2+} and strongly inward-rectifying (Parekh & Putney, 2005), replenishing signaling-dependent depletion of Ca^{2+} from internal Ca^{2+} stores of the endoplasmic reticulum. The Schlichter lab directly demonstrated that the membrane potential of microglia can influence the driving force for CRAC channels (Ohana et al., 2009): Ca^{2+} entry through CRAC channels increased by hyperpolarizing the cell to –90 mV, while depolarizing to –10 mV reduced it. Kir2.1, like other classical Kir channels, is expected to maintain a negative membrane potential and thereby regulate the driving force for ion fluxes, including Ca^{2+} influx. In

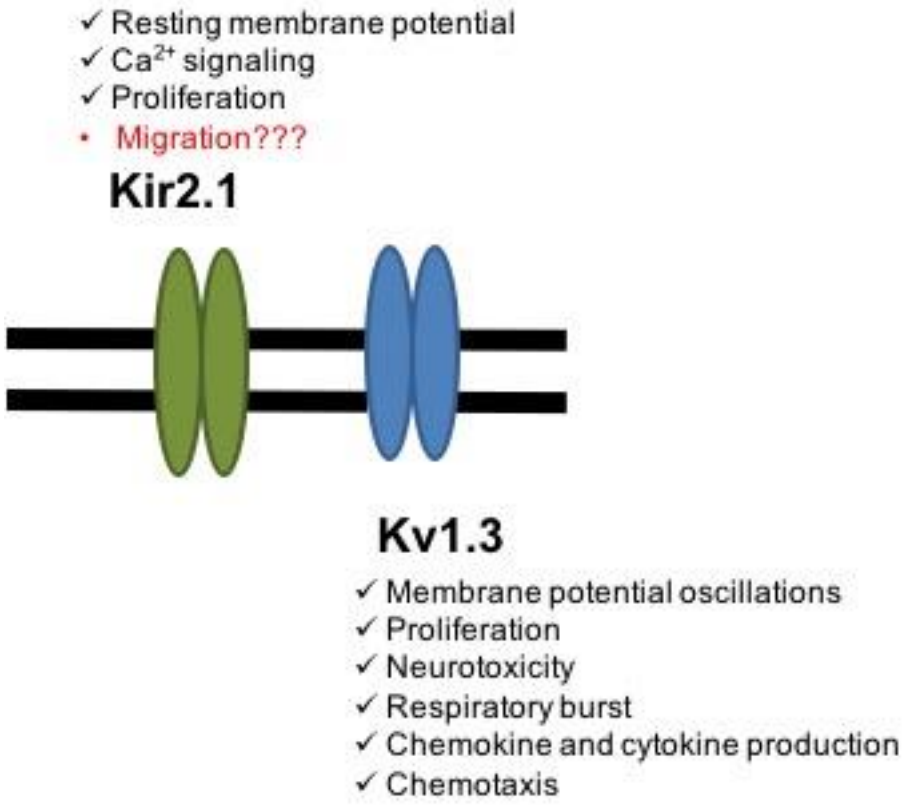

Figure 1.3. Known roles of Kv1.3 and Kir2.1 channels in microglial functions before I started my PhD studies. Only one study indirectly linked Kir2.1 activity to cell migration, but this was not directly tested.

microglia, blocking Kir2.1 channels reduced ATP-induced Ca^{2+} entry by prolonging membrane depolarization (Franchini et al., 2004), suggesting a link between Kir2.1 channel activity and Ca^{2+} entry. However, the source of Ca^{2+} entry was not identified, and whether blocking Kir2.1 was sufficient to affect Ca^{2+}-dependent cellular functions was not examined.

1.5.3 Cellular activity

When I began my PhD studies, there were already numerous papers from our lab and other research groups demonstrating that Kv1.3 and Kir2.1 contribute to a number of functions of rat microglial cells (Fig. 1.3). In particular, our lab showed that Kv1.3 channels are involved in functions associated with microglial activation, namely proliferation (Kotecha and Schlichter, 1999), neurotoxicity (Fordyce et al., 2005), and respiratory burst (Khanna et al., 2001). Other research groups have reported that Kv1.3 contributes to chemokine and cytokine production in activated rat microglia (Liu et al., 2012; Charolidi et al., 2015) and MCP-1 or ADP-induced chemotaxis in unstimulated rat microglia (Nutile-McMenemy et al., 2007). Little was known about the role of Kir2.1 in microglial functions, possibly due to the lack of specific channel blockers. In an early study, high concentrations of Ba^{2+} (5 and 10 mM) counteracted the increased proliferation of rat microglia induced by the mitogen, colony-stimulating factor-1 (CSF-1) (Schlichter et al. 1996). During my studies, only one study indirectly linked Kir2.1 activity to cell migration. In murine microglia, small GTPases, which are known to facilitate migration by regulating the actin cytoskeleton, modulated Kir2.1 current and cell spreading similarly, both increasing with Rac activation and decreasing with Rho activation (Muessel et al., 2013). It is not clear whether microglial functions are

modulated under different activation phenotypes *in vitro*, and whether or how Kir2.1 and Kv1.3 channels contribute.

1.6 RAT VERSUS MOUSE MODELS

Rats and mice are commonly used in biomedical research to model the human disease condition. Both rodent species have been used for many years to model CNS damage and disease. Rats have been favored for behavioral studies since they have many physiological similarities to humans, and are capable of learning a variety of tasks appropriate for cognition and memory research (Iannaccone and Jacob, 2009). Advances with molecular techniques have made mice more favorable for genetic manipulation (Nguyen and Xu, 2008; Sieger et al., 2013), but transgenic technology in rats is now advancing (Kawaharada et al., 2015). Surprisingly, only a few studies have directly compared the inflammatory response in rat and mouse CNS models: two studies compared the rodents' immune responses following acute CNS injury (Schroeter et al., 2003; Potter-Baker et al., 2014) and only one study directly compared responses of primary microglia isolated from the two rodent species (Patrizio and Levi, 1994). The literature on Kir channels suggests species differences in the regulation of channel activity in activated rat and mouse microglia (see §1.4.3), but whether this also extends to other microglial responses (e.g. gene expression changes, functional correlates, and other ion channel expression and activity) under different activation phenotypes is not known. This critical knowledge gap of how similar or different the immune response of microglia in these two commonly used models will affect the ability to translate experimental findings to the human condition.

1.7 RATIONALE AND HYPOTHESIS

K^+ channels are potential drug targets for autoimmune diseases. But before K^+ channels can be targeted in microglia, it is important to determine whether and how channel expression and activity contribute to microglial functions under different microglial activation states. For instance, very little is known about Kir2.1 and Kv1.3 channel expression in anti-inflammatory states (e.g. M2a and M2c), which help resolve M1 activation and promote repair. Kir2.1 channel is important for keeping the resting membrane potential very negative, and is proposed to regulate the driving force Ca^{2+} influx. Both migration and proliferation are Ca^{2+}-dependent functions. In **Chapter 3**, I hypothesized that Kir2.1 contributes to Ca^{2+} entry, and Ca^{2+}-dependent functions (e.g. migration and proliferation) of rat microglia. Here, I investigated the expression and contributions of Kir2.1 channels to migration and proliferation of untreated, and M2a- and M2c-activated rat microglia. The literature suggests species differences in the regulation of Kir2.1 current in M1-activated microglia, and stimulus dependent regulation of Kv1.3 currents. In **Chapter 4**, I hypothesize that these factors (i.e. species, stimulus) will affect whether and how these channels contribute to microglial migration under different activation phenotypes. I collaborated with Dr. Starlee Lively, a Research Associate in the Schlichter Lab, to compare rat and mouse microglial responses to different inflammatory cytokines. This comparative study examined the molecular responses and functional consequences (e.g. migration, and Kir2.1 and Kv1.3 channel activity) of M1, M2a, and M2c stimulated rodent microglia, and whether or not Kir2.1 and Kv1.3 modulate the functional consequences.

2 General Methods

This section will present the general procedures for the cellular and molecular techniques used in this thesis. Any specific differences are stated in the Methods section of each chapter.

2.1 Primary microglial cells

All procedures on animals were approved by the University Health Network Animal Care Committee (Animal Use Protocols 914 and 1573) and adhered to the Canadian Council on Animal Care guidelines for humane animal use. Pure neonatal microglia cultures were prepared by Dr. Xiaoping Zhu, Raymond Wong or myself from Sprague-Dawley rat pups (P1–P2) and C57BL/6 mouse pups (P0–P2). We selected this outbred rat strain and inbred mouse strain because they are both widely used in biomedical research, and specifically because C57BL/6 mice are the primary strain used in transgenic studies. Animals were purchased from Charles River (St-Constant, PQ, Canada). As we recently described for rat microglia (Siddiqui et al., 2012, 2014; Lively & Schlichter, 2013; Ferreira et al., 2014; Lam & Schlichter, 2015), brain tissue (excluding the cerebellum and meninges) was mashed, strained and centrifuged (300 ×*g*, 10 min) in cold Minimal Essential Medium (MEM; Invitrogen, Carlsbad, CA). The pellet was re-suspended in MEM, and seeded in 75 cm^2 flasks containing 20 mL of MEM supplemented with 10% fetal bovine serum (FBS; Wisent St-Bruno, PQ) and 0.05 mg/mL gentamycin (Invitrogen). Cells were incubated at 37°C with 5% CO_2, and after 48 h, the medium was changed to remove cellular debris and non-adherent cells. After 5–6 days (rat) or 10–14 days (mouse), microglia were harvested by shaking the flasks

(5 h, 65 rpm) on an orbital shaker in the incubator (37°C, 5% CO_2). Mouse cultures were grown longer to increase their numbers. The supernatant containing microglia was collected, centrifuged, and re-suspended in fresh MEM (2% FBS, 0.05 mg/mL gentamycin). Microglia were seeded onto UV-irradiated 15 mm glass coverslips (Fisher Scientific, Ottawa, ON) at different densities based on the experiment, as detailed below.

After seeding, microglia were allowed to settle for 2–3 days (37°C, 5% CO_2), and then were left unstimulated (control; CTL) or stimulated with 20 ng/mL IL-4 [M(IL-4)] or 20 ng/mL IL-10 [M(IL-10)] to induce anti-inflammatory states (Chapter 3), or with 20 ng/mL IFN-γ plus 50 ng/mL TNF-α to induce a pro-inflammatory state [M(I+T)] (Chapter 4). Our lab has previously validated that the cytokine concentrations and durations used in this thesis effectively induce gene expression changes of well-known classical and alternative activation markers (Lively & Schlichter, 2013; Ferreira et al., 2014; Siddiqui et al., 2014 & 2016). The recombinant cytokines (R & D Systems Inc., Minneapolis, MN) were specific to the rodent species; e.g., mIL-4 was used on mouse microglia.

2.2 Whole-cell patch clamp electrophysiology

For each assay, a coverslip bearing unstimulated or stimulated rodent microglia (7–9 $\times 10^4$ cells/coverslip) was mounted in a 300 µL volume perfusion chamber (Model RC-25, Warner Instruments, Hamden, CT). The standard bath solution consisted of (in mM): 125 NaCl, 5 KCl, 1 $CaCl_2$, 1 $MgCl_2$, 10 HEPES, 5 D-glucose, adjusted to pH 7.4 and 290–300 mOsm/kg H_2O. Bath solution, with or without a channel blocker, was perfused into the chamber using a gravity-driven perfusion system flowing at ~1 mL/min. Recording pipettes (5–8 MΩ resistance) were pulled from thin wall borosilicate glass

(WPI, Sarasota, FL) on a Narishige puller (Narishige Scientific, Setagaya-Ku, Tokyo), and fire polished with a microforge (MF 900; Narishige). Pipettes were filled with an intracellular solution containing (in mM): 40 KCl, 100 KAsp, 1 $MgCl_2$, 10 HEPES, 2 MgATP, (pH 7.2; 290–300 mOsm/kg H_2O), and with 0.5 $CaCl_2$ and 1 EGTA to buffer internal free Ca^{2+} to ~120 nM. Data were acquired using an Axopatch 200A amplifier, filtered at 5 Hz with a DigiDATA 1322A board, and analyzed with pCLAMP 10 software (all from Molecular Devices, Sunnyvale, CA). The ground electrode was inserted into an agar bridge made with bath solution in order to reduce junction potentials, which were then calculated with the pCLAMP utility. The voltage protocols for each experiment are indicated in the figure legends and Results text.

2.3 Gene Expression

2.3.1 RNA extraction

Microglia were seeded at 1–2 $\times 10^6$ cells/coverslip in a 35 mm dish, allowed to settle for 1–2 days (37°C, 5% CO_2), and then stimulated with cytokines for 6 or 24 h. Total RNA was extracted using TRIzol reagent (Invitrogen) and purified using an RNeasy Mini Kit (QIAGEN, Mississauga, ON, Canada) by Dr. Zhu, as previously described (Lively and Schlichter, 2013; Ferreira et al., 2014; Lam & Schlichter, 2015; Siddiqui et al., 2016). Samples were stored at –80ºC and used for NanoString and qRT-PCR assays.

2.3.2 Quantitative reverse transcriptase polymerase chain reaction (qRT-PCR)

The primers for genes of interest were designed by Dr. Zhu using "Primer3web" (http://bioinfo.ut.ee/primer3/). According to the manufacturer's instructions (Invitrogen), extracted RNA (0.25 µg) from unstimulated rat and mouse microglia were first reverse transcribed using SuperScriptII RNase reverse transcriptase, with dNTPs, oligo dT and DTT. cDNA was then amplified using ABI PRISM 7700 Sequence Detection System (PEBiosystems, Foster City, CA, USA), with the following protocol: 50˚C for 2 min, 95˚C for 10 min, 40 cycles at 95˚C for 15 s, 60˚C for 60 s, and three dissociation steps (95˚C for 15 s, 60˚C for 15 s, 95˚C for 15 s). The threshold cycle (CT) for each gene of interest was normalized to *Hprt1* (ΔCT), and converted to $2^{\Delta CT}$.

2.3.3 Multiplexed gene expression analysis (NanoString nCounter)

NanoString is as sensitive as qRT-PCR, without the need for reverse transcription or amplification, and is a relatively high-throughput method for analyzing multiple genes from a single RNA sample (Greiss et al., 2008). Our lab routinely uses NanoString to characterize microglial gene expression patterns of over 50 genes related to microglial activation (i.e., various pro- and anti-inflammatory mediators, receptors and signaling molecules) as well as putative activation markers, immunomodulators, nicotinamide adenine dinucleotide phosphate-oxidase (NOX) enzymes, purinergic and phagocytic receptors, and several potassium (K^+) channels (Ferreira et al., 2014; Siddiqui et al., 2014, Siddiqui et al., 2016). Extracted RNA (200 ng per sample) was sent to the Princess Margaret Genomics Centre (https://www.pmgenomics.ca/pmgenomics/;

Toronto, Canada), where the sample purity was assessed (using Nanodrop 1000), and a NanoString gene expression assay (i.e., hybridization, detection, scanning) was conducted for each species (Fig. 2.1). Code sets were designed and synthesized by NanoString nCounter technologies and include species-specific probes [Tables 2.1 and 2.2] for each mRNA of interest. Transcripts of interest in the 200 ng RNA sample (unstimulated or stimulated) were each recognized by a probe set consisting of a capture and a reporter probe, both of which contain 30-50 bases in length complementary to the target mRNA. The code sets also included negative and positive control reporter probes to minimize variability in the system unrelated to the samples. The negative and positive control reporter probes were developed by External RNA Control Consortium (ERCC) to detect foreign sequences that are not homologous to any organism. The 8 negative control reporter probes are not expected to detect the foreign transcripts in the samples and were used for background subtraction. The 6 positive control reporter probes recognize *in vitro* transcript for ERCC- mRNA targets that were pre-mixed with the code set, each at a different known concentration (0.125-128 fM), a range corresponding to the expression levels of most mRNA of interest.

Since the assays were run at different times, analysis of each species was conducted separately, and by Dr. Starlee Lively. Using nSolver Analysis Software (ver3.0), background levels were determined by calculating the geometric mean of the negative reporter probes for each sample (unstimulated or stimulated), which were then subtracted from the raw counts. If resulting mRNA counts were negative, they were adjusted to 1 by the software. Then, to control for the overall efficiency of probe hybridization and to identify the detection range of counting of experimental transcripts in each assay, a positive control scaling factor was determined. That is, the geometric

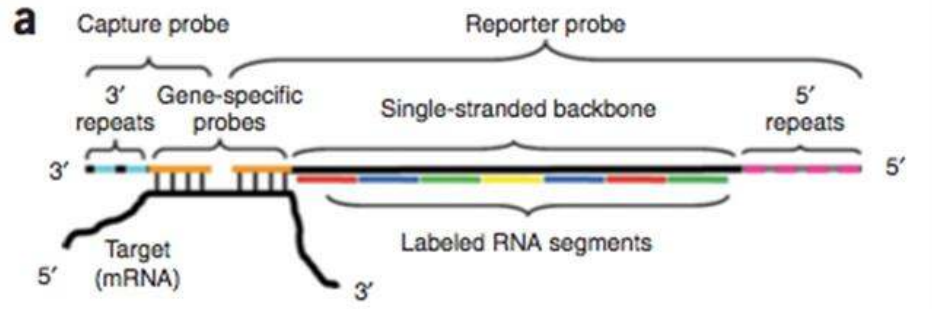
a
Capture probe
Reporter probe
3′ repeats
Gene-specific probes
Single-stranded backbone
5′ repeats
3′
5′
Target (mRNA)
5′
3′
Labeled RNA segments

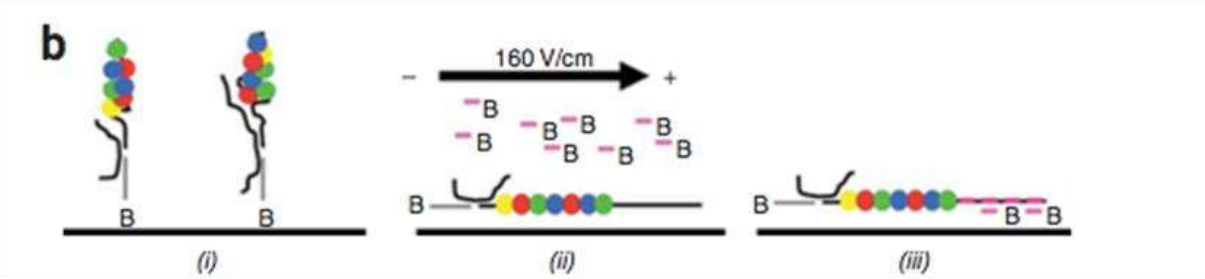
b
160 V/cm
–
+
B
(i)
(ii)
(iii)

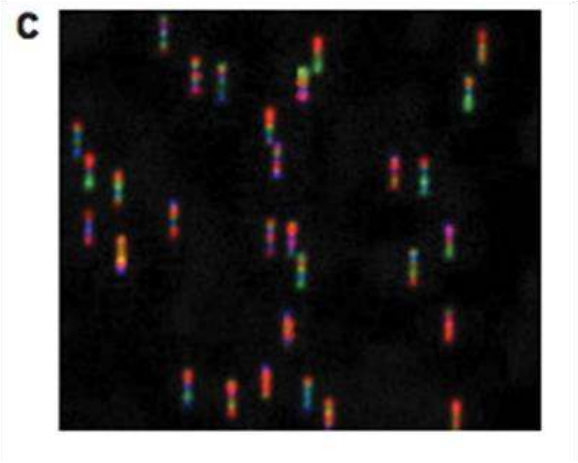
c

Figure 2.1. Overview of NanoString nCounter system for multiplexed gene expression analysis. A. A schematic representation of the hybridized complex (not to scale). The capture probe and reporter probe hybridize to a complementary target mRNA in solution via the gene-specific sequences (see Methods for details on capture and reporter probe construction). After hybridization, the tripartite molecule is affinity-purified first by the 3′ -repeat sequence and then by the 5′-repeat sequence to remove excess reporter and capture probes, respectively. **B.** Schematic representation of binding, electrophoresis, and immobilization. (i) The purified complexes are attached to a streptavidin-coated slide via biotinylated capture probes. (ii) Voltage is applied to elongate and align the molecules. Biotinylated anti-5′ oligonucleotides that hybridize to the 5′-repeat sequence are added. (iii) The stretched reporters are immobilized by the binding of the anti-5′ oligonucleotides to the slide surface via the biotin. Voltage is turned off and the immobilized reporters are prepared for imaging and counting. **C.** False-color image of immobilized reporter probes. [Figure and figure legend from Geiss et al., 2008. Reprinted by permission from Macmillan Publishers Ltd: NATURE BIOTECHNOLOGY, 2008]

mean was calculated for the counts obtained from one positive control probe in each sample (unstimulated and stimulated), and averaged across all samples. This averaged geometric mean was divided by the geometric mean of a given unstimulated or stimulated sample to obtain a sample-specific positive control scaling factor. nSolver considers scaling factors outside a range of 0.3–3 as an indication of suboptimal hybridization, but in both assays, positive control scaling factors for all samples fell within the optimal range. The sample-specific positive control scaling factor was then applied to all counts in the sample. Lastly, counts for each sample (unstimulated and stimulated) were adjusted by a reference gene scaling factor calculated in the same manner as the positive control scaling factor, except two housekeeping genes (*Hprt1* and *Gusb*) were used in lieu of the positive control probes. These scaled counts represent the relative mRNA counts of experimental transcripts in a sample and were used for graphical data (mean ± SEM) to highlight magnitude differences in mRNA levels observed among genes for each species.

Table 2.1. Rat target sequences used to create Custom CodeSet for nCounter Assay

Gene	Accession #	Target sequence
Aif1 (Iba1)	NM_017196.2	ATCGATATTATGTCCTTGAAGCGAATGCTGGAGAAACTTGGGGT TCCCAAGACCCATCTAGAGCTGAAGAAATTAATTAGAGAGGTGT CCAGTGGCTCCG
Arg1	NM_017134.2	ACGGGAAGGTAATCATAAGCCAGAGACTGACTACCTTAAACCA CCGAAATAAATGTGAATACATCGCATAAAAGTCATCTGGGGCAT CACAGCAAACCGA
Casp1 (ICE)	NM_012762.2	AGATTCTAAGGGAGGACATCCTTTCTCCTCAGAAACAAAAGAAA AACTGAACAAAGAAGGTGGCGCATTTCCTGGACCGAGTGGTTC CCTCAAGTTTTGC
Ccl22	NM_057203.1	TACATCCGTCACCCTCTGCCACCACGTTTCGTGAAGGAGTTCTA CTGGACCTCAAAGTCCTGCCGCAAGCCTGGCGTCGTTTTGATA ACCATCAAGAACC
Cd163	NM_001107887.1	CCTCTGTAATTTGCTCAGGAAACCAATCGCATACACTGTTGCCA TGTAGTTCATCATCTTCGGTCCAAACAACAAGTTCTACCATTGC AAAGGACAGTGA
Cd68 (ED1)	NM_001031638.1	CTCTCATTCCCTTACGGACAGCTTACCTTTGGATTCAAACAGGA CCGACATCAGAGCCACAGTACAGTCTACCTTAACTACATGGCA GTGGAATACAATG
Cx3cr1	NM_133534.1	ATGTGCAAGCTCACGACTGCTTTCTTCTTCATTGGCTTCTTTGG GGGCATATTCTTCATCACCGTCATCAGCATCGACCGGTACCTC GCCATCGTCCTGG
Cybb (Nox2)	NM_023965.1	CAGTACCAAAGTTTGCCGGAAACCCTCCTATGACTTGGAAATG GATCGTGGGTCCCATGTTCCTGTATCTGTGTGAGAGGCTGGTG CGGTTTTGGCGATC
Fcgr1a	NM_001100836.1	TGATGGATCATACTGGTGCGAGGTAGCCACGGAGGACGGCCG TGTCCTTAAGCGCAGCACCAAGTTGGAGCTATTTGGTCCCCAG TCATCAGATCCTGTC
Fcgr2b	NM_175756.1	CTGGTCCAAGGAATGCTGTAGATATGAAAGAAAACATCTAGAGT CCCTTCTGTGAGTCCTGAAACCAACAGACACTACGATATTGGTT CCCAATGGTTGA
Fcgr3a	NM_207603.1	GACTCTTGTTTGCAATAGACACAGTGCTGTATTTCTCGGTGCAG AGGAGTCTTCAAAGTTCCGTGGCAGTCTATGAGGAACCCAAAC TTCACTGGAGCAA
Gusb	NM_017015.2	TCATTTGATCCTGGATGAGAAACGAAAAGAATATGTCATCGGAG AGCTCATCTGGAATTTTGCTGACTTCATGACGAACCAGTCACCA CTGAGAGTAACA
Hprt1	NM_012583.2	AGCTTCCTCCTCAGACCGCTTTTCCCGCGAGCCGACCGGTTCT GTCATGTCGACCCTCAGTCCCAGCGTCGTGATTAGTGATGATG AACCAGGTTATGAC
Ifng	NM_138880.2	AAGGACGGTAACACGAAAATACTTGAGAGCCAGATTATCTCTTT CTACCTCAGACTCTTTGAAGTCTTGAAAGACAACCAGGCCATCA GCAACAACATAA
Ifngr1	NM_053783.1	CCTGTTACACATTCGACTACACTGTGTTTGTGAAACATTACAGG AGTGGGGAGATCCTACATACAGAACATAGCGTCCTAAAAGAAG ATTGTAGCGAAAC
Ifngr2	NM_001108313.1	TTTCTTAAGTTACACTTAGTAAAGCAGATGAGTCCGCAGGAGAC TTCAGCAAGAAAGAAGTTCCTACCGTCTCATCCCTTAGTTCTTC AAAGCCAAAGGA
Il10	NM_012854.2	ACAACATACTGCTGACAGATTCCTTACTGCAGGACTTTAAGGGT TACTTGGGTTGCCAAGCCTTGTCAGAAATGATCAAGTTTTACCT GGTAGAAGTGAT

Il10ra	NM_057193.2	TGTTTACATGTCACGACGGAGCATTATTTCACCGTGACCAACCT CAGCATTTTCTTCTTATCCATCCTGATACTCTGTGGAGCCCTGG TCTGCCTGGTTC
Il10rb	NM_001107111.1	CCTCCCTGGATCGTGGCCATCATCCTTATAGCCTCCGTCTTGAT AGTCTTCCTCTTCCTACTGGGCTGCTTCAGCATGGTGTGGTTCA TTTACAAGAAGA
Il13ra1	NM_145789.2	TAACGAATTTGAGTGTCTCTGTCGAAAATCTCTGCACAATAGTG TGGACATGGAGTCCTCCTGAGGGAGCCAGTCCAAATTGCAGTC TCAGATATTTTAG
Il1b	NM_031512.1	TGCACTGCAGGCTTCGAGATGAACAACAAAAATGCCTCGTGCT GTCTGACCCATGTGAGCTGAAAGCTCTCCACCTCAATGGACAG AACATAAGCCAACA
Il1r1	NM_013123.3	CTCATATTCTGGAGACTGCACACGTACGGTTAGTATACCCAGTT CCTGACTTCAAGAATTACCTCATCGGGGGCTTTGCCATCTTCAC AGCTACAGCCGT
Il1rn	NM_022194.2	TCATTGCTGGGTACTTACAAGGACCAAATACCAAACTAGAAGAA AAGATAGACATGGTGCCTATTGACTTTCGGAATGTGTTCTTGGG CATCCACGGGGG
Il4	NM_201270.1	TGCTGTCACCCTGTTCTGCTTTCTCATATGTACCGGGAACGGTA TCCACGGATGTAACGACAGCCCTCTGAGAGAGATCATCAACAC TTTGAACCAGGTC
IL4r	NM_133380.2	GGGTGTCAGCATCTCCTGCATCTGCATCCTATTGTTTTGCCTGA CCTGTTACTTCAGCATTATCAAGATTAAGAAGATATGGTGGGAC CAGATTCCCACT
Il6	NM_012589.1	GGAACAGCTATGAAGTTTCTCTCCGCAAGAGACTTCCAGCCAG TTGCCTTCTTGGGACTGATGTTGTTGACAGCCACTGCCTTCCCT ACTTCACAAGTCC
Itgam (Cd11b)	NM_012711.1	CATCCCTTCCTTCAACAGTAAAGAAATATTCAACGTCACCCTCC AGGGCAATCTGCTATTTGACTGGTACATCGAGACTTCTCATGAC CACCTCCTGCTT
Kcna2 (Kv1.2)	NM_012970.3	GCCGGCCAGGATCATAGCCATTGTATCTGTGATGGTCATTCTG ATCTCGATCGTCAGCTTCTGTCTGGAAACCTTGCCCATCTTCCG GGATGAGAACGAG
Kcna3 (Kv1.3)	NM_019270.3	GCCACCTTCTCCAGAAATATCATGAACCTGATAGACATTGTAGC CATCATCCCTTATTTTATTACTCTGGGCACTGAGCTGGCTGAGC GACAGGGTAATG
Kcna5 (Kv1.5)	NM_012972.1	ATCAGAAGGGGTAGCTGTCCTCTAGAAAAGTGTCACCTCAAGG CCAAGAGCAACGTGGACTTGCGGAGGTCCCTGTATGCCCTCTG TCTGGACACTAGCC
Kcnj2 (Kir2.1)	NM_017296.1	GTTCTTTGGCTGTGTGTTTTGGTTGATAGCTCTGCTCCACGGGG ATCTGGATGCTTCTAAAGAGAGCAAAGCGTGTGTGTCTGAGGT CAACAGCTTCACG
Mrc1	NM_001106123.1	CTTTGGAATCAAGGGCACAGAGCTATATTTTAACTATGGCAACA GGCAAGAAAAGAATATCAAGCTTTACAAAGGTTCCGGTTTGTGG AGCAGATGGAAG
Msr1 (SR-A)	NM_001191939.1	CACGTTCCATGACAGCATCCCTTCCTCACAACACTATAAATGGC TCCTCCGTTCAGGAGAAACTGAAGTCCTTCAAAGTTGCCCTCGT CGCTCTCTACCT
Myc	NM_012603.2	ACCGAGGAAAACGACAAGAGGCGGACACACAACGTCTTGGAAC GTCAGAGGAGAAACGAGCTGAAGCGTAGCTTTTTTGCCCTGCG CGACCAGATCCCTG
Ncf1	NM_053734.2	TCCATTCCCAGCATCCCATAATTGGGCTTGTCCGTGTTCCAACA TCTGGGCGGAATTTCACAGCCAAAGGTCAAGAGGACTGCTGTT ACGTTCAAGGTCG
Nfkbia (IκBα)	NM_001105720.2	TATTGTGCTTTTGGTTGAACCGCCATAGACTGTAGCTGACCCCA GTGTGCCCTCTCACGTAAGAACCAGGTGTTCAGTGGTATGTGC TTAAGTCATCCCC

Nos2	NM_012611.2	ACGGGACACAGTGTCGCTGGTTTGAAACTTCTCAGCCACCTTG GTGAGGGGACTGGACTTTTAGAGACGCTTCTGAGGTTCCTCAG GCTTGGGTCTTGTT
Nox1	NM_053683.1	CCGAGAAAGAAGATTCTTGGCTAAATCCCATCCAGTCTCCAAAC GTGACAGTGATGTATGCAGCATTTACCAGTATTGCTGGCCTTAC TGGAGTGGTCGC
Nox4	NM_053524.1	TGTTGGACAAAAGCAAGACTCTACATATCACCTGTGGCATAACT ATTTGTATTTTCTCAGGTGTGCATGTAGCTGCCCACTTGGTGAA CGCCCTGAACTT
Nr3c1	NM_012576.2	AGCTTTCCTTGAAGCGTATAAAGAGCCATGCTCCTTTAGTATGT GGGGAAGAAGAGAGCTGTCATAGTTTTGAGTACAGTGAGAAGA TGCGGTACTGTCT
P2rx7	NM_019256.1	ACTTTAAGAGGTCACATTAACCAGACTAGAAGCCATCGCATCTA ACCGCATACCAGACACAGTCTGACGCCTCATTGCTATGCTATG GTTCTAAGTGACT
P2ry12	NM_022800.1	TGATAACCATTGACCGATACCTGAAGACCACCAGACCATTTAAA ACTTCCAGCCCCAGCAATCTTTTGGGTGCGAAGATTCTTTCTGT TGCCATCTGGGC
P2ry2	NM_017255.1	GAGCTCTTTAGCCATTTTGTGGCTTACAGCTCTGTCATGCTGGG TCTGCTTTTTGCTGTGCCCTTTTCCATCATCCTGGTCTGTTACGT GCTCATGGCCC
Pparg	NM_013124.1	TTTATAGCTGTCATTATTCTCAGTGGAGACCGCCCAGGCTTGCT GAACGTGAAGCCCATCGAGGACATCCAAGACAACCTGCTGCAG GCCCTGGAACTCC
Ptgs2 (Cox-2)	NM_017232.3	TTCGGAGGAGAAGTGGGTTTTAGGATCATCAACACTGCCTCAAT TCAGTCTCTCATCTGCAATAATGTGAAAGGGTGTCCCTTTGCCT CTTTCAATGTGC
Ptk2b (Pyk2)	NM_017318.2	GCAGTGATCATGAAGAATCTTGACCACCCTCACATCGTCAAGCT GATTGGCATCATTGAAGAGGAACCCACATGGATCGTCATGGAA CTGTATCCTTATG
Ptpn6 (SHP-1)	NM_053908.1	GCAGAGTCACTGCTGCAGGCCAAGGGCGAGCCCTGGACATTT CTTGTGCGTGAGAGTCTCAGCCAACCTGGTGATTTTGTGCTCTC TGTGCTCAATGACC
Retnla (FIZZ1)	NM_053333.1	AGGAACTTCTAGCCCATCAAGATAACTATCCCTCTGCTGTAAGG AAGACCCTCTCATGCACTAATGTCAAGTCTATGAGCAAATGGGC CTCCTGCCCTGC
Socs1	NM_145879.1	CGGCCGCTGCAGGAGCTGTGTCGCCAGCGCATCGTGGCCGCC GTGGGTCGCGAGAACCTGGCACGCATCCCTCTTAACCCGGTAC TCCGTGACTACCTGA
Socs3	NM_053565.1	GGAAGACTGTCAACGGTCACCTGGACTCCTATGAGAAAGTGAC CCAGCTGCCTGGACCCATTCGGGAGTTCCTGGACCAGTATGAT GCTCCACTTTAAAG
Tgfb1	NM_021578.2	CGCCTGCAGAGATTCAAGTCAACTGTGGAGCAACACGTAGAAC TCTACCAGAAATATAGCAACAATTCCTGGCGTTACCTTGGTAAC CGGCTGCTGACCC
Tgfbr1	NM_012775.2	GTCTGCATTGCACTTATGCTGATGGTCTATATCTGCCATAACCG CACTGTCATTCACCACCGCGTACCAAATGAAGAGGATCCCTCA CTAGATCGCCCTT
Tgfbr2	NM_031132.3	CCAGCAGTCCTGACCTGTTGCTGGTCATTATCCAAGTGACGGG CGTCAGCCTCCTGCCTCCGCTGGGGATTGCCATAGCTGTCATT GCCATCTTCTACTG
Tlr2	NM_198769.2	TTTACAAACCCTTAGGGTAGGAAATGTTGACACTTTCAGTGAGA TAAGGAGAATAGATTTTGCTGGGCTGACCTCTCTCAACGAACTT GAAATTCAGGTA
Tlr4	NM_019178.1	GTCAGTGTGCTTGTGGTAGCCACTGTAGCATTTCTGATATACCA CTTCTATTTTCACCTGATACTTATTGCTGGCTGTAAAAAGTACAG CAGAGGAGAAA

Tnf	NM_012675.2	GGTGATCGGTCCCAACAAGGAGGAGAAGTTCCCAAATGGGCTC CCTCTCATCAGTTCCATGGCCCAGACCCTCACACTCAGATCATC TTCTCAAAACTCG
Tnfrsf1a	NM_013091.1	TATTCTTTATCTGCATCAGTCTACTGTGCCGATATCCCCAGTGG AGGCCCAGGGTCTACTCCATCATTTGTAGGGATTCAGCTCCTG TCAAAGAGGTGGA
Tnfrsf1b	NM_130426.4	AGGAGTTCAGATTCTTCCCATGGCAGCCACGGGACCCATGTCA ACGTCACCTGCATCGTGAACGTCTGTAGCAGCTCTGACCACAG CTCTCAGTGTTCTT
Trem2	NM_001106884.1	TCCGGCTGGCTGAGGAAGGGTGCCATGGAACCTCTCCACGTG TTTGTCCTGTTGCTGGTCACAGAGCTGTCCCAAGCCCTCAACA CCACAGTGCTGCAGG
Tspo	NM_012515.1	GCTGCCCGCTTGCTGTATCCTTACCTGGCCTGGCTGGCCTTTG CCACCATGCTCAACTACTATGTATGGCGTGATAACTCTGGTCGG CGAGGGGGCTCCC

Table 2.2. Mouse target sequences used to create Custom CodeSet for nCounter Assay

Gene	Accession #	Target sequence
Aif1 (Iba1)	NM_019467.2	CTGGAGCAGCCTGCAGACTTCATCCTCTCTCTTCCATCCCGGG GAAAGTCAGCCAGTCCTCCTCAGCTGCCTGTCTTAACCTGCAT CATGAAGCCTGAGG
Arg1	NM_007482.3	GTACATTGGCTTGCGAGACGTAGACCCTGGGGAACACTATATA ATAAAAACTCTGGGAATTAAGTATTTCTCCATGACTGAAGTAGA CAAGCTGGGGATT
Casp1 (ICE)	NM_009807.2	GACAATAAATGGATTGTTGGATGAACTTTTAGAGAAGAGAGTGC TGAATCAGGAAGAAATGGATAAAATAAAACTTGCAAACATTACT GCTATGGACAAG
Ccl22	NM_009137.2	CCAAGAATCAACTTCCACCCCTCTTCAACCACATGCTAGGGTCT TTTACTTTCTCTGCCCCACACCTTTGACTCCTTGCCTGTGTAGC TGATAGTCGAAG
Cd163	NM_053094.2	TCACGGCACTCTTGGTTTGTGGAGCCATTCTATTGGTCCTCCTC ATTGTCTTCCTCCTGTGGACTCTGAAGCGACGACAGATTCAGC GACTTACAGTTTC
Cd68 (ED1)	NM_009853.1	GCTCCCTGTGTGTCTGATCTTGCTAGGACCGCTTATAGCCCAA GGAACAGAGGAAGACTGTCCTCACAAAAAGGCCGTTACTCTCC TGCCATCCTTCACG
Cx3cr1	NM_009987.3	TATGCTTTGGTGTTGGTCTGTATTTCCCGCTGTCTCGGGTCACA TGGTTAAGCGTGCCTAGAGTGTGTCTATCCCACTTGTAATTCTG TCAATAAACATT
Cybb (Nox2)	NM_007807.2	ACAGAAGACTCTGTATGGACGGCCCAACTGGGATAACGAGTTC AAGACCATTGCAAGTGAACACCCTAACACCACAATAGGCGTTTT CCTGTGTGGCCCT
Fcgr1	NM_010186.5	GAGACAGTTCCACACAATGGTTTATCAACGGAACAGCCGTTCA GATCTCCACGCCTAGTTATAGCATCCCAGAGGCCAGTTTTCAG GACAGTGGCGAATA
Fcgr2b	NM_001077189.1	TTGGTTCCCAATGGTTGACTGTACTAATGACTCCCATAACTTAC AGCTTCCCAACTCAAGACTCTTCTGCTATCGATCCACACTGCCA CTAAAATTAATC
Fcgr3	NM_010188.5	TCTGACCTCCACCATCCACCATGGCAGGTGCACACAATAAATTA AAATGTCATGTATATTTTTAAACAAGAGACAGGGGCAGGCTAAG GGTTGATGGCAT
Gusb	NM_010368.1	AATACGTGGTCGGAGAGCTCATCTGGAATTTCGCCGACTTCAT GACGAACCAGTCACCGCTGAGAGTAATCGGAAACAAGAAGGG GATCTTCACTCGCCA
Hprt	NM_013556.2	TGCTGAGGCGGCGAGGGAGAGCGTTGGGCTTACCTCACTGCT TTCCGGAGCGGTAGCACCTCCTCCGCCGGCTTCCTCCTCAGAC CGCTTTTTGCCGCGA
Ifng	NM_008337.1	CTAGCTCTGAGACAATGAACGCTACACACTGCATCTTGGCTTTG CAGCTCTTCCTCATGGCTGTTTCTGGCTGTTACTGCCACGGCA CAGTCATTGAAAG
Ifngr1	NM_010511.2	AAGCATAATGTTACCTAAGTCCTTGCTCTCTGTGGTAAAAAGTG CCACGTTAGAGACAAAACCTGAATCGAAGTATTCACTTGTCACA CCGCACCAGCCA
Ifngr2	NM_008338.3	CATCCTGATTCCGTTGGGCATCTTCGCATTGCTGCTCGGCCTG ACGGGCGCCTGCTTCACCCTGTTCCTCAAATACCAAAGCCGAG TGAAGTACTGGTTT
Il10	NM_010548.1	GGGCCCTTTGCTATGGTGTCCTTTCAATTGCTCTCATCCCTGAG TTCAGAGCTCCTAAGAGAGTTGTGAAGAAACTCATGGGTCTTG GGAAGAGAAACCA

Il10ra	NM_008348.2	TGTTGTCGCGTTTGCTCCCATTCCTCGTCACGATCTCCAGCCTG AGCCTAGAATTCATTGCATACGGGACAGAACTGCCAAGCCCTT CCTATGTGTGGTT
Il10rb	NM_008349.5	CTTTACACCTGCGTTTCTCAGCCCCACAAATTGAGAATGAGCCT GAGACGTGGACCTTGAAGAACATTTATGACTCATGGGCTTACA GAGTGCAATACTG
Il13ra1	NM_133990.4	CTCAAACCGACCGACATAATATTTTAGAGGTTGAAGAGGACAAA TGCCAGAATTCCGAATCTGATAGAAACATGGAGGGTACAAGTT GTTTCCAACTCCC
Il1b	NM_008361.3	GTTGATTCAAGGGGACATTAGGCAGCACTCTCTAGAACAGAAC CTAGCTGTCAACGTGTGGGGGATGAATTGGTCATAGCCCGCAC TGAGGTCTTTCATT
Il1r1	NM_001123382.1	CTTCTTCGGAGTAAAAGATAAACTGTTGGTGAGGAATGTGGCTG AAGAGCACAGAGGGGACTATATATGCCGTATGTCCTATACGTTC CGGGGGAAGCAA
Il1rn	NM_031167.5	CAACCAGCTCATTGCTGGGTACTTACAAGGACCAAATATCAAAC TAGAAGAAAAGATAGACATGGTGCCTATTGACCTTCATAGTGTG TTCTTGGGCATC
Il4	NM_021283.1	TGCTTGAAGAAGAACTCTAGTGTTCTCATGGAGCTGCAGAGACT CTTTCGGGCTTTTCGATGCCTGGATTCATCGATAAGCTGCACCA TGAATGAGTCCA
IL4ra	NM_001008700.3	CCCACAGCAGTGCTGACGTTCCTAAGTCCTGGGCTTTCCTAGC TGATGTTGTCCTACCTACTCAGTCCCATTTTGTCCACCGAATAG ACCTGTCACTCAA
Il6	NM_031168.1	CTCTCTGCAAGAGACTTCCATCCAGTTGCCTTCTTGGGACTGAT GCTGGTGACAACCACGGCCTTCCCTACTTCACAAGTCCGGAGA GGAGACTTCACAG
Itgam (Cd11b)	NM_001082960.1	ATCCCTGTTCAGATCAACAATGTGACCGTATGGGATCATCCCCA GGTCATCTTCTCCCAGAACCTCTCAAGTGCCTGTCACACTGAG CAGAAATCCCCCC
Kcna2 (Kv1.2)	NM_008417.4	GTTAACTGATGTCTGATTGAAGCCTACTAATGTACTCACAGCTC AACAGGACTGATGCAGATGTTGCATAATAGCCTGCATTGTAGTC AGTGTTCTACAG
Kcna3 (Kv1.3)	NM_008418.2	CTGTTGGTTATGGTGATATGCACCCAGTGACCATAGGAGGCAA GATTGTGGGCTCTCTTTGTGCCATCGCAGGTGTCTTGACCATTG CATTGCCAGTTCC
Kcna5 (Kv1.5)	NM_145983.2	AAAAAGTATCGCATTCCATGACGCAGGAGCCGTTGAAGTGGTG AGCATTCACTGTAAGATGGATGTATTCATAGCCAGTTTTCTATAC CCAGCAGAGGGA
Kcnj2 (Kir2.1)	NM_008425.4	CTTAAGGCGAGAATCGGAGATATGACTGGCTGATTCCGTCTTT GGAATACTTACTTTGCTACACAGCCTGACGTTGGTCAGAGGTC CGAGACAGTTATAC
Mrc1	NM_008625.1	GTTCCGAAATGTTGAAGGGAAGTGGCTTTGGTTGAACGACAAT CCTGTCTCCTTTGTCAACTGGAAAACAGGCGATCCCTCTGGTG AACGGAATGATTGT
Msr1 (SR-A)	NM_001113326.1	GATTTCGTCAGTCCAGGAACATGGGAATTCACTGGATGCAATCT CCAAGTCCTTGCAGAGTCTGAATATGACACTGCTTGATGTTCAA CTCCATACAGAA
Myc	NM_010849.4	CCCTCAACGTGAACTTCACCAACAGGAACTATGACCTCGACTAC GACTCCGTACAGCCCTATTTCATCTGCGACGAGGAAGAGAATTT CTATCACCAGCA
Ncf1	NM_001286037.1	ACCATCCGCAACGCACAGAGCATCCACCAGCGTTCTCGGAAGC GCCTTAGCCAGGACACCTATCGCCGCAACAGCGTCCGATTCCT GCAGCAGCGCAGAC
Nfkbia (IκBα)	NM_010907.1	GTCAGAATTCACAGAGGATGAGCTGCCCTATGATGACTGTGTG TTTGGAGGCCAGCGTCTGACATTATAAGTGGAAAGTGGCAAAA AAGAATGTGGACTT

Nos2 (iNOS)	NM_010927.3	CCCCCCTCCTCCACCCTACCAAGTAGTATTGTACTATTGTGGAC TACTAAATCTCTCTCCTCTCCTCCCTCCCCTCTCTCCCTTTCCTC CCTTCTTCTCC
Nox1	NM_172203.1	CTCCAAACATGACAGTGATGTATGCAGCATTTACCAGTATTGCT GGCCTTACTGGAGTGATTGCCACTGTAGCTTTGGTTCTCATGGT AACGTCAGCTAT
Nox4	NM_015760.4	TCCCAGAAAGCTTCTCTTCACAACCATTCCTGGTCTGACGGGTG TCTGCATGGTGGTGGTATTGTTCCTCATGGTTACAGCTTCTACC TACGCAATAAGA
Nr3c1	NM_008173.3	ACCAGGATTCAGAAACTTACACCTGGATGACCAAATGACCCTTC TACAGTACTCATGGATGTTTCTCATGGCATTTGCCCTGGGTTGG AGATCATACAGA
P2rx7	NM_001038887.1	CTGGAGGAACTGGAAGTTAACCGTTCCTGCTGAGAAATCGGTG TGTTTCCTTTGGCTGCTCCTAGGTGAGGGTTTGCTGTGGTCTAG CCTGGGAAGTAGG
P2ry12	NM_027571.3	GATCACCCAGGTTCTCTTCCCATTGCTGTACACCGTCCTGTTCT TTGCTGGGCTCATCACGAACAGCTTGGCAATGAGGATTTTCTTT CAGATCCGCAGT
P2ry2	NM_008773.3	TAGCCATTTTGTGGCTTACAGCTCCGTCATGCTGGGTCTGCTTT TTGCTGTGCCCTTTTCCGTAATCCTGGTCTGTTACGTGCTTATG GCCAGGCGGCTG
Pparg	NM_011146.1	ACCAAGTGACTCTGCTCAAGTATGGTGTCCATGAGATCATCTAC ACGATGCTGGCCTCCCTGATGAATAAAGATGGAGTCCTCATCT CAGAGGGCCAAGG
Ptgs2 (Cox-2)	NM_011198.3	CCATCAGTTTTTCAAGACAGATCATAAGCGAGGACCTGGGTTCA CCCGAGGACTGGGCCATGGAGTGGACTTAAATCACATTTATGG TGAAACTCTGGAC
Ptk2b (PYK2)	NM_001162365.1	CTTCCGCCGCTTCACAACCGCCAGTGATGTCTGGATGTTTGCT GTATGCATGTGGGAGATCCTCAGCTTTGGGAAGCAGCCTTTCT TCTGGCTCGAAAAT
Ptpn6 (SHP-1)	NM_013545.2	GACCGAGGCCCAGTACAAGTTTATTTACGTGGCCATTGCCCAG TTCATCGAAACGACCAAGAAGAAACTGGAGATCATACAATCCCA GAAGGGCCAGGAG
Retnla (FIZZ1)	NM_020509.3	GAATACTGATGAGACCATAGAGATTATCGTGGAGAATAAGGTCA AGGAACTTCTTGCCAATCCAGCTAACTATCCCTCCACTGTAACG AAGACTCTCTCT
Socs1	NM_009896.2	CAGCTTGTGTCTGGGGCCAGGACCTGAATTCCACTCCTACCTC TCCATGTTTACATATTCCCAGTATCTTTGCACAAACCAGGGGTC GGGGAGGGTCTCT
Socs3	NM_007707.2	CCGCGACAGCTCGGACCAGCGCCACTTCTTCACGTTGAGCGTC AAGACCCAGTCGGGGACCAAGAACCTACGCATCCAGTGTGAG GGGGGCAGCTTTTCG
Tgfb1	NM_011577.1	GGAGTTGTACGGCAGTGGCTGAACCAAGGAGACGGAATACAG GGCTTTCGATTCAGCGCTCACTGCTCTTGTGACAGCAAAGATAA CAAACTCCACGTGG
Tgfbr1	NM_009370.2	TCAGAAGTAGTGGCCAGCTGTGTCTCTAGTAGGACAGTAAAGG CATGAAGCTCAGCCTGTAATCCTGCTACTACAGTAGTACTCCAG AAGTGCCTTGAGG
Tgfbr2	NM_009371.2	TGTGCAAGTTTTGCGATGTGAGACTGTCCACTTGCGACAACCA GAAGTCCTGCATGAGCAACTGCAGCATCACGGCCATCTGTGAG AAGCCGCATGAAGT
Tlr2	NM_011905.2	GCAGGCGGTCACTGGCAGGAGATGTGTCCGCAATCATAGTTTC TGATGGTGAAGGTTGGACGGCAGTCTCTGCGACCTAGAAGTGG AAAAGATGTCGTTC
Tlr4	NM_021297.2	AACGGCAACTTGGACCTGAGGAGAACAAAACTCTGGGGCCTAA ACCCAGTCTGTTTGCAATTAATAAATGCTACAGCTCACCTGGGG CTCTGCTATGGAC

Tnf	NM_013693.1	TTCCTGAGTTCTGCAAAGGGAGAGTGGTCAGGTTGCCTCTGTC TCAGAATGAGGCTGGATAAGATCTCAGGCCTTCCTACCTTCAGA CCTTTCCAGACTC
Tnfrsf1a	NM_011609.2	CTCCTTGCCAAGCTGACAAGGACACGGTGTGTGGCTGTAAGGA GAACCAGTTCCAACGCTACCTGAGTGAGACACACTTCCAGTGC GTGGACTGCAGCCC
Tnfrsf1b	NM_011610.3	GTGTGTGTCCATGTTTGCATGTATGTGTGTGCCAGTGTGTGGA GGCCAGAGGTTGGCTTTGGGTGTGTTTGATCACTCTCAGTTACT GAGGCAGGGCTCT
Trem2	NM_031254.2	GGGCGCCTACCCTAGTCCTGACTGTTGCTCAATCCAGGAGCAC AGTTCCTGTGGGCTGAGCCTGACTGGCTTGGTCATCTCTTTTCT GCACTTCAAGGGA
Tspo	NM_009775.4	GACACTGGCTCCCATCTGGGGCACACTGTATTCAGCCATGGGG TATGGCTCCTACATAGTCTGGAAAGAGCTGGGAGGTTTCACAG AGGACGCTATGGTT

2.4 Microglia staining

Microglia were seeded at 7–9 $\times 10^4$ cells/coverslip, and stimulated with cytokines for 24 h. They were briefly washed in phosphate-buffered saline (PBS), and fixed in 4% paraformaldehyde (Electron Microscopy Sciences, Hatfield, PA) at room temperature for 15 min. After permeabilizing the cells with 0.2% Triton X-100 for 5 min, they were washed in PBS (3×, 5 min), and labeled with Alexa Fluor 488-conjugated phalloidin (1:50 in PBS for 1 h; Invitrogen) to visualize filamentous (F) actin, and with 4′,6-diamidino-2-phenylindole (DAPI; 1:3000 in PBS for 10 min; Invitrogen) to label nuclei. After washing (3×, 5 min), coverslips were mounted on glass slides using Dako mounting medium (Dako, Glostrup, Denmark) and stored in the dark at 4°C. Five random fields were imaged at 20× or 40× magnification using the deconvolution microscope (DECON; Carl Zeiss, Jena, Germany).

2.5 Proliferation assay

CyQuant NF assay (Invitrogen) was used to measure cell proliferation, as previously described (Ferreira et al., 2014). Microglia were seeded at 2–3x10^4 cells per well of a 96-well flat-bottom plate and cultured in MEM with 2% FBS for 1–2 days. Then, cells were unstimulated or stimulated with a cytokine in the presence or absence of a channel blocker (Ba^{2+}, ML133 or AgTx-2). After 24 h, the CyQuant dye solution was added to each well, and incubated for 30 min (37°C, 5% CO_2). The fluorescence intensity was measured using a multi-label plate reader (Victor^3 1420, Perkin Elmer, Woodbridge, ON, Canada), with excitation at 485 nm and emission at 535 nM. Readings were taken for 0.1 s at 3 mm from the bottom of the plate in duplicate,

averaged, and background was subtracted before normalizing to the unstimulated (control) group.

2.6 Transwell migration assay

Microglia were seeded at 3×10^4 cells per insert filter (which bore 8 µm-diameter holes), and placed in the upper well of a Transwell migration chamber (VWR, Mississauga, ON, Canada) containing 500 µL MEM with 2% FBS, as recently described (Ferreira et al., 2014; Siddiqui et al., 2014; Lam & Schlichter, 2015). After 30 min, 500 µL of MEM with 2% FBS was added to the lower well, and microglia were left unstimulated (control) or stimulated for 24 h (37°C, 5% CO_2) with I+T, IL-4 or IL-10, as above. When used, a channel blocker (5 nM AgTx-2 or 20 µM ML133) was added at the time of cytokine addition. Transwell inserts were then briefly washed with PBS, fixed for 10 min in 4% paraformaldehyde, and washed again in PBS (3×, 5 min). A Q-tip was used to remove microglia from the top of the Transwell inserts. Cells that had migrated to the underside of the membrane were stained with 0.3 % crystal violet in methanol (~1 min) and washed with PBS. Cells from 5 random fields at 40× magnification were counted using an Olympus CK2 inverted microscope (Olympus, Tokyo), summed and normalized to the unstimulated (CTL) group.

2.7 Single-cell fluorescence imaging

Fura-2AM (Invitrogen) is a ratiometric fluorescent Ca^{2+} indicator that was used to measure changes in intracellular Ca^{2+}. Unstimulated or stimulated microglia ($7–8\times10^4$ cells/coverslip) were incubated (40 min, room temperature) with 3.5 µg/mL Fura-2AM in standard bath solution containing 2 mM $CaCl_2$. The coverslip was mounted in a

perfusion chamber and washed to remove any residual external Fura-2. Individual cells within the field of view were selected using the region of interest tool, which defines the area of the cell to be measured. Fluorescent intensity measurements were acquired at room temperature using a Nikon Diaphot inverted microscope (with a Nikon Fluor 40X objective), Retiga-EX camera (Q-imaging, Burnaby, BC, Canada), DG-4 arc lamp with excitation wavelength changer (Sutter Instruments, Novato, CA), and Northern Eclipse image acquisition software (Empix Imaging, Missisauga, ON, Canada). Cells were exposed to 340 and 380 nm excitation wavelengths every 2-3 s, with the excitation shutter closed between acquisitions to prevent photobleaching. Ratios (340/380) were obtained using a 505 nm dichroic mirror and a 510 nm emission filter. In using this ratiometric Ca^{2+} indicator, uneven dye loading into cells within and between treatment conditions are corrected. For nominally Ca^{2+}-free solution, $CaCl_2$ was omitted. EGTA was not added because we found that it can rapidly deplete Ca^{2+} from immune cells (Schlichter and Sakellaropoulos, 1994).

2.8 Griess (nitric oxide) assay

The colorimetric Griess assay (Invitrogen) was used to measure nitrite levels as an indirect measure of nitric oxide production. Cells were seeded at 7-9x10^4 onto glass coverslips and were either left unstimulated, or stimulated for 24 h with I+T, IL-4 or IL-10, in the presence or absence of a channel blocker (ML133 or AgTx-2). For the Griess reaction, 200 µL of media from microglia samples was added to wells of a 96-well plate containing 25 µL of sulfanilic acid. Then, 25 µL of 0.1% N-(1-naphthyl) ethylenediamine was added, and the media was kept at room temperature in the dark for 30 min to allow the reaction to occur. The colorimetric change in the samples was quantitated using a

multi-label plate counter (Victor^3 1420, Perkin Elmer, Woodbridge, ON) set at an absorbance wavelength of 570 nm. Nitrite concentrations of the samples were interpolated from a standard curve generated from a series of samples of known concentration.

2.9 Reagents

For patch-clamp recordings and functional assays, Ba^{2+} or ML133 were used to block Kir2.1, and agitoxin-2 was used to block Kv1.3 channels. Stock solutions were prepared in DMSO for ML133 (Tocris Bioscience, MO) and in double distilled water for Ba^{2+} and agitoxin-2, to which 0.02% BSA was added (all from Sigma). To examine Ca^{2+} signaling, thapsigargin and BTP2 (both from EMD Millipore Calbiochem, San Diego, CA) were prepared in DMSO. Inhibitor solutions were diluted to a working final concentration of 0.01%, aliquoted and stored at –20°C until used.

2.10 Statistics

All graphical data are presented as mean ± SEM for the number of replicates indicated on each figure. The statistical significance was analyzed using GraphPad ver 6.01 (GraphPad Software, San Diego, CA) or Origin v9.0 (OriginLab, Northampton, MA, USA). Specific statistical tests and post-hoc analyses will be stated within the method section of each chapter. Results were considered significant if $p<0.05$.

3 Expression and contributions of the Kir2.1 inward-rectifier K^+ channel to proliferation, migration, and chemotaxis of rat microglia in unstimulated and anti-inflammatory states

3.1 INTRODUCTION

Members of the Kir2 inward-rectifier K^+ channel family (which includes Kir2.1) are expressed in both excitable and non-excitable cells, where their primary function is to maintain a hyperpolarized membrane potential (Lu 2004; Hibino et al. 2010). Kir2.1 currents have often been reported in cultured rodent microglia (Kettenmann et al. 1993; Eder 2005; Kettenmann et al. 2011) in both unstimulated (often called 'resting') and classical-activated (pro-inflammatory) states (Draheim et al. 1999; Nörenberg et al. 1992 & 1994; Visentin et al. 1995; Schlichter et al. 1996; Chung et al. 1999; Prinz et al. 1999; Franchini et al. 2004; Newell and Schlichter 2005; Moussaud et al. 2009). The current has also been recorded in microglia in brain slices (Brockhaus et al. 1993; Lyons et al. 2000; Boucsein et al. 2000 & 2003; Schilling and Eder 2007 & 2015). After CNS damage, microglia can also enter anti-inflammatory states that help resolve classical activation and promote repair (Hanisch and Kettenmann 2007; Colton 2009; Czeh et al. 2011). However, it is not known if Kir2.1 is expressed in microglia in these states; i.e., following 'alternative' activation (evoked by interleukin-4) or 'acquired deactivation' (evoked by IL-10).

After CNS injury, the population of microglia at damage sites will depend on both proliferation and migration; thus, it is important to compare these functions in pro- and anti-inflammatory states. It is well known that cell proliferation and migration are Ca^{2+}-dependent processes. Our early study showed that when rat microglia were exposed to CSF-1 to increase proliferation; this was reduced by Ba^{2+} (5–10 mM) (Schlichter et al. 1996) but the microglial activation state was not determined. Another study showed that Ba^{2+} block of Kir2.1 reduced ATP-induced Ca^{2+} entry in rat microglia by prolonging membrane depolarization (Franchini et al. 2004). While suggestive of a link between Kir2.1, proliferation and Ca^{2+} signaling, previous studies have not addressed whether the microglial activation state affects Kir2.1 contributions.

We recently found that stimulation of rat microglia with IL-4 or IL-10 increases their migration, ATP-induced chemotaxis and invasion through ECM while classical activation (induced by LPS) reduces these functions (Lively and Schlichter 2013; Ferreira et al. 2014; Siddiqui et al. 2014). Both their migration and chemotaxis depend on Ca^{2+} influx through Ca^{2+}-release activated Ca^{2+} (CRAC/Orai1) channels (Siddiqui et al. 2012; Ferreira and Schlichter 2013), which are highly expressed in unstimulated rat microglia (Ohana et al. 2009; Siddiqui et al. 2012). However, CRAC-mediated Ca^{2+} entry has not been compared for microglia in alternative- or acquired-deactivation states. CRAC is activated by depleting intracellular Ca^{2+} stores and is strongly inward-rectifying at negative membrane potentials (Derler et al. 2012; Shim et al. 2015); thus, Ca^{2+} influx through CRAC is enhanced with hyperpolarization. Kir2.1, like other classical Kir channels, is expected to maintain a negative membrane potential.

Based on these previous results, we hypothesized that Kir2.1 will contribute to CRAC-mediated Ca^{2+} entry in unstimulated, IL-4- and IL-10-stimulated rat microglia,

and this will be reflected by its contributions to proliferation and migration. Real-time qRT-PCR was used to monitor expression of Kir2.1 (encoded by the *Kcnj2* gene) and patch-clamp recordings were used to compare Kir2.1 currents. Fura-2 imaging was used to quantify the contribution of Kir2.1 to CRAC-mediated Ca^{2+} signaling. Then, after demonstrating the utility of the recently developed Kir2-family inhibitor, ML133, we used Ba^{2+} and ML133 to assess Kir2.1 contributions to proliferation, migration and chemotaxis.

3.2 METHODS

Refer to Chapter 2 for the general procedure for each technique listed below, and for RNA extraction, and intracellular Ca^{2+} measurements.

Primary microglial cells. Rat microglia cultures, which were prepared by Dr. Zhu. Microglia were unstimulated or stimulated for 6 or 24 h with 20 ng/mL of rat recombinant IL-4 or 20 ng/mL or rat recombinant IL- 10.

Whole-cell patch clamp electrophysiology. After junction potential (–12.6 mV) and head stage leak (~ –3 mV) correction, all voltages were ~ –15 mV more negative than shown in the figures, Results text and voltage protocols.

Reagents. Inhibitor solutions were diluted to working concentrations of 100 µM or 1 mM Ba^{2+}, 20 µM ML133, 5 nM AgTx-2, 1 µM thapsigargin and 10 µM BTP2.

qRT-PCR. Dr. Zhu prepared RNA samples from rat microglia that were unstimulated or stimulated with IL-4 or IL-10 for 6 or 24 h. Primers for *Kcnj2* (which encodes the Kir2.1 channel) and the housekeeping gene, *Hprt1*, were designed by Dr. Zhu using "Primer3Tes" as follows. *Kcnj2*: forward (5'- ACCGCTACAGCATCGTCTCT -3') and reverse (5'-CTGCACTGTTGTCGGGTATG -3'); *Hprt1*: forward (5'-

CAGTACAGCCCCAAAATGGT -3') and reverse (5'- CAAGGGCATATCCAACAACA -3'). The threshold cycle (CT) for *Kcnj2* was normalized to that of *Hprt1*.

Microglia staining: cell morphology & viability. Microglia were untreated or stimulated for 24 h with IL-4 or IL-10. When a Kir2.1 inhibitor (Ba^{2+} or ML133) was used, it was added at the same time as the cytokine. To examine viability, microglia were incubated with propidium iodide (500 nM, Invitrogen) for 1 h (37°C, 5% CO_2) before fixing with 4% paraformaldehyde (Electron Microscopy Sciences, Hatfield, PA) for 10 min at room temperature. Cells were permeabilized, washed, and stained with FITC-conjugated tomato lectin (TL; 1:500, 15 min), and the nuclear dye, 4', 6-diamidino-2-phenylindole (DAPI; 1:3000, 5 min; Invitrogen). After washing, coverslips were mounted on glass slides using Dako mounting medium (Dako, Glostrup, Denmark). Counts of dead microglia (cells double-labeled with PI and DAPI) were normalized to the total number of DAPI-positive cells in 5 fields of view for each treatment condition.

Proliferation assay. Microglia were unstimulated or stimulated with IL-4 or IL-10 in the presence or absence of a channel blocker (Ba^{2+} or ML133).

Transwell migration assay. Microglia were left untreated or stimulated with IL-4 or IL-10. When used, a channel inhibitor (Ba^{2+} or ML133) was added for a further 23 h (24 h total incubation period). For chemotaxis, ATP (300 µM) was added to the lower well.

Statistics. Electrophysiology and Fura-2 experiments were analyzed using Origin v9.0 (OriginLab,Northampton, MA, USA), while dose response curve-fitting and all other data were analyzed using GraphPad v6.01 (GraphPad Software, San Diego, CA). For statistical analysis, paired or unpaired Student's t-test and one-way analysis of variance (ANOVA) with Bonferroni post hoc analysis were used. Results were considered significant if $p<0.05$.

3.3 RESULTS

3.3.1 Inward-rectifier Kir2.1 current is blocked by Ba^{2+} and ML133

We isolated whole-cell Kir2.1 currents from unipolar rat microglia that had a distinct lamellum and a uropod. This morphology corresponds with a high migratory capacity (Vincent et al. 2012; Siddiqui et al. 2012; Lively and Schlichter 2013; Ferreira et al. 2014; Siddiqui et al. 2014). Before performing cell function assays, it was important to examine the efficacy of the two blockers (Ba^{2+}, ML133) that we planned to use to test the role of Kir2.1 in microglia. ML133 is a recently identified small molecule inhibitor of the Kir2-family, and it blocks Kir2.1 heterologously expressed in HEK cells with an IC_{50} of 1.8 μM at 7.4 pH (less effective at lower pH) (Wang et al. 2011). Very few studies have used ML133 (Wang et al. 2011; Masia et al. 2015), and it has not been reported for microglia.

Kir2.1 presents as a rapidly activating, strongly inward-rectifying current, due to relief at negative potentials of block by internal Mg^{2+} and polyamines (Hibino et al. 2010; Baronas and Kurata 2014), and time-dependent block by external Na^{+} at very negative potentials (Kubo et al. 1993; Nörenberg et al. 1994). As illustrated in Figure 3.1A, the Kir current in rat microglia shows the hallmark rapid voltage-independent activation at negative potentials and time-dependent relaxation at very negative potentials. ML133 (at 20 μM) fully blocked the microglial Kir2.1 current at all voltages tested (Fig. 3.1A–C). Importantly, ML133 blocked the small component of outward current just above the reversal potential (E_{rev}) (Fig. 3.1C, inset). As expected for Kir2.1 current, there was strong inward rectification and E_{rev} was about –82 mV after junction potential and head stage leak correction, which is very close to the calculated Nernst potential with the bath

and pipette solutions used (E_K= –85 mV). Although external Ba^{2+} is commonly used to block Kir2.1 currents in rodent microglia (Brockhaus et al. 1993; Nörenberg et al. 1994; Schlichter et al. 1996; Chung et al. 1999a; Franchini et al. 2004), block is voltage dependent and decreases with membrane depolarization (Schlichter et al. 1996; Franchini et al. 2004). The outward Kir2.1 current in rat microglia was not well blocked by 100 µM external Ba^{2+} (Fig. 3.1D). Caution is needed when using higher Ba^{2+}concentrations in functional assays because millimolar Ba^{2+} also inhibit some voltage-dependent K^+ channels (Armstrong and Taylor 1980; Armstrong et al. 1982), and activates some SK channels (Cao and Houamed 1999; Soh and Park 2001). Therefore, in several of the following functional studies, we compared effects of ML133 with Ba^{2+}.

We next examined the time dependence of block by bath-applied ML133 because it is known to act on an internal site (Wang et al. 2011) and should thus take time to enter the cell. As expected, full block by 20 µM ML133 required several minutes (Fig. 3.1E). Note that in the absence of ML133, there was some time-dependent current rundown; i.e., to 79.4±6.8 % (n=5) of the initial current at 5 min. This rundown is expected in whole-cell recordings due to loss of cytoplasmic components; e.g., lipid kinases that generate phosphatidylinositol 4,5-bisphosphate, that are required to sustain Kir2.1 channel function (Hilgemann et al. 2001; Fürst et al. 2014). Finally, a dose-response curve for ML133 block was constructed and yielded an IC_{50} of 3.5 µM (n=4–7) cells for each point, Fig. 3.1F). This value is comparable to the reported values in HEK cells (Wang et al. 2011) and murine neutrophils (Masia et al. 2015).

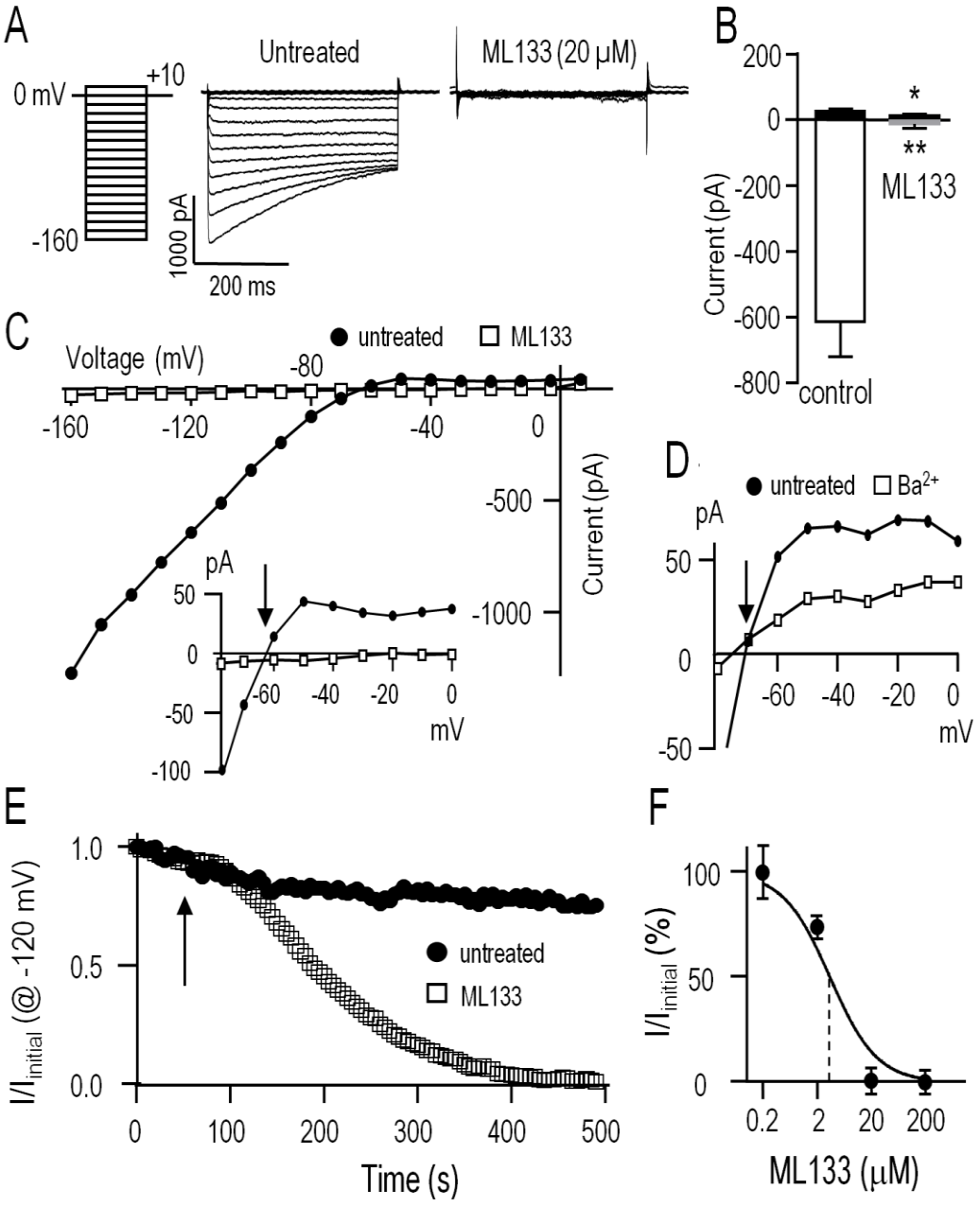
A
Untreated
ML133 (20 μM)
0 mV
+10
-160
1000 pA
200 ms
B
200
0
-200
-400
-600
-800
Current (pA)
*
**
ML133
control
C
untreated
ML133
Voltage (mV)
-80
-160
-120
-40
0
-500
-1000
Current (pA)
pA
50
0
-50
-100
-60
-40
-20
0
mV
D
untreated
Ba2+
pA
50
0
-50
-60
-40
-20
0
mV
E
1.0
0.5
0.0
I/Iinitial (@ -120 mV)
untreated
ML133
0
100
200
300
400
500
Time (s)
F
100
50
0
I/Iinitial (%)
0.2
2
20
200
ML133 (μM)

Figure 3.1 The inward-rectifier Kir2.1 current in rat microglia is blocked by Ba^{2+} and ML133. For all recordings, the standard bath solution contained 5 nM AgTx-2 to block the Kv1.3 current. Whole-cell currents were then recorded in response to the voltage protocol shown in panel A; i.e., test pulses between –160 and +10 mV in 10-mV increments from a holding potential of 0 mV. Note: in this, and all subsequent figures, the liquid junction potential and headstage leak were not corrected; thus, all voltages are ~15 mV more negative than indicated. **A.** Representative currents with and without the specific Kir2.x-family inhibitor, ML133 (20 µM). **B.** Summary of amplitudes of inward current (at –120 mV) and outward current (at –50 mV) (mean ± SEM; n=5 each) with and without 20 µM ML133. **p*<0.05, ***p*<0.01; paired Student's t-test. **C.** Current-voltage (I-V) relations from the same cell as in A, before and after adding 20 µM ML133. *Inset:* I-V relations, plotted on an expanded Y-axis. Note the outward Kir2.1 current above the reversal potential, E_{rev} (arrow) before, but not after adding ML133. **D.** I-V relations for a different cell before and after adding 100 µM Ba^{2+}. Note the incomplete block of outward current. **E.** Time course of block by 20 µM ML133, which was added to the bath at the time indicated by the arrow. Voltage steps to –120 mV from a holding potential of 0 mV were repeatedly applied at an interpulse interval of 5 s. **F.** Dose-response curve for ML133 block of Kir2.1 current, normalized to the value without drug and presented as a semi-logarithmic function (mean ± SEM, n=4–7 cells for each concentration). The IC_{50} (3.5 µM) is indicated by the vertical dashed line.

3.3.2 Kir2.1 expression in anti-inflammatory microglial activation states

We previously found that alternative activation and acquired deactivation are elicited by 24 h stimulation of rat microglia with IL-4 or IL-10, respectively (Lively and Schlichter 2013; Ferreira et al. 2014; Siddiqui et al. 2014). However, there are apparently no reports addressing expression of *Kcnj2* mRNA (which codes for Kir2.1) or Kir2.1 currents in microglia following stimulation with IL-4 or IL-10. Levels of *Kcnj2* mRNA did not significantly differ at 6 or 24 h after stimulation with IL-4 or IL-10 (Fig. 3.2A). Nevertheless, it was important to compare the current amplitude in the different activation states because it can be affected by factors beyond mRNA expression; particularly, protein expression, trafficking to the surface membrane and post-translational modulation. We waited until 24 h after stimulation with IL-4 or IL-10 to allow time for such changes to occur. Representative currents are shown in Figure 3.2B. Figure 3.2C summarizes the current densities; i.e., the current measured at −120 mV was normalized to the cell capacitance, which is a measure of cell surface area. Current densities were not different between unstimulated cells and after IL-4 or IL-10.
The capacitance did not statistically differ with treatments; i.e., it was 25±2 pF (n=18) for unstimulated microglia versus 24±2 pF (n=17) for IL-10-stimulated cells; however, there was a trend toward a smaller cell size after IL-4 stimulation (19±2 pF, n=17; p=0.14). We previously noted that IL-4 stimulated cells were generally smaller (Lively and Schlichter 2013) but did not monitor their capacitance in that study.

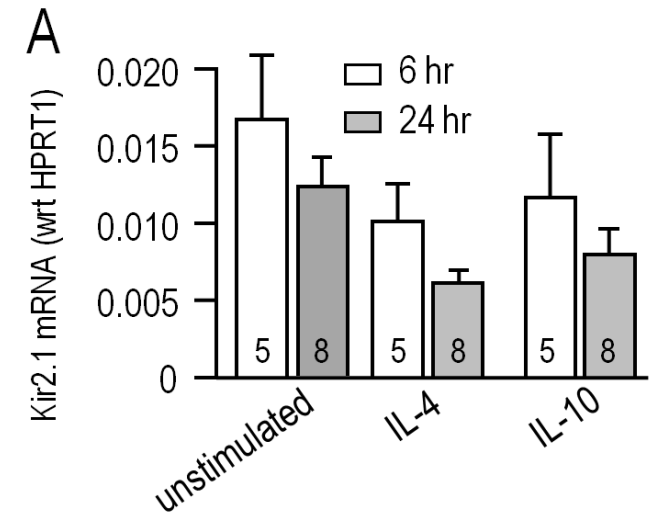
A
Kir2.1 mRNA (wrt HPRT1)
0.020
0.015
0.010
0.005
0
6 hr
24 hr
5
8
5
8
5
8
unstimulated
IL-4
IL-10

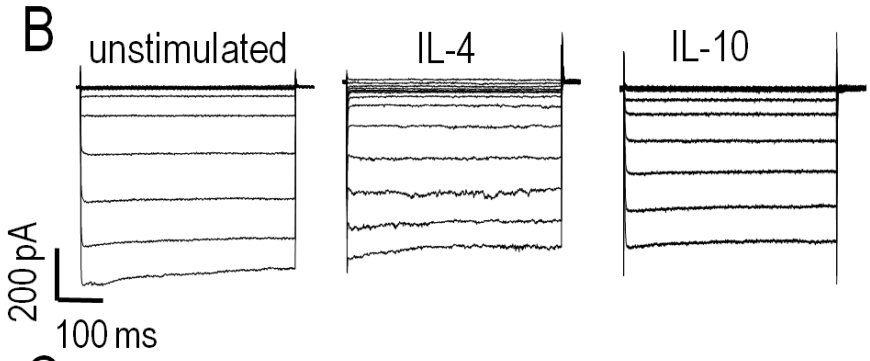
B
unstimulated
IL-4
IL-10
200 pA
100 ms

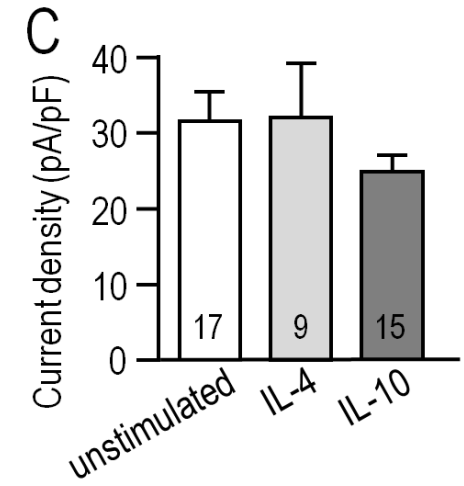
C
Current density (pA/pF)
40
30
20
10
0
17
9
15
unstimulated
IL-4
IL-10

Figure 3.2. **Kir2.1 expression and current is unaffected by IL-4 or IL-10 stimulation.** **A.** *Kcnj2* (Kir2.1) mRNA levels were monitored using real-time qRT-PCR at 6 and 24 h from cells that were unstimulated or stimulated with 20 ng/mL IL-4 or IL-10. Channel expression was normalized to the housekeeping gene, *Hprt1*, and shown as mean ± SEM for the number of microglia cultures indicated on the bars. Comparisons based on a two-way ANOVA followed by Tukey's post-hoc test, indicate no significant differences. **B.** Whole-cell Kir2.1 currents were recorded in response to voltage steps, as in Figure 1A. Representative recordings are shown for an unstimulated microglial cell and individual cells stimulated for 24 h with 20 ng/mL IL-4 or IL-10. **C.** Summarized Kir2.1 current densities recorded at –120 mV, plotted as mean ± SEM for the number of cells indicated on each bar. A one-way ANOVA followed by a Bonferroni post-hoc test indicates non-significant differences.

3.3.3 Kir2.1 contributes to microglial proliferation, migration and chemotaxis

We previously reported that rat microglia are migratory, with most cells having a unipolar morphology with a fan-shaped lamellum at the leading edge and a trailing uropod whether unstimulated or stimulated with IL-4 or IL-10 (Siddiqui et al. 2012 & 2014; Vincent et al. 2012; Lively and Schlichter 2013). This morphology was also prevalent in the present study (Fig. 3.3A–C). However, when classically activated by LPS, they become non-migratory and dramatically change their morphology to nearly spherical (Lively and Schlichter, 2013; Siddiqui et al. 2014). Because both Kir2.1 blockers (Ba^{2+}, ML133) greatly reduced migration (see below), we asked whether their morphology changed to that of LPS-stimulated cells. It did not; and blocking Kir2.1 did not obviously affect their unipolar morphology under any of the activation states examined (Fig. 3.3A–C). Time-lapse imaging for 2 h (not shown) also showed that the blockers did not obviously affect their morphology. In addition, their viability, monitored with propidium-iodide, was >90% during the longest stimulation period (24 h) and was unaffected by activation state or treatment with ion channel blockers (not shown). However, from the images, we noted apparent differences in cell density after blocking Kir2.1, which we then quantified using the CyQuant assay in a microplate reader format. As we recently showed for IL-4 (Ferreira et al. 2014), proliferation was not affected by 24 h stimulation with IL-4 or IL-10 alone (Fig. 3.3D). However, the Kir2.1 blockers significantly increased cell density (by 130–146%) of both unstimulated- and IL-4-stimulated microglia. Together, our results show that blocking Kir2.1 increased their

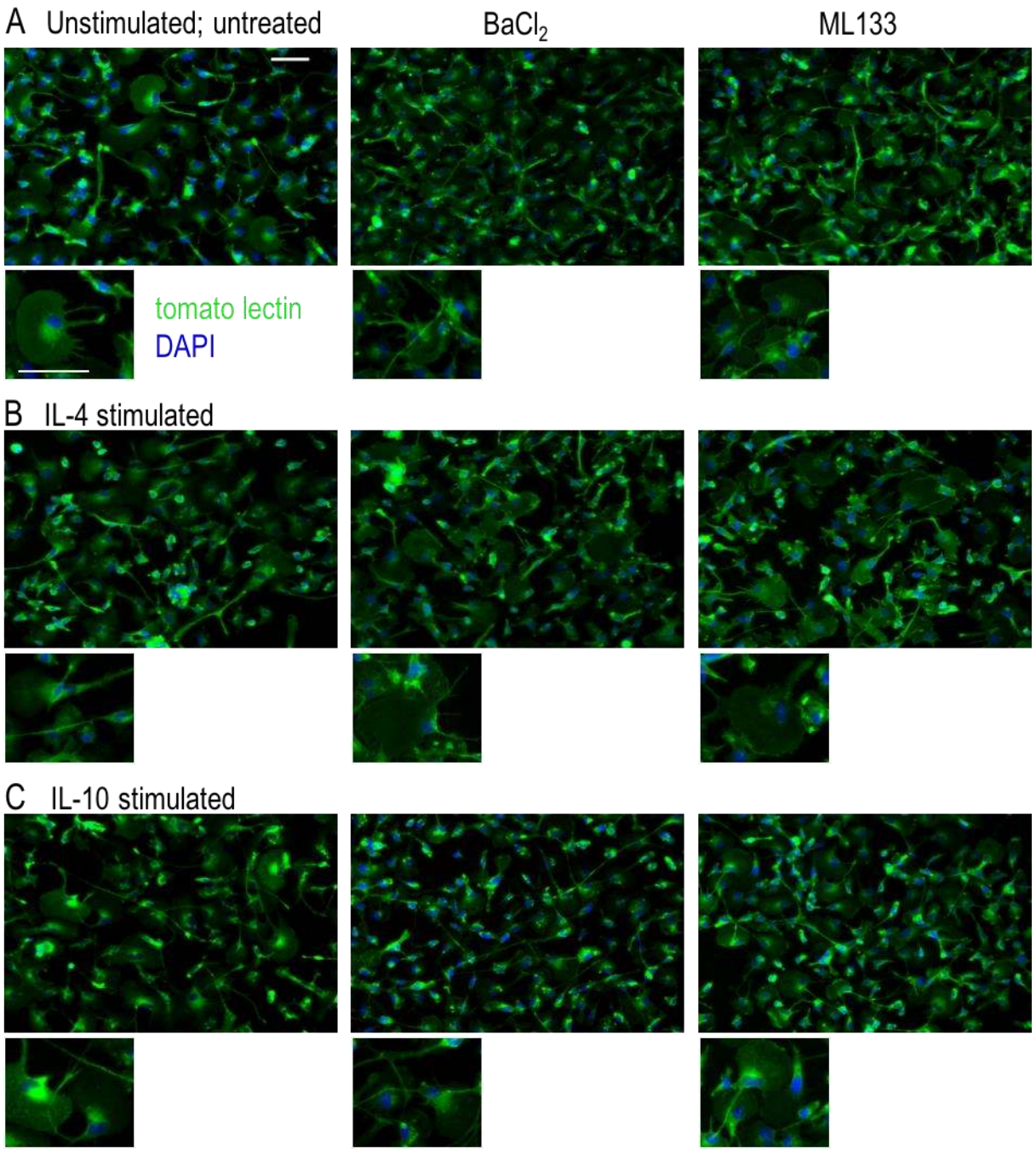
A Unstimulated; untreated
BaCl2
ML133
tomato lectin
DAPI
B IL-4 stimulated
C IL-10 stimulated
D
unstimulated
IL-4
IL-10
Fold change wrt control
2.0
1.5
1.0
0.5
0.0
***
*
**
**
12
Control
+BaCl2
+ML133
IL-4
IL-10

Figure 3.3. Blocking Kir2.1 increases proliferation of unstimulated and IL-4-stimulated microglia. Microglial cells were left unstimulated or stimulated with IL-4 or IL-10 for 24 h. When Kir2.1 blockers were used, they were added to the bath after the first hour and remained for the following 23 h. **A–C.** Representative images of cells labeled with the microglia marker, tomato-lectin (green), and the nuclear dye, DAPI (blue): untreated (left panels), 1 mM Ba^{2+} (middle), 20 µM ML133 (right panels). [Note the purity of the microglial cultures, as all cells labeled with tomato lectin.] Scale bars are 50 µm and apply to all images. **D.** For the CyQUANT proliferation assay, microglia were stimulated for 24 h with IL-4 or IL-10 in the presence or absence of Ba^{2+} or ML133 treatment. Results are expressed as fold change (mean ± SEM, n=12 cultures per treatment) with respect to the untreated unstimulated control (dashed lines), and a one-way ANOVA with Bonferroni post-hoc test was performed. *p<0.05, **p<0.01, ***p<0.001

proliferation without affecting viability. In contrast, this proliferative effect of blocking Kir2.1 was not seen in IL-10 stimulated microglia.

We next asked if Kir2.1 is important for their migratory capacity. Transwell inserts were used to examine 3-dimensional migration in the absence (random transmigration) and presence of the chemoattractant, ATP (chemotactic migration). Consistent with our previous findings (Lively and Schlichter 2013; Ferreira et al. 2014; Siddiqui et al. 2014), random transmigration was increased by stimulation with IL-4 (by 343%; n=11) or IL-10 (344%; n=8) (Fig. 4). Transmigration of unstimulated cells was reduced by blocking Kir2.1 with Ba^{2+} (by 61%) or ML133 (by 73%) (Fig. 3.4A). Similar, large reductions were seen in IL-4-stimulated cells (76% by Ba^{2+}, 90% by ML133; Fig. 3.4B) and IL-10-stimulated cells (77% by Ba^{2+}, 85% by ML133; Fig. 4C), and their migration was at or below the level of unstimulated cells (dotted lines). ATP-induced chemotactic migration was several-fold higher than random transmigration for all three activation states, and was dramatically reduced by treatment with Kir2.1 blockers; i.e., to about the same level as random transmigration of unstimulated cells (1.0 for the normalized data). It is important to note that these reductions are likely underestimated for unstimulated and IL-4-stimulated cells because the blockers increased proliferation (by 1.3–1.46 fold over 24 h; Fig. 3.3D) and thus, increased the number of cells available to migrate during the assay.

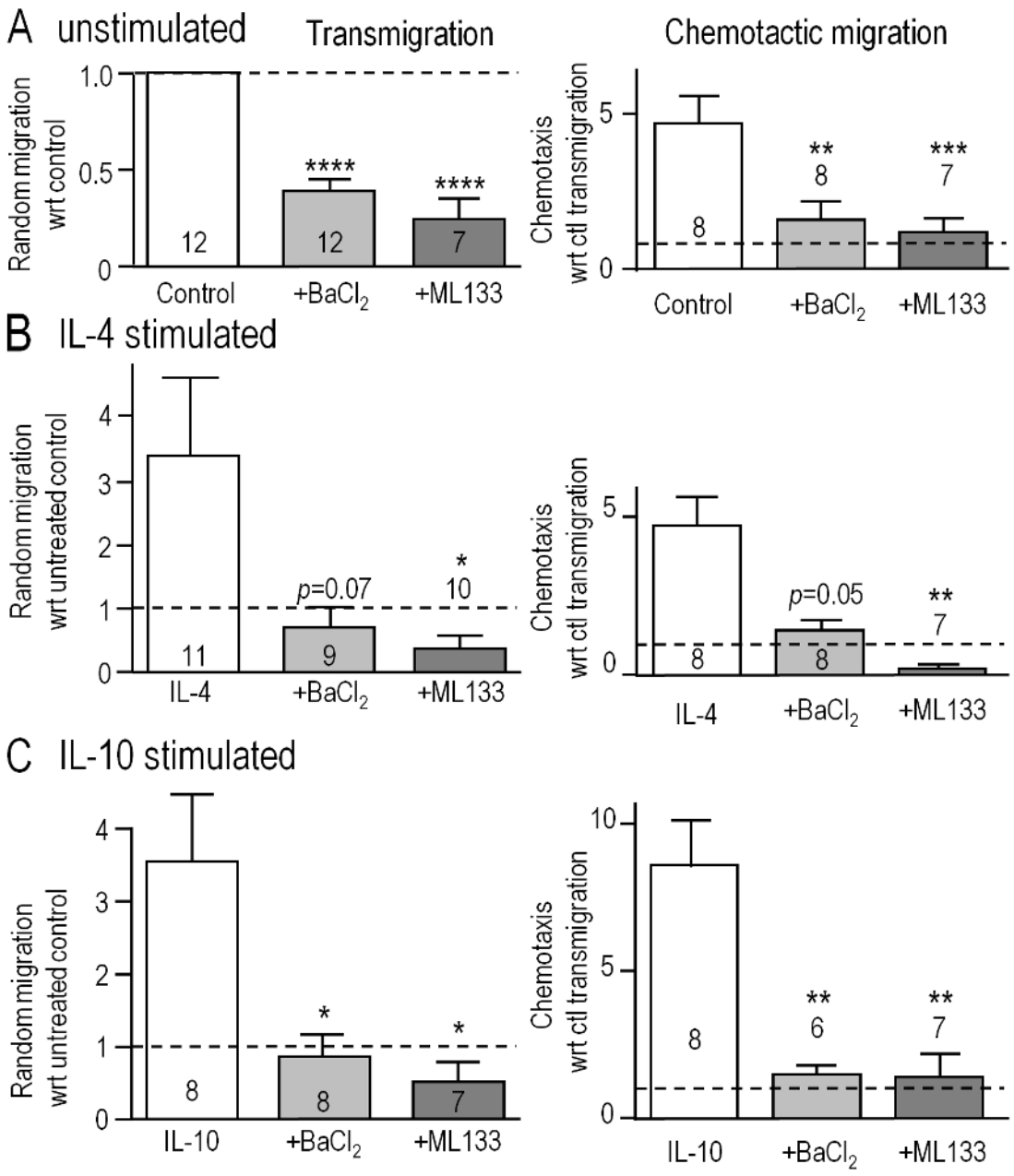
A unstimulated
Transmigration
Chemotactic migration
Random migration wrt control
1.0
0.5
0
****
****
12
12
7
Control
+BaCl2
+ML133
Chemotaxis wrt ctl transmigration
5
0
**
***
8
8
7
Control
+BaCl2
+ML133
B IL-4 stimulated
Random migration wrt untreated control
4
3
2
1
0
p=0.07
*
11
9
10
IL-4
+BaCl2
+ML133
Chemotaxis wrt ctl transmigration
5
0
p=0.05
**
8
8
7
IL-4
+BaCl2
+ML133
C IL-10 stimulated
Random migration wrt untreated control
4
3
2
1
0
*
*
8
8
7
IL-10
+BaCl2
+ML133
Chemotaxis wrt ctl transmigration
10
5
0
**
**
8
6
7
IL-10
+BaCl2
+ML133

Figure 3.4. Blocking Kir2.1 reduces migration of unstimulated, IL-4- and IL-10-stimulated microglia. A–C. Microglial cells were seeded on filters bearing 8 µm diameter pores in the upper wells of 3D Transwell^{TM} chambers. We quantified random transmigration (left panels) and chemotactic migration induced by adding 300 µM ATP to the lower well (right panels). Microglia were unstimulated **(A)** or stimulated with IL-4 **(B)** or IL-10 **(C)** for 24 h, and when used, 1 mM Ba^{2+} or 20 µM ML133 was added after the first hour and for the remaining 23 h. All results are expressed as fold change with respect to random transmigration of untreated (control) unstimulated cells (i.e., 1.0 indicated by the dashed lines). Data are mean ± SEM for the number of microglial cultures indicated on each bar, and were analyzed using one-way ANOVA with Bonferroni post-hoc test. *p<0.05, **p<0.01, ***p<0.001, ****p<0.0001

3.3.4 Blocking Kir2.1 reduces store-operated Ca^{2+} influx

To examine whether Kir2.1 regulates CRAC-mediated Ca^{2+} influx in microglia, we isolated this component in Fura-2-loaded cells. As in our earlier study (Ohana et al. 2009), CRAC was activated by depleting Ca^{2+} stores using a 5-min treatment with 1 µM thapsigargin in a Ca^{2+}-free bath solution. The baseline Fura-2 signal was low and stable, a large rise occurred when external Ca^{2+} was restored, and unstimulated microglia often displayed Ca^{2+} oscillations (Fig. 3.5A). As expected for CRAC, the Ca^{2+} rise required influx and was rapidly eliminated by removing external Ca^{2+}. Further evidence that the rise was CRAC-mediated was that it was eliminated by perfusing the CRAC blocker, 10 µM BTP2, into the bath.

Next, we assessed contributions of CRAC and Kir2.1 to Ca^{2+} influx in the different activation states (Fig. 3.5B). To allow time for block by ML133 (Fig. 3.1E) and BTP2 to develop (Fig. 3.5A); each blocker was added to separate coverslips of cells for the duration of the experiment. Without channel blockers, the Ca^{2+} response of unstimulated microglia usually reached a plateau during the 5 min exposure to Ca^{2+}; whereas, in IL-4- or IL-10-stimulated cells, there was usually a rapid rise followed by a spontaneous decline (Fig. 3.5B). The Fura-2 signal, integrated over the 5-min exposure to external Ca^{2+}, was ~50% lower in IL-4-stimulated microglia than in unstimulated- ($p<0.0001$) or IL-10-stimulated cells ($p<0.0001$; Fig. 3.5C). The CRAC blocker, BTP2, reduced Ca^{2+} entry by 96% in both unstimulated and IL-10-stimulated cells ($p<0.0001$), but was slightly less effective in IL-4-stimulated cells (reduced by 82%, $p<0.0001$). As we predicted, blocking Kir2.1 with ML133 reduced Ca^{2+} entry in unstimulated cells (by

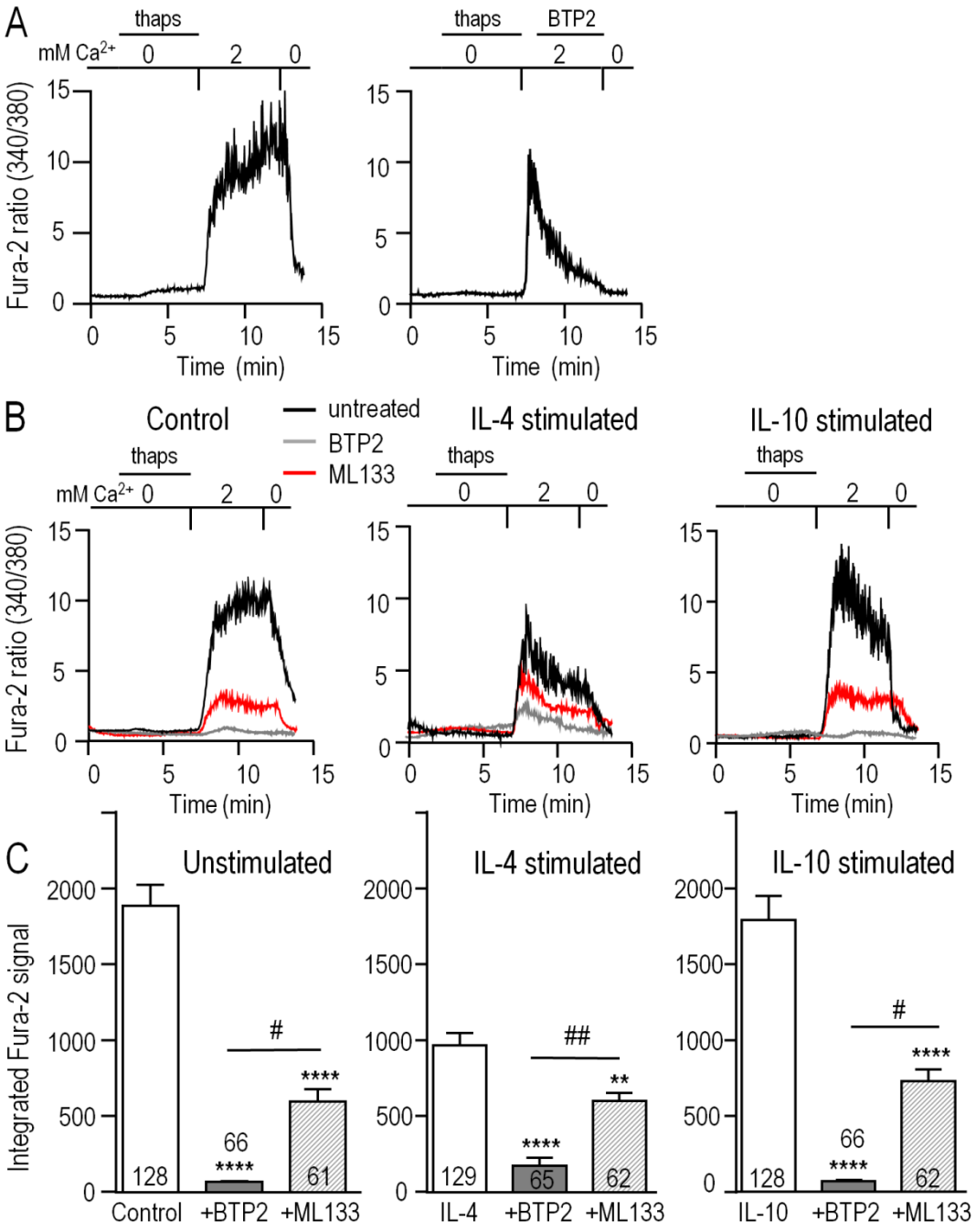
A
thaps
BTP2
mM Ca2+ 0 2 0
Fura-2 ratio (340/380)
Time (min)
B
Control
IL-4 stimulated
IL-10 stimulated
untreated
BTP2
ML133
C
Unstimulated
IL-4 stimulated
IL-10 stimulated
Integrated Fura-2 signal
Control +BTP2 +ML133
IL-4 +BTP2 +ML133
IL-10 +BTP2 +ML133

Figure 3.5. Blocking Kir2.1 reduces CRAC-mediated Ca^{2+} influx. Microglia were unstimulated or stimulated for 24 h with 20 ng/mL IL-4 or IL-10, and then loaded with the Ca^{2+}-sensitive dye, Fura-2. The Ca^{2+} levels are reported as the ratio of the signal at 340 and 380 nm excitation wavelengths. **A.** CRAC-mediated Ca^{2+} influx. As indicated by the horizontal bars above the traces, microglia were exposed for 5 min to Ca^{2+}-free bath solution containing 1 µM thapsigargin (thaps) to deplete intracellular Ca^{2+} stores and activate CRAC. Then, Ca^{2+} influx was restored by perfusing in a solution containing 2 mM Ca^{2+}. After 5 min, the dependence on external Ca^{2+} was confirmed by re-perfusing the bath with Ca^{2+}-free solution. Right panel: A different cell, showing the response to the CRAC-channel blocker, 10 µM BTP2, added to the bath where indicated. **B.** Reduction of the CRAC-mediated Ca^{2+} rise by blocking CRAC or Kir2.1. Representative recordings from unstimulated and IL-4- or IL-10 stimulated microglia, using the same protocol as in panel A. Ca^{2+} was monitored in separate coverslips of cells with or without 10 µM BTP2 or the Kir blocker, 20 µM ML133 present throughout the recording. **C.** The area under each Fura-2 trace was integrated over the 5 min period of exposure to 2 mM Ca^{2+}, and expressed in arbitrary units as mean ± SEM for the number of cells indicated on each bar. Three independent cell cultures were used to test each blocker (BTP2, ML133) and control cells were from the same 6 cell cultures. Results were analyzed using one-way ANOVA with a Bonferroni post-hoc test. Statistical effects of each channel blocker within each activation state (stimulus) are indicated as $^{**}p<0.01$, $^{****}p<0.0001$. Statistical differences between the blockers are indicated as $^{\#}p<0.05$, $^{\#\#}p<0.01$

~68%, $p<0.001$), and to a similar degree in IL-10-stimulated cells (~59%, $p<0.0001$). After adding ML133 to IL-4-stimulated cells, the remaining signal was about the same as in unstimulated and stimulated cells. The percent reduction by ML133 was lower (~38%, $p<0.01$), because the control IL-4 response was lower. Together, these results show that Ca^{2+} entry in microglia was mainly CRAC-mediated under all three activation states, and required Kir2.1 activity for maximal influx.

3.4 DISCUSSION

There are several salient findings in this study. ***(i)*** Expression of *Kcnj2* mRNA and Kir2.1 current were comparable in rat microglia that were unstimulated or had undergone alternative activation (with IL-4) or acquired deactivation (with IL-10). ***(ii)*** Proliferation was comparable in all three microglial activation states. It was slightly increased by blocking Kir2.1 in unstimulated and IL-4-stimulated microglia, but not after IL-10 stimulation. ***(iii)*** Migration and chemotaxis were increased by IL-4 and by IL-10, and were dramatically decreased by blocking Kir2.1 with Ba^{2+} or ML133, regardless of activation state. ***(iv)*** Blocking Kir2.1 with ML133 reduced Ca^{2+} influx through BTP2-sensitive, Ca^{2+}-release-activated Ca^{2+} (CRAC) channels in all three activation states.

Reports of changes in Kir2.1 current with microglial activation have been inconsistent, possibly species dependent, and very little is known about anti-inflammatory states. For cultured murine microglia, several studies show that classical activation decreases Kir2.1 current; i.e., after exposure to lipopolysaccharide (LPS) or the pro-inflammatory cytokines, IFN-γ or TNF-α (Draheim et al. 1999; Prinz et al. 1999; Boucsein et al. 2003). In contrast, effects on the current in rat microglia range from no change, to a small increase (LPS), to a large increase (IFN-γ) (Nörenberg et al. 1992;

Visentin et al. 1995). For microglia in brain slices, Kir2.1 was observed in the murine corpus callosum and within the peri-infarct region after ischemia (middle cerebral artery occlusion) in rats (Brockhaus et al. 1993; Lyons et al. 2000). More recent studies have compared Kir2.1 currents in rodent microglia under different conditions: rat microglia in the facial nucleus before and after facial nerve axotomy, murine microglia from acute and cultured hippocampal slices, and murine microglia from young adult and aged animals (Schilling and Eder 2007 & 2015; Boucsein et al. 2000). The current was initially small in microglia from rat facial nucleus, acute murine hippocampal slices and young adult mice, and it increased in the denervated facial nucleus, in cultured slices, and in aged mice. However, microglial activation states were not determined. TGF-β, like IL-10, is considered a resolving cytokine (Suzumura et al. 1993; Pratt and McPherson 1997), and in primary murine microglia or cell lines (BV-2, C8-B4) the current density was not affected by stimulation with TGF-β1 or TGF-β2 (Schilling et al. 2000; Moussaud et al. 2009). Here, we found that neither *Kcnj2* mRNA nor the Kir2.1 current differed under any of the activation states examined: unstimulated, IL-4- or IL-10-stimulated.

After comparing the Kir2.1 current in the different activation states, it was important to assess its contributions to microglial functions, for several reasons. The Kir2.1 current amplitude represents a snapshot in time, and changes in other currents could affect its relative contribution to the membrane potential and microglia functions over a longer period. In addition, Kir2.1 is subject to post-translational modulation (Hilgemann et al. 2001; Hibino et al. 2010; Fürst et al. 2014), which might differ in intact cells, with time, and with activation state. Results of functional studies using the common blocker, Ba^{2+}, have been inconsistent; thus, it is important to consider its

limitations, in particular that block is voltage dependent. The present study shows that Ba^{2+} is a poor blocker of outward Kir2.1 current in microglia. The reported bi-stable distribution of microglial membrane potentials (about –35 and –70 mV) (Nörenberg et al. 1994; Visentin et al. 1995; Boucsein et al. 2003) might explain why Ba^{2+} depolarized some rat microglial cells but did not affect others (Chung et al. 1999a), and reduced the ATP-induced Ca^{2+} signal in some microglia but not others (Franchini et al. 2004). Here, we found that a higher Ba^{2+} concentration (1 mM) affected all the functions that were examined (proliferation, migration, chemotaxis) but relevant off-target effects have been reported. For instance, KCa2.3 and KCa3.1 channels are expressed in rat microglia (Kaushal et al. 2007; Schlichter et al. 2010; Siddiqui et al. 2012; Ferreira et al. 2014; Siddiqui et al. 2014); 1 mM Ba^{2+} blocks cloned KCa3.1 channels (by 88%; Joiner et al. 1997), and sub-millimolar Ba^{2+} moderately activates cloned KCa2 and KCa3.1 channels (Cao and Houamed 1999; Soh and Park 2001). We previously showed that migration of rat microglia depends on KCa3.1 (Ferreira and Schlichter 2013; Ferreira et al. 2014); thus, its block by Ba^{2+} could contribute to inhibition of migration and chemotaxis in the present study. Therefore, rather than relying only on Ba^{2+}, we determined that the selective inhibitor, ML133 (Wang et al. 2011) blocked in a voltage-independent manner, with essentially complete block of both inward and outward Kir2.1 currents at 20 μM. Most importantly, ML133 greatly reduced CRAC-mediated Ca^{2+} entry and had the same effects as Ba^{2+} in increasing proliferation and reducing migration and chemotaxis. Each of these functional outcomes will be discussed in light of the literature.

The prevailing view is that Kir2.1 channel activity helps maintain a negative membrane potential in many cell types, and thereby regulates the driving force for ion fluxes, including Ca^{2+} influx. In rat microglia, Ca^{2+} can enter through several pathways,

including Ca^{2+}-release activated Ca^{2+} (CRAC/Orai1) and TRPM7 channels (Jiang et al. 2003; Ohana et al. 2009; Siddiqui et al. 2014), ionotropic purinergic receptors (Inoue 2008), and reversed Na^{+}/Ca^{2+} exchange (Newell et al. 2007). Here, we focussed on CRAC-mediated Ca^{2+} entry because the channel is highly Ca^{2+}-selective and strongly inward-rectifying and thus, Ca^{2+} entry will be facilitated by hyperpolarization. CRAC accounted for essentially all of the store-operated Ca^{2+} entry (i.e., it was fully blocked by BTP2) in unstimulated and IL-10-stimulated microglia, and most of the Ca^{2+} entry in IL-4-stimulated cells. Blocking Kir2.1 with ML133 substantially reduced Ca^{2+} entry in all three microglial activation states, which provides the first evidence that Kir2.1 regulates microglia functions by promoting CRAC-mediated Ca^{2+} influx. Although beyond the scope of the present study, several observations regarding store-operated Ca^{2+} entry would be worth following up in future; i.e., differences in the shape of the Ca^{2+} signal in unstimulated versus IL-4- or IL-10-stimulated microglia after Ca^{2+} was restored to the bath; and the lower Ca^{2+} response and BTP2-insensitive component in IL-4-stimulated cells.

Microglia must migrate and invade through extracellular matrix (ECM) to reach damage sites, and this is stimulated by ATP release from damaged cells (Davalos et al. 2005; Farber and Kettenmann 2006; Inoue 2008; Tozaki-Saitoh et al. 2012). Cultured rat microglia are highly migratory (Vincent et al. 2012; Siddiqui et al. 2012; Lively and Schlichter 2013; Ferreira and Schlichter 2013; Ferreira et al. 2014; Siddiqui et al. 2014), and both migration and invasion are increased in IL-4 and in IL-10 stimulated microglia (Lively and Schlichter 2013; Ferreira et al. 2014; Siddiqui et al. 2014). Microglial migration is a Ca^{2+}-dependent process involving CRAC channels (Siddiqui et al. 2012; Ferreira and Schlichter 2013; Michaelis et al. 2015), as well as Ca^{2+}-permeable TRPM7

channels in IL-4- and IL-10-stimulated cells (Siddiqui et al. 2014). In migrating rat microglia, CRAC/Orai1 is enriched in podosomes, which are tiny multi-molecular structures used for adhesion and ECM degradation during migration and invasion (Vincent et al. 2012; Siddiqui et al. 2012); and blocking CRAC reduced podosome expression, invasion and transmigration (Siddiqui et al. 2012). Consistent with the role of Kir2.1 in CRAC-mediated Ca^{2+} entry, we found that blocking Kir2.1 greatly reduced migration and ATP-induced chemotaxis in unstimulated, IL-4 or IL-10 stimulated microglia. Previous studies did not directly assess the role of Kir2.1 in migration. However, in murine microglia the Kir2.1 current and cell spreading were increased by activated Rac and decreased by activated Rho, which are small GTPases that regulate actin and facilitate cell migration (Muessel et al. 2013).

Neonatal rat microglia proliferate in culture (Schlichter et al. 1996). Consistent with our recent IL-4 study (Ferreira et al. 2014); proliferation was not altered by 24 h stimulation with IL-4 or IL-10. However, in unstimulated or IL-4-stimulated cells (but not after IL-10), proliferation was increased 40–46% by 1 mM Ba^{2+} and 30–46% by ML133. In our early study using CSF-1, 1 mM Ba^{2+} increased proliferation by 25%, while higher concentrations decreased it with an apparent IC_{50} of 1.5 mM (Schlichter et al. 1996). We now think that the inhibition at 5 and 10 mM Ba^{2+} was an off-target effect, possibly on KCa3.1, as noted above. Some studies have used targeted knockdown of Kir2.1 to avoid the problems associated with Ba^{2+}. Consistent with our results using ML133 (and 1 mM Ba^{2+}), proliferation of endothelial progenitor cells was increased after silencing Kir2.1 with siRNA or blocking it with Ba^{2+} (Jang et al. 2011) but the mechanism was not identified. The contribution of Kir2.1 to proliferation is somewhat controversial and might also depend on cell type. There was no effect or even reduced proliferation in Schwann

cells, mesenchymal stem cells, smooth muscle cells, and fibroblasts after treatment with Ba^{2+} (10–500 μM) or dominant-negative suppression of Kir2.1 (Sobko et al. 1998; Karkanis et al., 2003; Zhang et al., 2012a; Zhang et al., 2012b; Qi et al. 2015). The mechanism by which Kir2.1 inhibition affects cell proliferation is not known. Numerous studies show that Ca^{2+} entry is important for cell proliferation (Capiod 2011; Borowiec et al. 2014), and that cell cycle progression correlates with changes in K^+ channel activity (Pardo 2004; Blackiston et al. 2009; Urrego et al. 2014), which is expected to affect the membrane potential. Unfortunately, detailed studies of membrane potential during the cell cycle are lacking for microglia and other cells. What is known is that the membrane K^+ permeability is generally higher during the G1 phase and lower during other phases of the cell cycle, and this variation appears to be necessary because artificially sustained hyperpolarization blocks DNA synthesis (Urrego et al. 2014). One possibility is that blocking Kir2.1 increased microglia proliferation by depolarizing the membrane, and shortening the G1 phase or increasing the rate of transition through S, G2 and M phases. If so, the lack of effect of blocking Kir2.1 on proliferation of IL-10-stimulated microglia might result from another K^+ channel type providing the necessary high K^+ permeability. Future studies will need to analyze K^+ channel activity, membrane potential, and Ca^{2+} entry during the cell cycle, and determine whether they differ with microglial activation states.

In summary, the similar expression of Kir2.1 in unstimulated and anti-inflammatory activation states suggested that this channel is important for homeostatic functions of microglia. Proliferation and migration are two such functions, and there is evidence that these processes involve Ca^{2+} signaling and CRAC/Orai1 channels. The involvement of Kir2.1 in regulating membrane potential in other cell types, and the

present results showing that Kir2.1 regulates CRAC-mediated Ca^{2+} entry in unstimulated and anti-inflammatory states, suggest a convergent mechanism. While this study did not examine classical-activated microglia, we have previously reported that LPS-stimulated rat microglia are much less migratory than unstimulated or anti-inflammatory (IL-4- or IL-10-stimulated) cells (Lively and Schlichter 2013; Ferreira et al. 2014; Siddiqui et al. 2014), and there is evidence that the Kir2.1 current is decreased in classical-activated mouse microglia (Draheim et al. 1999; Prinz et al. 1999; Boucsein et al. 2003). In future, the selective inhibitor, ML133, should prove useful for examining roles of Kir2.1 in classical-activated microglia (e.g. migration) and in other cell functions involved in CNS injury.

4 A rat versus mouse comparison of microglia in different activation states: Molecular profiles, K^+ channels and migration

4.1 INTRODUCTION

When damaged, cells in the central nervous system (CNS) release 'damage-associated molecular pattern' molecules ('alarmins') and other soluble mediators, including high-mobility group box 1, purine metabolites, nucleic acids, and cytokines. In response, microglia 'activate', and this is accompanied by dramatic changes in morphology, molecular profiles and functional properties (Kettenmann et al., 2011; Hanisch et al., 2013). Rats have been used for many years to model CNS damage and disease because they have many physiological similarities to humans and can learn a wide variety of tasks, making them useful for behavioral studies (Iannaccone and Jacob, 2009). More recently, mice have been favored because of the ease of genetic manipulation (Nguyen and Xu, 2008; Sieger et al., 2013), although transgenic technology in rats is now advancing (Kawaharada et al., 2015). Immune responses of mice and humans are increasingly being compared (Mestas et al., 2004; Bryant et al., 2012; Thomas and Mattila, 2014), and it is also important to determine the similarities and differences between commonly used rodent species. Surprisingly few studies of microglia have compared their responses in both rodent species (Patrizio and Levi, 1994; Du et al., 2016), and this knowledge gap could affect the ability to translate experimental findings to human treatments. The present study directly compares

numerous molecular responses and several functional outcomes in primary microglia from rat and mouse.

After acute CNS injury, microglial activation is thought to evolve over time, with pro- and anti-inflammatory states lying at opposite ends of a continuum (Lynch, 2009; Kettenmann et al., 2011; Hanisch, 2013). Changes in activation states are expected to affect the capacity of microglia to produce immune mediators, migrate, proliferate, and phagocytose dead cells and debris. *In vitro* studies are commonly used to elucidate responses to stimuli that can skew microglia toward a particular activation state. The terminology is evolving (Colton et al., 2009; Hanisch, 2013; Cherry et al., 2014; Murray et al., 2014; Mitchell-Robinson et al., 2015), and for clarity, we will use the following. 'Classical' activation (M1), which is a pro-inflammatory phenotype thought to exacerbate tissue damage, is usually induced *in vitro* by bacterial lipopolysaccharide (LPS) with or without IFN-γ. Recently, we have begun to use a combination of IFN-γ and TNF-α to induce a pro-inflammatory state (Siddiqui et al., 2016), which we denote as M(I+T). Several anti-inflammatory (M2) states have been implicated in tissue repair, matrix deposition, and resolution of pro-inflammatory states. Of these, 'alternative activation' (M2a; induced by IL-4 and/or IL-13) and 'acquired deactivation' (M2c; induced by IL-10, TGF-β1 or glucocorticoids) have received the most attention. Here, we assessed an M(IL-4) state and an M(IL-10) state. Microglial activation states are usually identified by altered expression of marker molecules, but less is known about functional correlates. Recently, we reported that several functions of rat microglia are activation state dependent. Migration was drastically reduced in a M(LPS) state but increased in M(IL-4) and M(IL-10) states (Lively and Schlichter, 2013; Siddiqui et al., 2014; Lam and

Schlichter, 2015), and myelin phagocytosis was increased in M(I+T) and M(IL-10) states but was unaffected in an M(IL-4) state (Siddiqui et al., 2016).

In attempting to identify therapeutic targets to modulate microglial activation, numerous studies are addressing the expression and contributions of several K^+ channels. Following acute CNS injury, rodent microglia *in situ* express inward-rectifier and outward-rectifier K^+ currents (Lyons et al., 2000; Boucsein et al., 2000; Menteyne et al., 2009) but their prevalence is controversial. *In vitro* studies have implicated Kir2.1 (Schlichter et al., 1996; Schilling et al., 2000; Muessel et al., 2013; Lam and Schlichter, 2016), and Kv1.3 channels (Schlichter et al., 1996; Kotecha and Schlichter, 1999; Draheim et al., 1999) in several microglia functions. However, there is evidence that expression of Kir and Kv currents can change with microglial activation and this is expected to affect channel contributions to cell functions. For instance, in rat microglia, Kir2.1 activity is required for migration under unstimulated, M(IL-4) and M(IL-10) states (Lam and Schlichter, 2015); whereas, in M(LPS) cells, Kv1.3 expression increased and contributed to neurotoxicity (Fordyce et al., 2005). Published results hint at differences in Kv1.3 and Kir2.1 currents between rat and mouse microglia.

Here, we directly compared responses of primary microglia from rat and mouse to the pro-inflammatory stimulus, I+T, and the anti-inflammatory stimuli, IL-4 and IL-10. First, gene expression patterns were compared for a wide variety of pro- and anti-inflammatory mediators, receptors, activation markers and immune modulators. Then, we compared Kir2.1 and Kv1.3 expression and channel activity (currents), and examined channel involvement in microglial migration. Our results show similarities and differences between these rodent species.

4.2 METHODS

Refer to Chapter 2 for the general procedure for each technique listed below.

Primary microglial cells. Pure rat and mouse microglia cultures were prepared by Dr. Xiaoping Zhu, Raymond Wong and myself. Microglia were unstimulated (control; CTL) or stimulated with 20 ng/mL IFN-γ plus 50 ng/mL TNF-α to induce a pro-inflammatory state [M(I+T)], or with 20 ng/mL IL-4 [M(IL-4)] or 20 ng/mL IL-10 [M(IL-10)] to induce anti-inflammatory states. For mRNA analysis and migration assays, cells were stimulated for 24 h. Patch clamping was conducted 30 h after stimulation to allow more time for trafficking and post-translational modifications.

Microglia staining. Dr. Lively conducted this experiment labelling microglia with Alexa Fluor 488-conjugated phalloidin (1:50 in PBS for 1 h; Invitrogen) to visualize filamentous (F-) actin.

Whole-cell patch clamp electrophysiology. A –15 mV correction was made at all voltages examined to account for the junction potential (–12.6 mV) and headstage leak (~ –3 mV), as indicated in the figure legends, Results text and voltage protocols.

Gene expression. Dr. Zhu prepared RNA samples from rat and mouse microglia that was unstimulated or stimulated with cytokines for 24 h. Samples were stored at –80ºC and used for NanoString and real-time qRT-PCR assays.

qRT-PCR*.* The expression of Kir2 subfamily members were compared in unstimulated rat and mouse microglia. qRT-PCR primers were designed by Dr. Zhu using "Primer3web" to detect the genes encoding *Kcnj2* (Kir2.1): forward (5'-ACCGCTACAGCATCGTCTCT-3') and reverse (5'-CTGCACTGTTGTCGGGTATG-3'); *Kcnj12 (*Kir2.2): forward (5'- AACCCCTACAGCATCGTATC-3') and reverse (5'-

GCACCTTGCCATTGCCAAA-3'); *Kcnj4* (Kir2.3): forward (5'-AACAAGTCCCAGCGCTACATG-3') and reverse (5'-AGGAAGGCCGCGGAGAAG-3'); and *Kcnj14* (Kir2.4): forward (5'-AGTGCATCGCAGGCT GTGTG-3') and reverse (5'-CACTGCGTTCTCACTGAAGAC-3'). Primers for the housekeeping gene, *Hprt1*, were: forward (5'-CAGTACAGCCCCAAAATGGT-3') and reverse (5'-CAAGGGCATATCCAACAACA-3').

Reagents. Inhibitor solutions were diluted to working concentrations of 20 μM ML133 and 5 nM AgTx-2.

Transwell migration and proliferation assay. Microglia were unstimulated or stimulated with I+T, IL-4 or IL-10 in the presence or absence of a channel blocker (ML133 or AgTx-2). Transmigration assay and data analysis was conducted by Dr. Lively.

Statistics. All graphical data are presented as mean ± SEM for the number of replicates indicated. The statistical significance was analyzed using GraphPad ver 6.01 (GraphPad Software, San Diego, CA) with either a one-way or two-way analysis of variance (ANOVA) with Dunnett's, Bonferroni, or Tukey's post-hoc analysis. For NanoString expression data, scaled counts were log2-transformed for statistical analysis. Main effect p values for each gene were determined using a one-way ANOVA, and adjusted using a 5% false discovery rate correction for multiple comparisons (Benjamini and Yekutieli, 2001) in R (version 3.3.1). Effects of stimulation on expression of a given gene were then determined using Dunnett's post-hoc analysis. Results were considered significant if $p < 0.05$. Nanostring data analysis was conducted by Dr. Lively.

4.3 Results

4.3.1 Morphology of rodent microglia depends on the activation state

Because the functional analysis in this study concerned microglial migration, we first compared microglia morphology between species and in response to activating stimuli. Previously, we had shown that rat microglia migrate in the direction of the lamellum, which usually contains a prominent ring of F-actin-rich podosomes that we called a 'podonut' (Vincent et al., 2012; Siddiqui et al., 2012; Lively and Schlichter, 2013). Podosomes are subcellular structures involved in adhesion and matrix degradation (Linder and Weisner, 2015).

(i) Unstimulated cells. Microglia of both species showed a similar initial morphology. They were mostly unipolar, with a uropod and a large lamellum containing a podonut (Fig. 4.1). There were both similarities and differences in their morphological responses to activating stimuli. Because the terminology for microglial activation is evolving, we will define our terminology according to the stimulus and three previously identified states.

(ii) M(I+T). To evoke a pro-inflammatory state (classical activation, M1), microglia were stimulated as before (Siddiqui et al., 2016) with a combination of IFN-γ and TNF-α. The shape of the cells changed dramatically, with subtle species differences. Rat microglia were clustered into chains of cells, while mouse microglia were more evenly distributed.

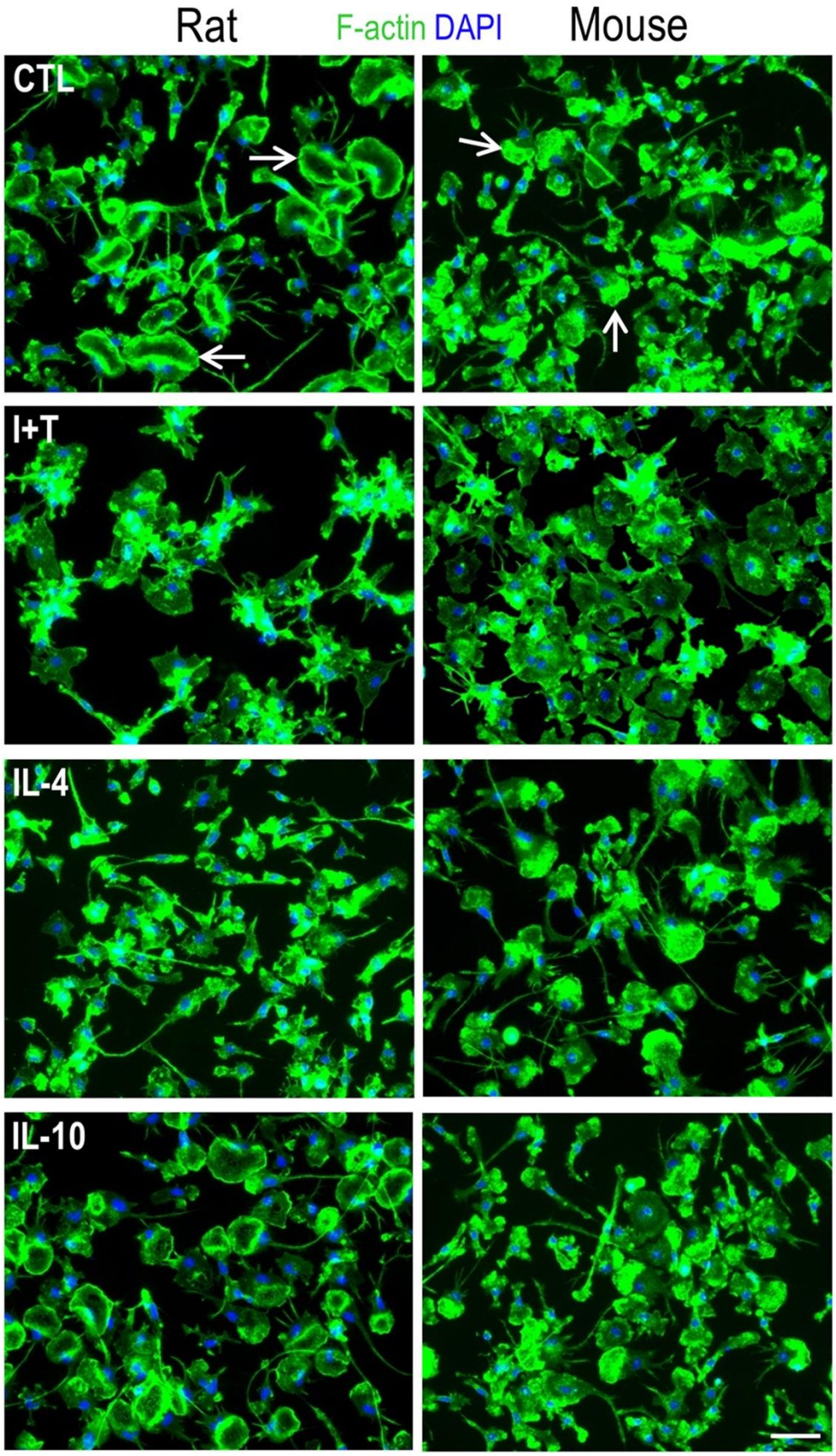
Rat
F-actin DAPI
Mouse
CTL
I+T
IL-4
IL-10

Figure 4.1. Effect of activation state on cell morphology. Rat and mouse microglia were unstimulated (CTL) or stimulated with IFN-γ and TNF-α (I+T), IL-4 or IL-10 for 24 h. Representative images of neonatal rat and mouse primary microglia labeled with phalloidin to visualize F-actin (green) and DAPI to label nuclei (blue). Arrows show examples of F-actin-rich podosomes organized into a ring-like structure (which we call a podonut) in the lamellum of unipolar microglia. Scale bar, 50 µm. Microglia staining was performed by Dr. Starlee Lively.

For both species, but especially in mouse microglia, individual cells often appeared flat and circular or amoeboid. There was no apparent cell polarity and, if cell processes were present, there were often more than three. ***(iii)*** M(IL-4). Microglia were stimulated with IL-4 to skew them towards an anti-inflammatory state (alternative activation, M2a). Both species showed many unipolar cells with podonuts. However, the morphology of rat microglia was more heterogeneous and lamellae were often smaller than in unstimulated rat cells or M(IL-4) mouse cells. ***(iv)*** M(IL-10). Microglia were stimulated with IL-10 to skew them toward an acquired deactivation state (M2c). For rat microglia, we previously reported that IL-10 increases the proportion of cells containing podonuts (Siddiqui et al., 2014), and this was the case in the present study. However, for IL-10–treated mouse microglia, an increase in podonuts was not evident and they continued to resemble unstimulated cells.

4.3.2 Comparing the inflammatory expression profile of rat and mouse microglia

Studies of CNS damage and disease can use mRNA expression to assess the evolution of inflammatory responses to injury. There is considerable interest in identifying markers to distinguish between pro- and anti-inflammatory states. Here, we used gene profiling to compare responses of rat and mouse microglia to the stimulation paradigms. Transcript expression was quantified for 58 genes that are known to be expressed in rodent microglia, and considered molecular markers for identifying microglia and its activation states (i.e., M1 and/or M2a phenotype) *in vitro* and *in vivo*. This includes pro- and anti-inflammatory mediators and their receptors, other immunomodulators, NOX

enzymes, as well as purinergic and phagocytic receptors. The nomenclature of some genes differs between rat (Table 2.1) and mouse (Table 2.2); for simplicity, the rat names will be used in the text.

Pro-inflammatory genes. (i) Unstimulated. As previously shown (Sivagnanam et al., 2010; Lively and Schlichter, 2013; Siddiqui et al., 2016), unstimulated (control; CTL) rat microglia were in a relatively resting state, exemplified by very low transcript levels (<100 mRNA counts) of typical pro-inflammatory mediators (*Nos2*, *Il6*, *Ptgs2* (COX-2), *Ifng* (IFN-γ) (Fig. 4.2). A similar starting state was seen for mouse microglia. Both species showed moderate transcript levels (>500 counts) of receptors for IFN-γ and TNF-α (except for very low *Ifngr2* in rat; 32±4 counts). ***(ii)*** M(I+T). *Rat:* We recently reported that I+T stimulation skews rat microglia toward a pro-inflammatory state, with elevated *Nos2*, *Tnf*, *Ptgs2* and *Il6* (Siddiqui et al., 2016), and this was confirmed here. In addition, there was increased transcript expression of *caspase 1 (Casp1;* also known as interleukin-1 converting enzyme (ICE), the protein kinase *Ptk2b* (PYK2), and TNF receptors (*Tnfrsf1a*, *Tnfrsf1b*). Expression was not altered for *Ifng* and its receptors (*Ifngr1, Ifngr2)*, or for *Il1b* and its receptor (*Il1r1*). *Mouse:* I+T treatment induced a similar transcript expression profile to rat, except for an increase in *Ifngr2* and lack of change in *Tnfrsf1b*. There were some species differences in the magnitude of gene induction. For instance, *Nos2* increased 1321 fold in rat microglia versus 230 fold in mouse, and *Ptgs2* increased 4 fold in rat versus 189 fold in mouse. ***(iii)*** M(IL-4). IL-4 treatment either did not alter transcript levels of the pro-inflammatory mediators or it decreased them (*Tnf* in rat; *Il1b* in both species). None were up-regulated. ***(iv)*** M(IL-10). IL-10 did not alter pro-inflammatory transcript levels, except for small increases in *Tnfrsf1a* (both species) and *Tnfrsf1b* (rat only). Overall, only I+T treatment increased the

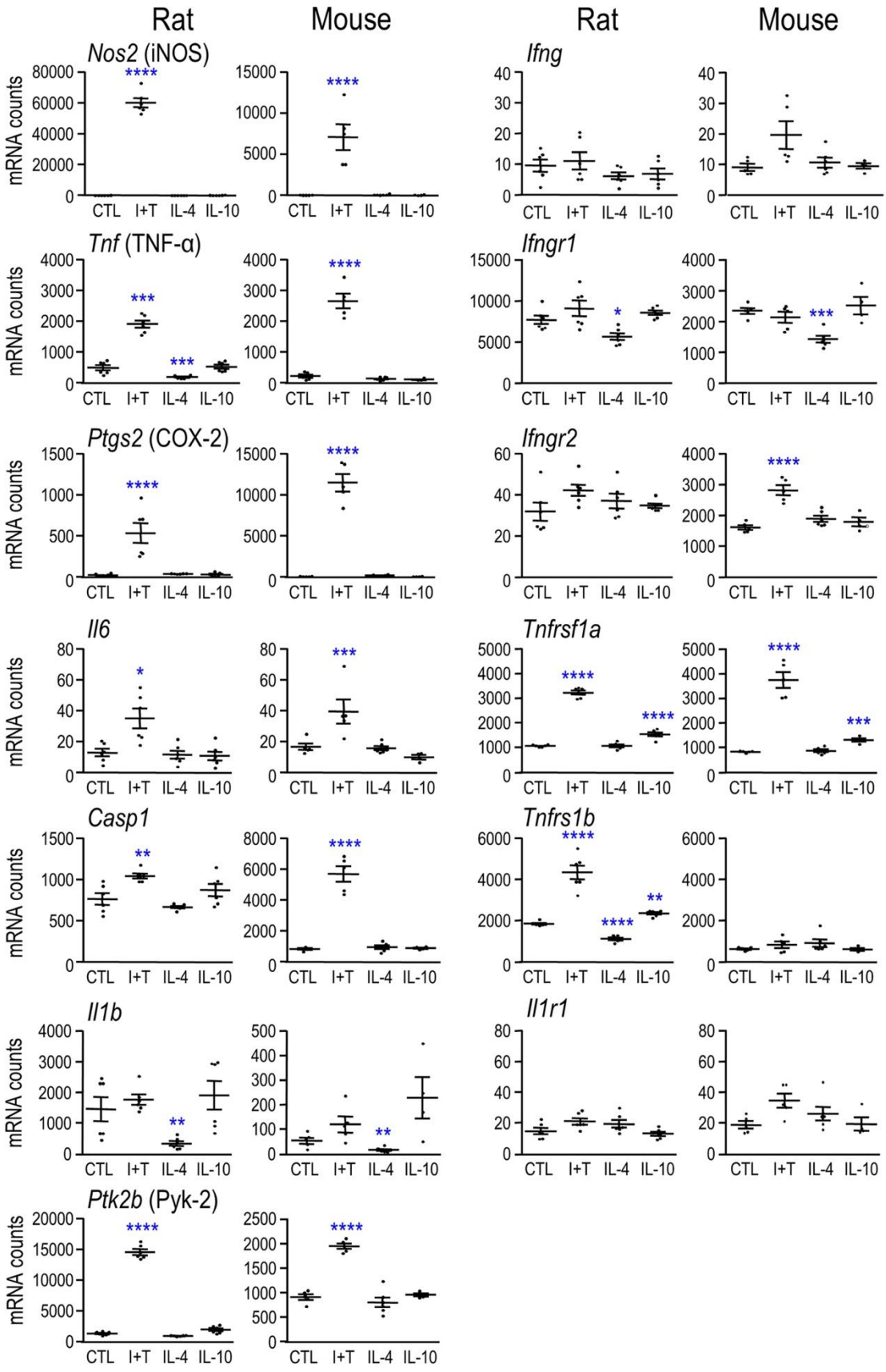
Rat
Mouse
Rat
Mouse
Nos2 (iNOS)
Ifng
Tnf (TNF-α)
Ifngr1
Ptgs2 (COX-2)
Ifngr2
Il6
Tnfrsf1a
Casp1
Tnfrs1b
Il1b
Il1r1
Ptk2b (Pyk-2)
mRNA counts
CTL
I+T
IL-4
IL-10

Figure 4.2. Transcript expression of pro-inflammatory mediators. Rat and mouse microglia were unstimulated (CTL) or stimulated with IFN-γ and TNF-α (I+T), IL-4 or IL-10 for 24 h. Relative mRNA counts for each gene were normalized to two housekeeping genes (described in Methods) and are shown as mean ± SEM (n=4–6 individual cultures). One symbol indicates p<0.05, two symbols, p<0.01, three symbols, p<0.001. NanoString data analyzed by Dr. Starlee Lively.

expression of pro-inflammatory genes, and some quantitative differences were seen between rat and mouse.

Anti-inflammatory and 'alternative' activation genes. It was previously found that IL-4 can up-regulate several molecules in mouse microglia, including arginase (ARG1), 'found in inflammatory zone' 1(FIZZ1), mannose receptor (MRC1), CCL22, CD163, and peroxisome proliferator-activated receptor gamma (PPAR-γ) (Franco and Fernandez-Suarez, 2015). Although less is known about IL-10–induced changes, it has been suggested that they are similar to LPS, but smaller (Chhor et al., 2013). It is not known whether responses to IL-4 or IL-10 differ between rat and mouse microglia. ***(i)*** Unstimulated. Under control conditions, microglia from both species had low transcript levels of several markers (*Arg1*, *Ccl22*, *Retnla* (FIZZ1), *Cd163*), and moderate levels of *Myc*, *Mrc1* and *Il1rn* (Fig. 4.3). Minor species differences were seen, in that *Pparg* levels were very low in mouse but moderate in rat. ***(ii)*** M(I+T). In both species, I+T increased transcript levels of *Il1rn* and decreased *Mrc1* and *Myc*. Species differences were an increase in *Arg1* in rat and *Ccl22* in mouse, and a decrease in *Pparg* in rat. ***(iii)*** M(IL-4). In both species, IL-4 increased transcript levels of *Arg1*, *Ccl22*, *Myc*, and *Mrc1*. Species differences were that in rat cells, only *Cd163* increased and *Il1rn* decreased; while in mouse, *Retnla*, *Pparg*, and *Il1rn* increased. ***(iv)*** M(IL-10). In both species, IL-10 elicited very different responses from IL-4. That is, IL-10 had very little effect, except for increasing *Il1rn* in rat microglia, and increasing *Mrc1* and decreasing *Myc* in mouse microglia. Several of these genes have been used to indicate 'alternative activation' (M2a) of rodent microglia but our results show that not all are reliable; e.g., the M1 stimulus (I+T) increased *Arg1* in rat and *Ccl22* in mouse.

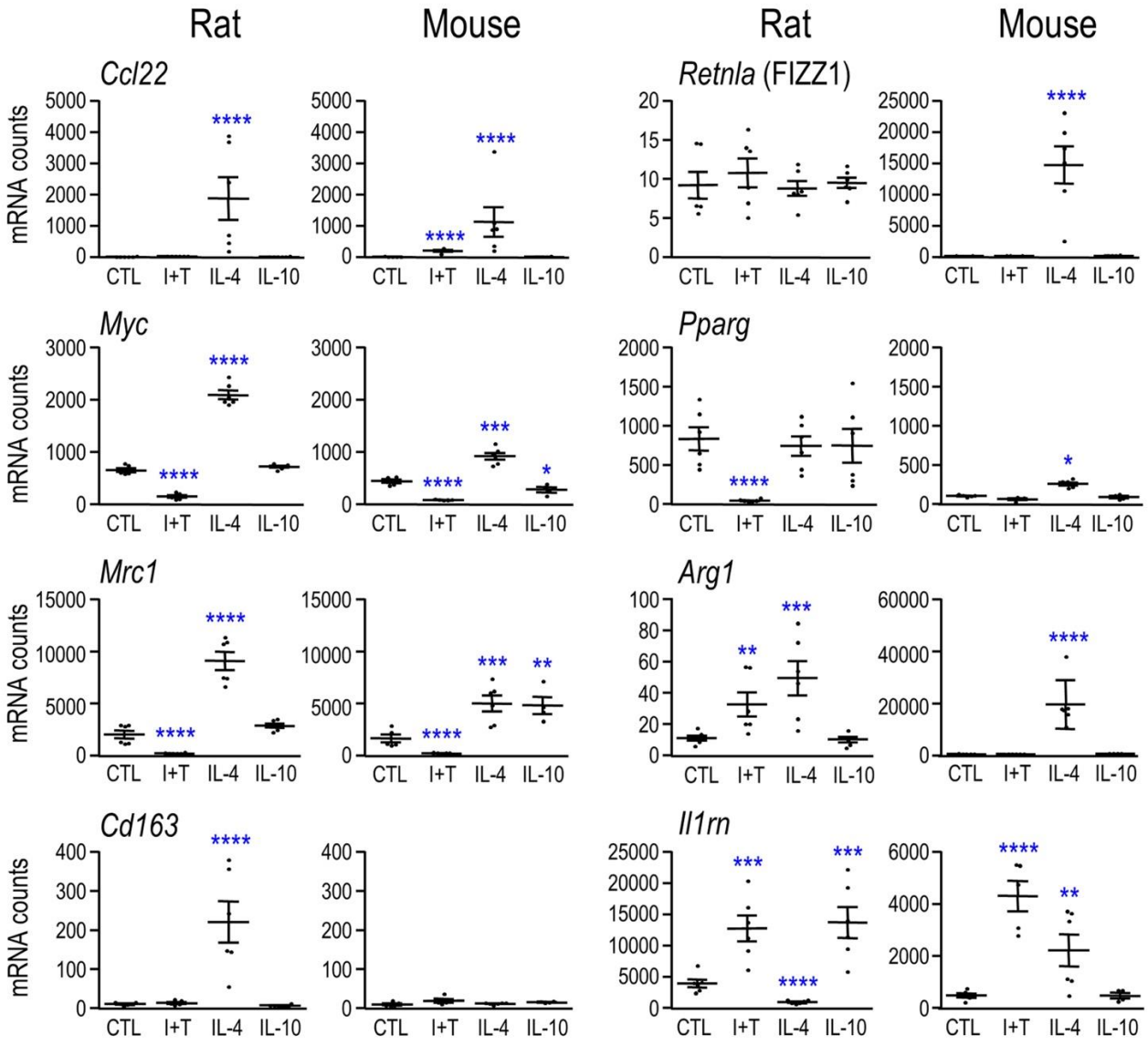

Figure 4.3. Transcript expression of markers associated with alternative (M2a) activation. Rat and mouse microglia were unstimulated (CTL) or stimulated with IFN-γ and TNF-α (I+T), IL-4 or IL-10 for 24 h. Relative mRNA counts for each gene were determined as in Figure 2, and are expressed as mean ± SEM (*n*=4–6 individual cultures). One symbol indicates $p<0.05$, two symbols, $p<0.01$, three symbols, $p<0.001$. NanoString data analyzed by Dr. Starlee Lively.

We next compared expression of the anti-inflammatory cytokines, IL-4, IL-10 and TGF-β1, and their receptors. ***(i)*** Unstimulated. In both species, *Il4* and *Il10* transcripts were initially very low. *Tgfb1* and the receptors for all three cytokines were moderately to highly expressed, except for low *Il4r* in mouse microglia (Fig. 4.4). ***(ii)*** M(I+T). In both species I+T stimulation increased transcript levels of *Il4r*, *Il13ra1*, *Il10ra* and *Tgfbr2*. Species differences were that *Tgfb1* decreased only in rat, *Il4* slightly decreased in mouse, *Il10rb* increased in rat, and *Tgfbr1* increased in mouse only. ***(iii)*** M(IL-4). In both species, IL-4 increased *Tgfb1* transcripts, and decreased *Il13ra1* and *Tgfbr2*. Species differences were decreases in *Il10rb* and *Tgfbr1* in rat only, and *Il10ra* in mouse only. ***(iv)*** M(IL-10). There was little effect on cytokine expression, except for an increase in *Tgfb1* transcripts in rat. In both species, IL-10 up-regulated expression of the receptors, *Il4r*, *Il13ra1* and *Tgfbr2*. *Il10rb* was increased in rat only.

4.3.3 Microglia markers, immune modulators

Next, we examined molecules that have been routinely used to identify 'activated' microglia after acute brain injury, as well as several immunomodulatory molecules (Fig. 4.5). ***(i)*** Unstimulated. Microglia of both species expressed low transcript levels of *Socs1* (suppressor of cytokine signaling 1) and *Socs3*. Both species showed moderate to very high levels of the other molecules: *Itgam* (CD11b), *Cd68*, *Cx3cr1*, toll-like receptor 2 (*Tlr2*), *Tlr4*, *Nfkbia* (IκBα; an endogenous inhibitor of NFκB), *Tspo* (translocator protein), *Nc3r1* (glucocorticoid receptor), and *Ptpn6* (Src homology region 2 domain-containing phosphatase-1; SHP-1). Surprisingly, *Aif1* (ionized Ca^{2+} binding adapter molecule 1, Iba1) was highly expressed in rat cells (>20,000 mRNA counts) but very low in mouse.

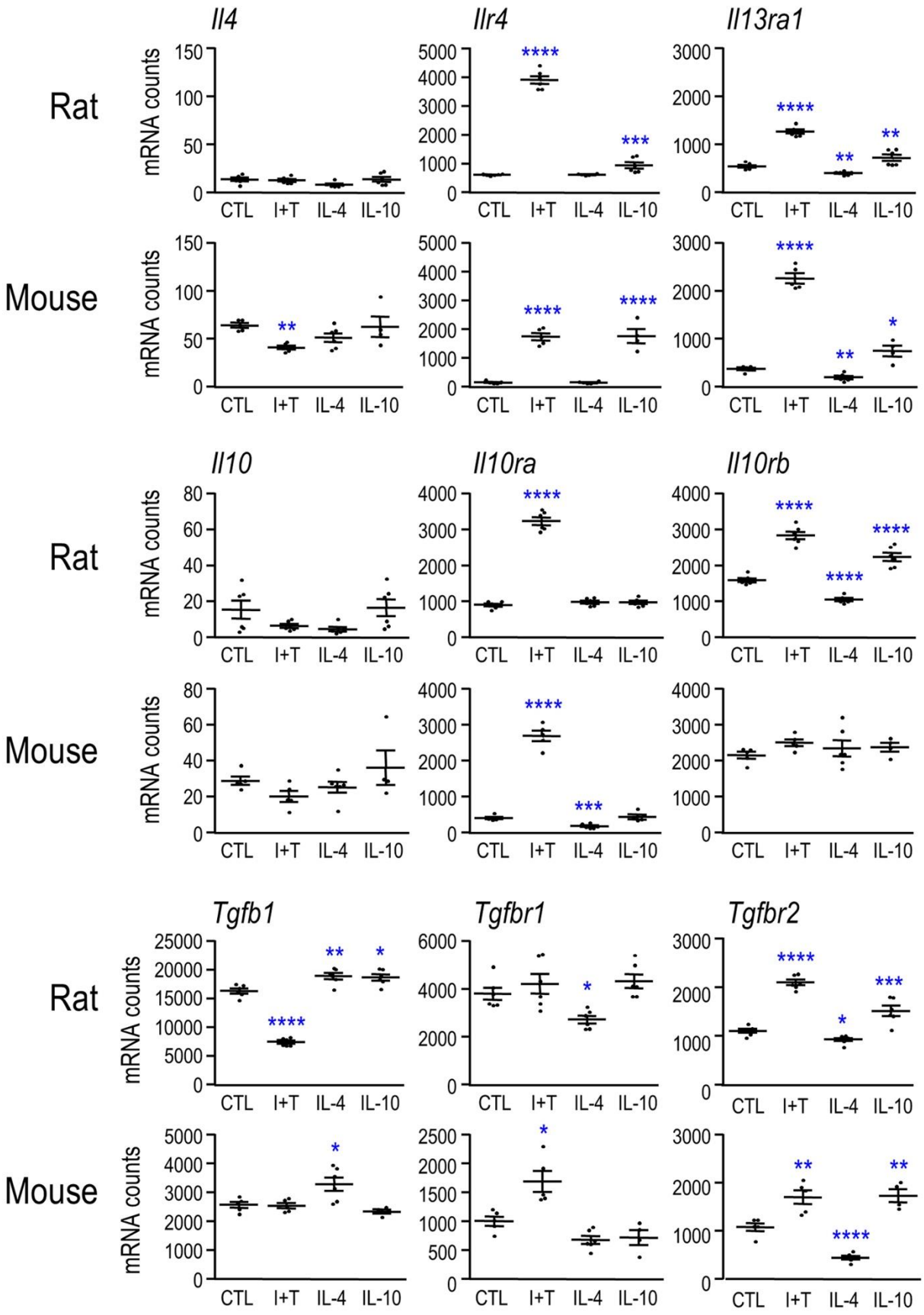
Il4
Ilr4
Il13ra1
Il10
Il10ra
Il10rb
Tgfb1
Tgfbr1
Tgfbr2
Rat
Mouse
mRNA counts
CTL
I+T
IL-4
IL-10

Figure 4.4. **Transcript expression of anti-inflammatory cytokines and their receptors.** Rat and mouse microglia were unstimulated (CTL) or stimulated with IFN-γ and TNF-α (I+T), IL-4 or IL-10. Relative mRNA counts for each gene were determined as in Figure 4.2, and are expressed as mean ± SEM (n=4–6 individual cultures). One symbol indicates $p<0.05$, two symbols, $p<0.01$, three symbols, $p<0.001$. NanoString data analyzed by Dr. Starlee Lively.

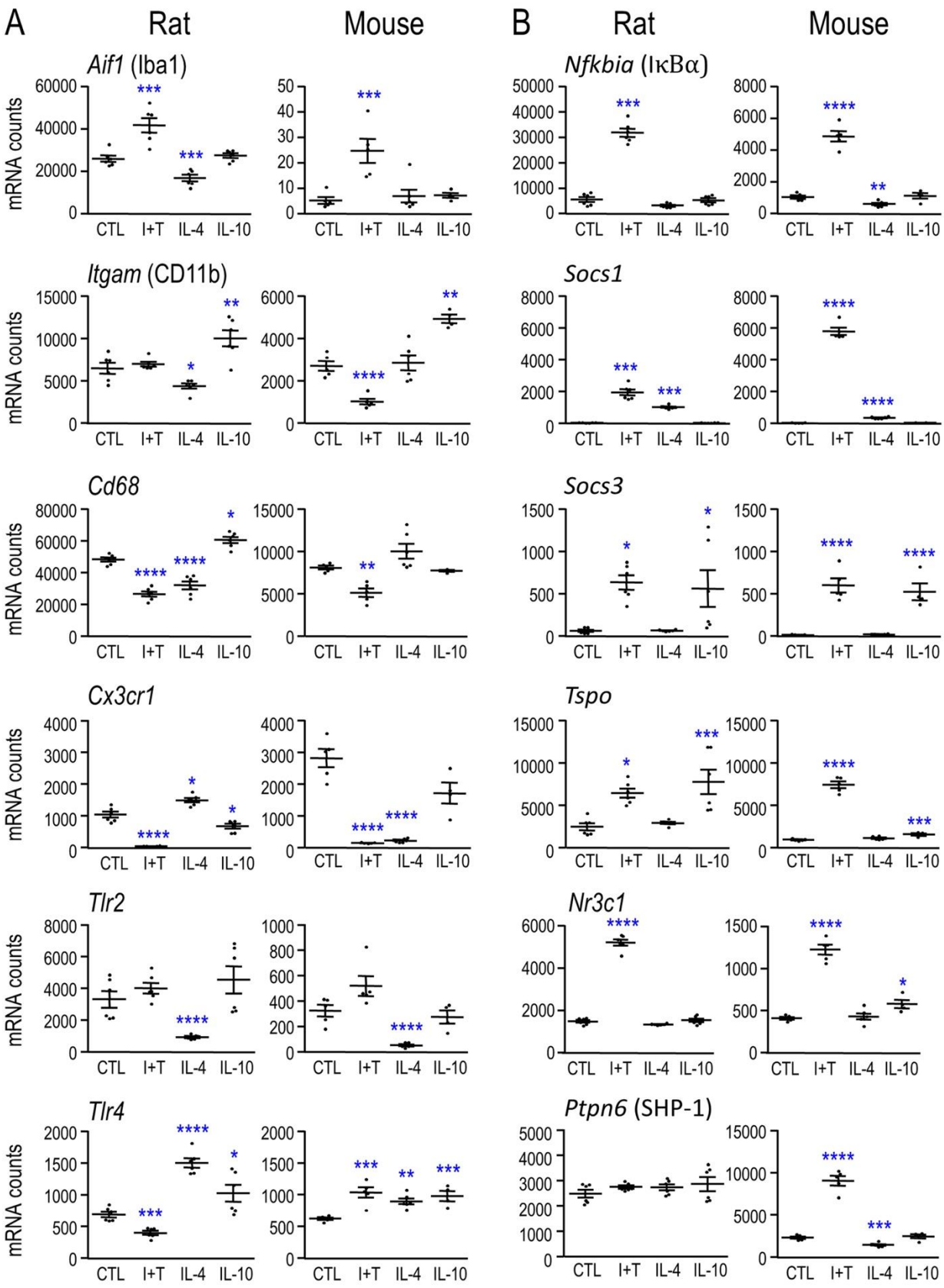
A
Rat
Mouse
B
Rat
Mouse
Aif1 (Iba1)
Nfkbia (IκBα)
Itgam (CD11b)
Socs1
Cd68
Socs3
Cx3cr1
Tspo
Tlr2
Nr3c1
Tlr4
Ptpn6 (SHP-1)
mRNA counts
CTL
I+T
IL-4
IL-10

Figure 4.5. Transcript expression of other microglia markers and immunomodulatory molecules. Rat and mouse microglia were unstimulated (CTL) or stimulated with IFN-γ and TNF-α (I+T), IL-4 or IL-10. Relative mRNA counts for each gene were determined as in Figure 4.2, shown as mean ± SEM (n=4–6 individual cultures). One symbol indicates $p<0.05$, two symbols, $p<0.01$, three symbols, $p<0.001$. NanoString data analyzed by Dr. Starlee Lively.

(ii) M(I+T). In both species, I+T stimulation increased expression of *Aif1*, *Nc3r1*, *Nfkbia*, *Socs1*, *Socs3*, and *Tspo* but decreased *Cd68* and *Cx3cr1*. Species differences were increases in *Ptpn6* and *Tlr4* in mouse only, and decreases in *Itgam* in mouse and *Tlr4* in rat. ***(iii)*** M(IL-4). In both species, IL-4 increased expression of *Tlr4* and *Socs1*, and decreased *Tlr2*. Species differences were an increase in *Cx3cr1* expression in rat versus a decrease in mouse; decreased *Aif1*, *Itgam* and *Cd68* in rat only; and decreased *Nfkbia* and *Ptpn6* in mouse only. ***(iv)*** M(IL-10). In both species, IL-10 increased expression of *Itgam*, *Tlr4*, *Socs3*, and *Tspo*. Species differences were an increase in *Cd68* and decrease in *Cx3cr1* in rat only; and a small increase in *Nc3r1* in mouse only. Interestingly, *Itgam* (in rat and mouse microglia) and *Cd68* (in rat) were the only genes selectively up-regulated by IL-10 treatment. Our results suggest that increased transcript expression of *Nfkbia*, *Aif1*, and possibly *Nc3r1* (but it also increased slightly after IL-10 treatment in mouse) mark the pro-inflammatory state in both species. The other genes examined were not selective activation state markers in either species: *Itgam*, *Cd68*, *Cx3cr1*, *Tlr2*, *Tlr4*, *Socs1*, *Socs3*, *Tspo*, and *Ptpn6*. It is also notable that the pro-inflammatory I+T treatment decreased *Cx3cr1*, which is often used to identify microglia; and *Cd68*, which is often used to identify phagocytic cells.

4.3.4 Purinergic and phagocytic receptors and NADPH oxidase enzymes

We have included some additional data (Fig. A.1) that will not be discussed in detail but are a useful resource. To follow on our recent study of rat microglia that examined myelin phagocytosis and consequent production of reactive oxygen species (ROS)

(Siddiqui et al., 2016), we have included a species comparison of transcript levels of several phagocytic receptors, and NOX enzymes. Several purinergic receptors were also examined because they can modulate phagocytosis, ROS production, cytokine secretion, and migration of microglia (Pocock and Kettenmann, 2007). ***(i)*** Unstimulated. Microglia from both species had low transcript levels (<500 mRNA counts) of *Nox1*, *Nox4*, *P2rx7*, *P2ry2*, and *P2ry12;* and high levels (>2500 mRNA counts) of *Cybb* (NOX2), *Fcgr2b*, *Fcgr3a*, and *Msr1* (SR-A). The main species differences were the much higher levels of *Ncf1, Fcgr1a and Trem2* in rat. ***(ii)*** M(I+T). In both species, this pro-inflammatory treatment increased transcript levels of *Ncf1*, *Cybb*, and *Fcgr3a*, and decreased *Trem2*. Species differences were opposite changes in *Fcgr1a*, and an increase in *P2ry2* and decreases in *Msr1 and P2ry12* in rat only. ***(iii)*** M(IL-4). Expression of *Cybb* and *Fcgr1a* was decreased in both species, but all other changes were species dependent. This anti-inflammatory treatment affected most of the genes examined in rat microglia, but few in mouse cells. In rat only, *Fcgr2b*, *P2ry2* and *P2ry12* increased, while *Ncf1, Fcgr3a*, *Trem2* and *Msr1* decreased. Interestingly, *P2ry12* decreased in mouse cells. The only other mouse-specific change was a small increase in *Nox1*. ***(iv)*** M(IL-10). In both species, IL-10 treatment increased *Fcgr1a*, *Fcgr2b*, *Fcgr3a* and *Msr1* transcripts. There were several species differences. *Cybb* and *P2ry2* increased only in rat, while *Trem2* increased in rat but decreased in mouse. Of note, *P2rx7* transcripts remained low in both species and were unaffected by any treatment tested.

4.3.5 Comparing expression of Kir2 and Kv1 channel genes

Primary rat and mouse microglia express Kir2.1 mRNA and protein (Muessel, 2013; Lam & Schlichter, 2015) but other Kir2-family members have not been assessed. Because these channels can function as homotetramers or heterotetramers (Hibino et al., 2010), we first compared expression of *Kcnj2* (Kir2.1), *Kcnj12* (Kir2.2), *Kcnj4* (Kir2.3) and *Kcnj14* (Kir2.4). [Kir2.5 was omitted because it is electrically silent and Kir2.6 omitted because it is expressed primarily in skeletal muscle (Ryan et al., 2010; Dassau et al., 2011).] In both rodent species, transcript expression of Kir2.1 predominated (Fig. 4.6A), and expression of *Kcnj12*, *Kcnj4* and *Kcnj14* was not affected by the microglial activation state (not shown). Thus, homomeric Kir2.1 channels likely produce the inward-rectifying K^+ current in both species, which is important because the blocker we used (ML133) can affect other Kir2 members (Wang et al., 2011).

Kv1.2, Kv1.3 and Kv1.5 mRNA and protein have been detected in primary rat microglia (Kotecha & Schlichter, 1999; Khanna et al., 2001; Fordyce et al., 2005; Li et al., 2008). In primary mouse microglia, Kv1.3 and Kv1.5 have been detected (Pannasch et al., 2006), but we found no reports of Kv1.2 expression. We used NanoString to compare species transcript expression of *Kcna2* (Kv1.2), *Kcna3* (Kv1.3) and *Kcna5* (Kv1.5), and *Kcnj2* (Kir2.1) in different activation states (Fig. 4.6B). Again, quantitative expression was reported as relative mRNA counts per 200 ng of RNA. ***(i)*** Unstimulated. The main species difference was in the magnitude of *Kcnj2* expression, which was high (1901 ± 256 counts) in rat microglia and moderate in mouse cells (379 ± 36 counts). Both species expressed low levels of *Kcna2*, *Kcna3* and *Kcna5* (≤100 counts).

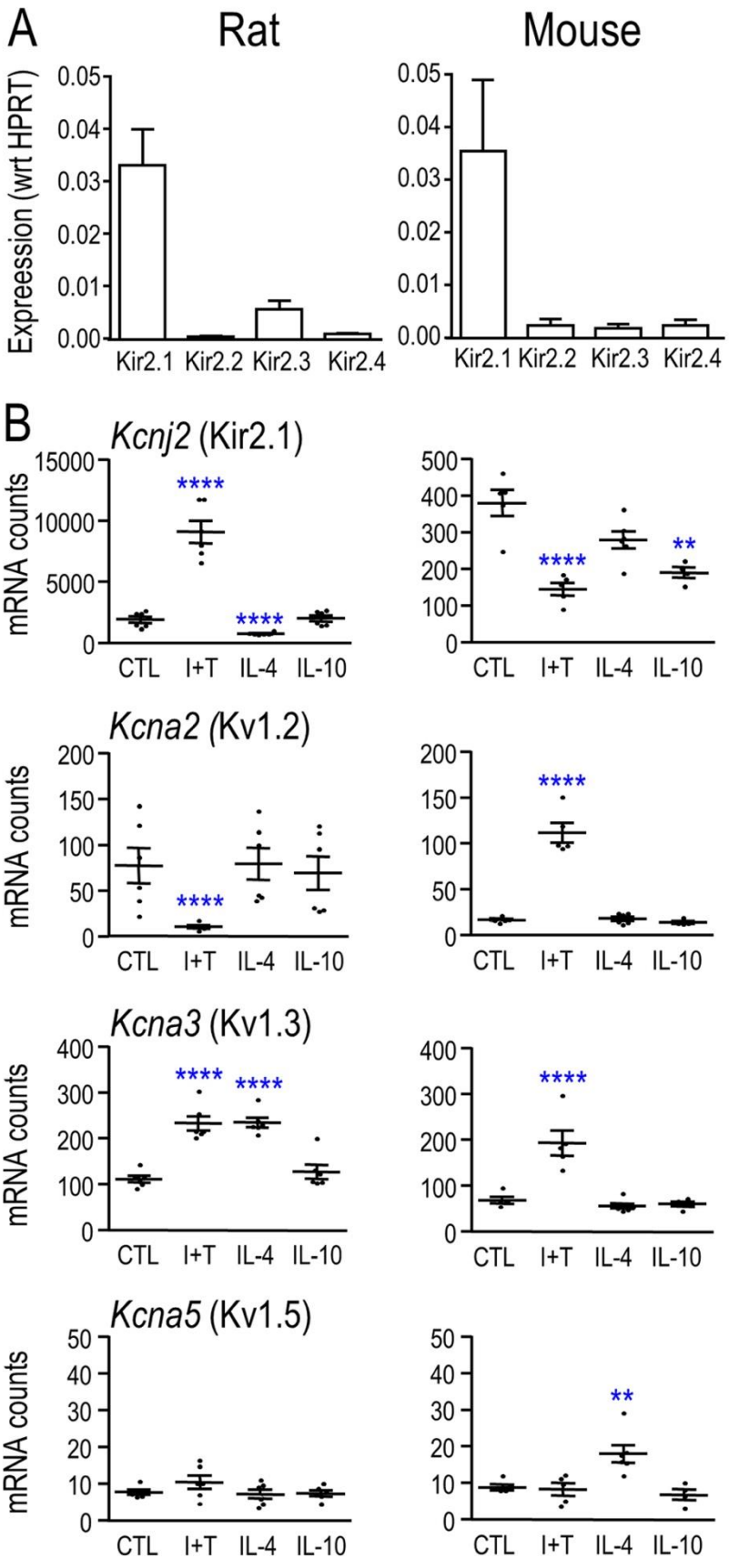
A
Rat
Mouse
Expression (wrt HPRT)
0.05
0.04
0.03
0.02
0.01
0.00
Kir2.1 Kir2.2 Kir2.3 Kir2.4
B
Kcnj2 (Kir2.1)
Kcna2 (Kv1.2)
Kcna3 (Kv1.3)
Kcna5 (Kv1.5)
mRNA counts
CTL I+T IL-4 IL-10
****
**

Figure 4.6. K^+ channel transcript expression. Rat and mouse microglia were unstimulated (CTL) or stimulated with IFN-γ and TNF-α (I+T), IL-4 or IL-10. **A.** Real-time qRT-PCR analysis of the expression of Kir2 subfamily members in rat and mouse unstimulated microglia (*n*=6 individual cultures. **B.** As in Figure 4.2, Relative mRNA counts for each K^+ channel gene was determined (*n*=4–6 individual cultures). Data are shown as mean ± SEM. One symbol indicates $p<0.05$, two symbols, $p<0.01$, three symbols, $p<0.001$, four symbols, 0.0001. Primers used for qRT-PCR were designed by Dr. Xiaoping Zhu and NanoString data analyzed by Dr. Starlee Lively.

(ii) M(I+T). *Kcnj2* expression showed a striking species difference. It increased 4.8 fold in rat microglia (to 9087 ± 907 counts) but decreased 2.6 fold in mouse. Conversely, *Kcna2* decreased 7.4 fold in rat but increased 6.8 fold in mouse. In both species, *Kcna3* increased (2.1 fold in rat, 2.8 fold in mouse) while *Kcna5* was not affected. ***(iii)*** **M(IL-4).** In mouse microglia, there was little to no effect on K^+ channel expression, and although Kcna5 increased 2 fold, the level remained very low (18 counts). However, in rat cells, Kcna3 increased 2.1 fold (to 235 ± 11 counts) and Kcnj2 decreased 2.5 fold (to 750 ± 45 counts). **(iv)** M(IL-10). The only effect seen was a 2 fold decrease in Kcnj2 in mouse cells.

The most notable species differences in K^+ channel mRNA expression were the opposite changes evoked by I+T in *Kcnj2* and *Kcna2*, and the IL-4 evoked increase in *Kcna3* in rat only. However, channel activity can also be regulated post-translationally, including trafficking to the surface membrane and second-messenger signaling. Kir2.1 and Kv1.3 currents have been well characterized in microglia *in vitro* (Eder, 2005; Kettenmann et al., 2011), and here we undertook a direct comparison under each activation state. Total inward and outward currents were monitored and then, specific voltage protocols and channel blockers were used to isolate and quantify Kir2.1 and Kv1.3 currents. Because the microglial morphology changed with activation state (Fig. 4.1), we first compared the cell capacitance as an indicator of the cell size. The capacitance did not differ under any activation condition or between species (Table 3.3). Subsequently, currents were recorded from microglia with the most prevalent morphologies; i.e., unipolar for unstimulated, M(IL-4) and M(IL-10); rounded or amoeboid for M(I+T).

Table 4.1. Comparison of cell capacitance in rat and mouse microglia in different activation states

		Capacitance (pF); mean ± SEM (n)		Rat versus mouse differences
	Morphology	**Rat**	**Mouse**	
control	Unipolar	25.8 ± 1.2 (54)	24.1 ± 1.4 (46)	*NS*
I+T	Amoeboid	29.8 ± 2.4 (30)	25.0 ± 1.0 (45)	*NS*
IL-4	Unipolar	25.4 ± 1.4 (48)	24.8 ± 1.2 (29)	*NS*
IL-10	Unipolar	28.1 ± 1.3 (34)	29.0 ± 2.0 (27)	*NS*

Data are expressed as mean pF ± SEM (number of cells). Two-way ANOVA with Bonferroni's post-hoc test reported no statistical differences (NS) between species for each stimulation paradigm, as well as across activation states within a given species (not shown).

4.3.6 Comparing the inward-rectifier (Kir) current

Microglia Kir currents displayed the stereotypical features of Kir2.1 (Fig. 4.7A). This current activates at negative potentials due to relief of channel block by internal Mg^{2+} and polyamines (Hibino et al., 2010; Baronas and Kurata, 2014), and then the current relaxes at very negative potentials due to time-dependent block by external Na^{+} (Kubo et al., 1993; Nörenberg et al., 1994).

To quantify the Kir2.1 component of the whole-cell current, we used ML133, a membrane-permeant blocker (Wang et al., 2011) that acts in a time-dependent manner with an IC_{50} ~3.5 μM in rat microglia (Lam & Schlichter, 2015). Regardless of the microglial activation state, most of the Kir current (82–86% in rat, 85–95% in mouse) was blocked by 20 μM ML133 (Fig. 4.7B), and the small remaining current had a linear current-versus-voltage (I-V) relation (not shown). Thus, to examine whether microglial activation states affect channel activity, we compared the total Kir current density. In both species, the I-V relations showed inward rectification and reversal at about –82 mV with junction potential and headstage leak correction, which is close to the K^{+} Nernst potential (Fig. 4.7C). ***(i)*** Unstimulated. Both rodent species displayed a similar magnitude of Kir2.1 current (Fig. 4.7A, C) despite the differences in mRNA counts (Fig. 4.6B). Species differences were seen under all activation states examined (Fig. 4.7C). ***(ii)*** M(I+T). The Kir2.1 current decreased in mouse cells but was unchanged in rat. ***(iii)*** M(IL-4). The Kir2.1 current decreased substantially in rat cells but was unchanged in mouse. ***(iv)*** M(IL-10). The Kir2.1 current decreased in mouse cells but was unchanged in rat. Overall, the Kir2.1 current amplitude is not a reliable indicator of the microglial activation state, but instead depends on both the rodent species and activating stimulus.

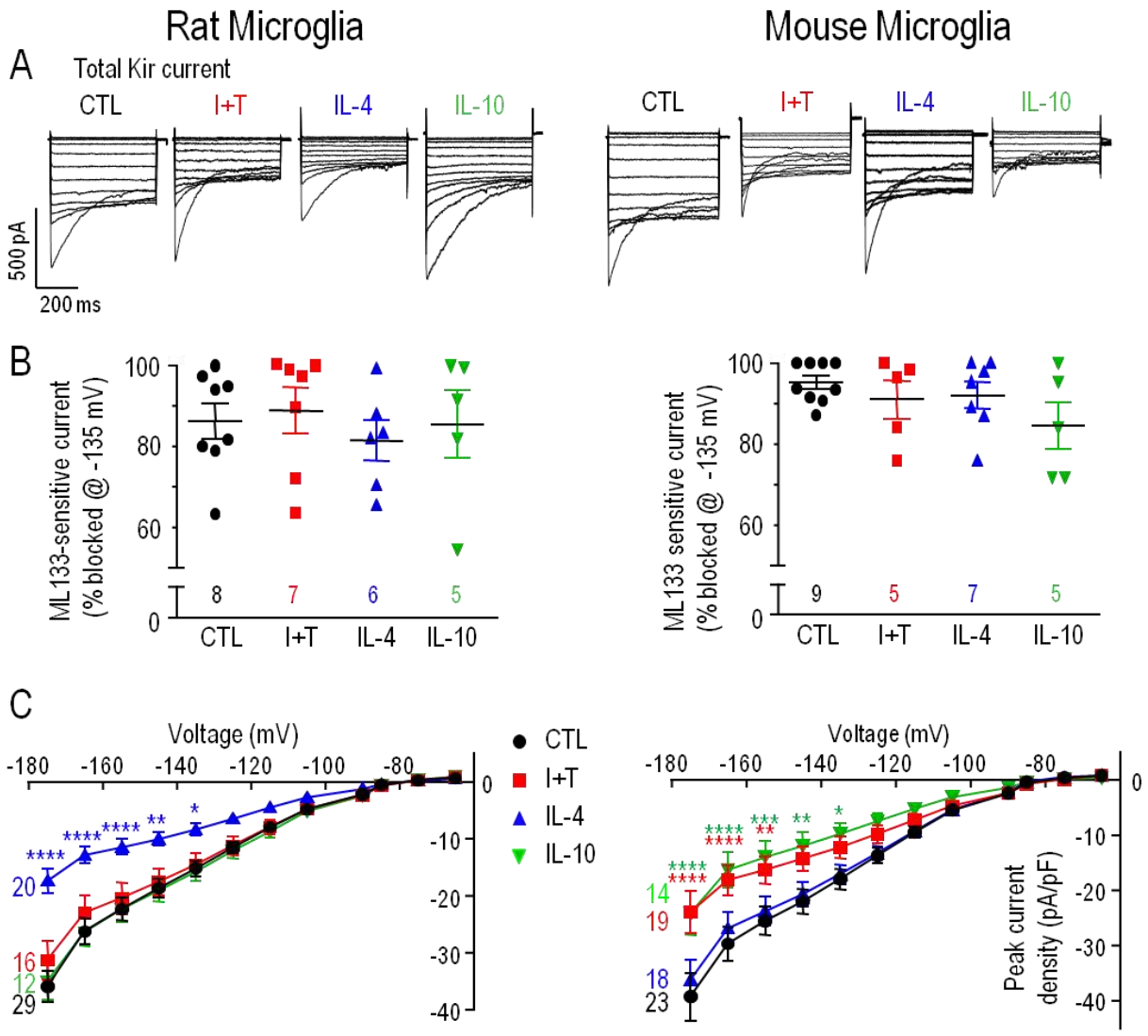
Rat Microglia
Mouse Microglia
A
Total Kir current
CTL
I+T
IL-4
IL-10
500 pA
200 ms
B
ML133-sensitive current
(% blocked @ -135 mV)
ML133 sensitive current
(% blocked @ -135 mV)
100
80
60
0
8
7
6
5
9
5
7
5
C
Voltage (mV)
-180
-160
-140
-120
-100
-80
0
-10
-20
-30
-40
Peak current
density (pA/pF)
20
16
12
29
14
19
18
23

Figure 4.7. Inward-rectifier (Kir) current versus activation state. Rat and mouse microglia were unstimulated (CTL) or stimulated for 30 h with IFN-γ and TNF-α (I+T), IL-4 or IL-10. Whole-cell Kir currents were recorded in response to a voltage protocol with test pulses between –175 and –65 mV in 10 mV increments from a holding potential of -15 mV. **A.** Representative traces of total Kir current in primary rat (left column) and mouse (right column) microglia. **B.** Scatterplot of individual cells showing the proportion of the peak inward current (at –135 mV) that was blocked by 20 μM ML133. **C.** Current-voltage (I-V) relations for the total Kir current, where peak current density (pA/pF) was plotted as a function of voltage. Data are shown as mean ± SEM (number of cells). One symbol indicates $p<0.05$, two symbols, $p<0.01$, three symbols, $p<0.001$, four symbols, 0.0001

4.3.7 Comparing the outward-rectifier (Kv) current

Kv1-family members are activated by depolarization but inactivate with sustained depolarization. Thus, the current amplitude depends on both the holding potential and test potential. The voltage dependence of activation and steady-state inactivation can also be modulated, as shown for Kv1.3 (Bowlby et al., 1997; Chung & Schlichter, 1997a, b), so it is crucial to quantify the current over a range of potentials. In addition, a hallmark of Kv1.3 is cumulative inactivation, which is seen as a use-dependent decrease in current if successive depolarizing pulses are delivered with too little interpulse delay (Grissmer et al., 1994; Nörenberg et al., 1994; Kotecha & Schlichter, 1999; Cayabyab et al., 2000). For rat microglia, substantial cumulative inactivation is evoked by repetitive pulses every 1 s (Nörenberg et al., 1994) or 5 s (Cayabyab et al., 2000; Kotecha & Schlichter, 1999), while an interpulse interval of 60 s ensures complete recovery from inactivation (Kotecha & Schlichter, 1999). Therefore, to quantify Kv currents in rat microglia, we used a holding potential of –105 mV to relieve channel inactivation, and used 60 s intervals between successive depolarizing steps. Agitoxin-2 (AgTx-2) is an extremely potent Kv1.3 blocker (Garcia et al., 1994), with a K_d of 177 pM in activated T lymphocytes (Kotecha & Schlichter, 1999). To quantify the Kv1.3 component, 5 nM AgTx-2 was perfused into the bath, and the remaining unblocked current was subtracted. The entire rat protocol required ~20 min per recording. Because recordings from mouse microglia did not usually last as long, it was necessary to modify the protocol. A voltage ramp from –75 to +45 mV was applied from the –105 mV holding potential, after the protocol was validated by ensuring that the amplitude at +45 mV was the same as for a single voltage step.

Rat microglia. Kv currents were observed in every rat microglial cell examined under all activation conditions (Fig. 4.8A), and the proportion blocked by AgTx-2 was similar (64–77%; Fig. 4.8B). The remaining current had a nearly linear I-V relation without time dependence during steps (not shown), and was not identified. In all activation states, the total Kv current and AgTx-2 sensitive Kv1.3 component activated in a time- and voltage-dependent manner above about –50 mV (corrected for junction potential), and it increased with depolarization (Fig. 4.8A, C). Time-dependent inactivation was also apparent during depolarizing test pulses. M(I+T) cells had increased total Kv current and AgTx-2 sensitive components. M(IL-4) treatment also increased the currents but to a lesser degree. The currents in M(IL-10) cells did not differ from unstimulated cells.

Mouse microglia. Examples of Kv currents in mouse microglia under each activation state are shown in Figure 4.9A. The first striking species difference was their lower prevalence in mouse; i.e., ~56% (19/34) of unstimulated cells, ~42% (10/24) of M(IL-4) cells, and ~56% (9/16) of M(IL-10) cells. In contrast, ~92% of M(I+T) cells had Kv currents (23/25 cells). A second species difference was that in mouse cells expressing a Kv current, AgTx-2 blocked a lower proportion of the Kv current: ~42% (15 cells) in unstimulated cells, ~37% (7 cells) in M(IL-4) cells, ~37% (8 cells) in M(IL-10) cells, and ~61% (17 cells) in M(I+T) cells (Fig. 4.9B). This suggests that mouse microglia express other Kv currents. The AgTx-2 sensitive Kv1.3 current in mouse microglia activated at about –50 mV (Fig. 4.9C), similar to rat cells. We then compared the total Kv and AgTx-2 sensitive current densities under the different activation states. M(I+T) cells had larger Kv and Kv1.3 currents (Fig. 4.9C), which was consistent with the mRNA data (Fig. 4.6A), and similar to rat microglia (Fig. 4.8). Unlike rat, M(IL-4) mouse

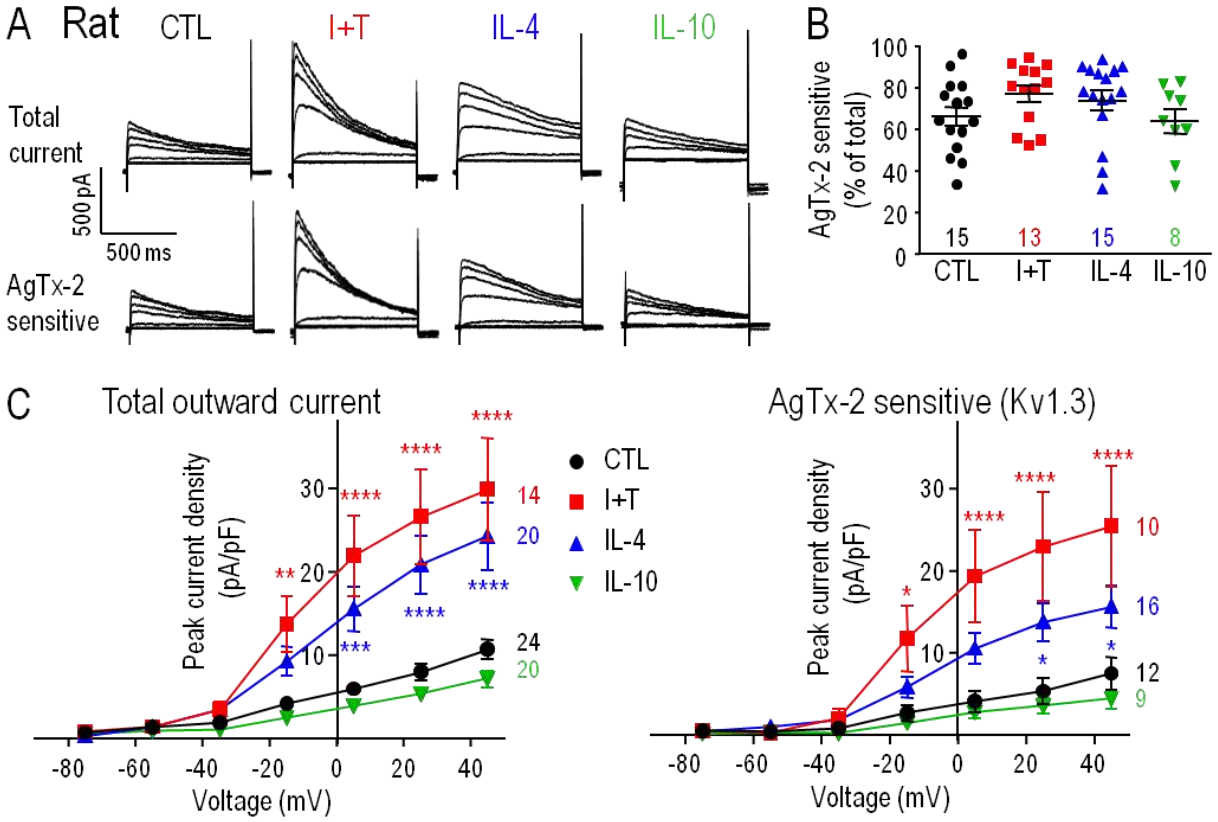

Figure 4.8. Rat microglia: AgTx-2 sensitive Kv1.3 currents versus activation state. Whole-cell Kv currents were isolated using a voltage clamp protocol holding at –105 mV, followed by 1s long voltage steps from –75 to +45 mV in 20 mV increments, applied every 60 s. **A.** Representative traces of total Kv current in unstimulated (CTL) rat microglia, and in cells stimulated for 30 h with IFN-γ and TNF-α (I+T), IL-4 or IL-10. For each cell, 5 nM AgTx-2 was perfused into the bath to record the AgTx-2 insensitive component, which was then subtracted from the total current to yield Kv1.3 current. **B.** Scatter plot of individual cells showing the proportion of the peak current (at +45 mV) that was blocked by AgTx-2. **C.** Peak current density (pA/pF) as a function of voltages for the total Kv (left) and the AgTx-2 sensitive Kv1.3 (right) currents. Data are shown as mean ± SEM (number of cells). One symbol indicates $p<0.05$, two symbols, $p<0.01$, three symbols, $p<0.001$, four symbols, $p<0.0001$

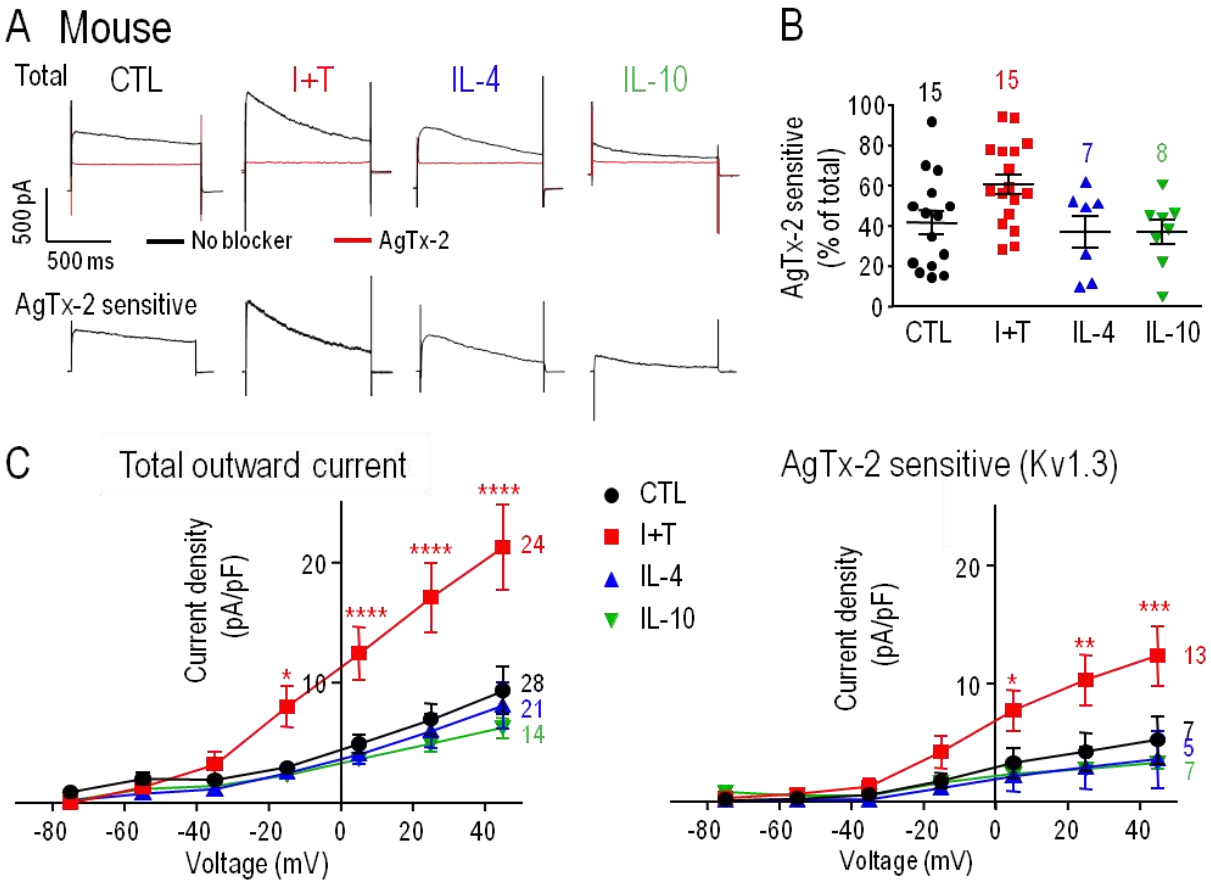
A Mouse
Total
CTL
I+T
IL-4
IL-10
500 pA
500 ms
No blocker
AgTx-2
AgTx-2 sensitive
B
AgTx-2 sensitive (% of total)
15
15
7
8
CTL
I+T
IL-4
IL-10
C
Total outward current
Current density (pA/pF)
Voltage (mV)
CTL
I+T
IL-4
IL-10
24
28
21
14
AgTx-2 sensitive (Kv1.3)
13
7
5
7

Figure 4.9. Mouse microglia: AgTx-2 sensitive Kv1.3 currents versus activation state. Whole-cell Kv currents were recorded using a modified voltage protocol. From a holding potential of –105 mV, a single step to +45 mV was applied for 1 s before returning to –105 mV for 60 s, and then a voltage ramp was applied from –75 to +45 mV over 120 ms. **A.** Representative traces of Kv currents in the absence and presence of 5 nM AgTx-2 at +45 mV in unstimulated (CTL) cells, and in cells stimulated for 30 h with IFN-γ and TNF-α (I+T), IL-4 or IL-10. For each cell, AgTx-2 was perfused into the bath to record the AgTx-2 insensitive component, which was then subtracted from the total current to yield the Kv1.3 current. **B.** Scatter plot of individual cells showing the proportion of the peak current (at +45 mV) that was blocked by AgTx-2. **C.** Peak current density (pA/pF) as a function of voltage was plotted from the voltage-ramp component: total Kv current (left), AgTx-2 sensitive Kv1.3 current (right). All data are shown as mean ± SEM (number of cells). One symbol indicates $p<0.05$, two symbols, $p<0.01$, three symbols, $p<0.001$, four symbols, $p<0.0001$

cells had the same current densities as unstimulated cells. In both species, M(IL-10) had no effect.

While changes in the prevalence and amplitude of Kv and Kv1.3 currents were seen with the stimuli tested, theses currents are apparently not reliable indicators of the microglial activation state and also differ with the species.

4.3.8 Kir2.1 and Kv1.3 channel activity contribute to microglial migration

Very little is known about migration of mouse microglia in different activation states or roles of Kir2.1 and Kv1.3 channels in migration of rodent microglia (see Discussion). Thus, we compared these aspects in both species under all four states. ***Rat.*** M(I+T) cells migrated less (2.9 fold) than unstimulated cells, while M(IL-4) and M(IL-10) migrated more, by 1.8 fold and 2.4 fold, respectively (Fig. 4.10A). Blocking Kir2.1 channels (20 μM ML133) reduced migration by 2.6 fold in M(IL-4) cells and 3.7 fold in M(IL-10) cells (Fig. 4.10B). Although ML133 reduced migration by 2.8 fold in unstimulated cells and 4 fold in M(I+T) cells, the ANOVA result did not show statistical significance, likely because migration was not as high as with IL-4 or IL-10 treatment. Blocking Kv1.3 (5 nM AgTx-2) increased migration of unstimulated microglia (2.9 fold), M(IL-4) cells (1.7 fold), and M(IL-10) cells (1.6 fold). ***Mouse.*** Effects of the activation state on migration were similar to rat. Migration decreased 1.6 fold in M(I+T) cells, increased 1.9 fold in M(IL-4) cells, and 3.3 fold in M(IL-10) cells. Blocking Kir2.1 also inhibited migration of mouse microglia: by 7.2 fold in M(IL-4) cells, and 14.2 fold in M(IL-10) cells. Again, while ML133 apparently reduced migration by 5.8 fold in unstimulated

mouse microglia and by 20.8 fold in M(I+T) cells, the ANOVA result did not show statistical significance. Similar to rat cells, blocking Kv1.3 with AgTx-2 increased migration of unstimulated mouse microglia (2.9 fold), M(IL-4) cells (1.9 fold), and M(IL-10) cells (1.4 fold). While AgTx-2 appeared to increase migration of M(I+T) cells (3.2 fold), it was not statistically significant. For both species, we ruled out changes in the number of cells available to migrate. A CyQuant NF assay showed that neither channel blocker altered the cell density over the 24 h migration period, regardless of activation state (not shown).

Together, our results suggest that in microglia of both species, Kir2.1 activity facilitates migration and Kv1.3 activity inhibits it, regardless of the activation state.

4.4 Discussion

The present results highlight similarities and differences between primary rat and mouse microglia. Several activation paradigms and outcomes were examined; thus, for clarity, the most relevant literature will be discussed under four topics: molecular profiling of responses; Kir2.1 channel expression and current; Kv1.3 channel expression and current; and contributions of Kir2.1 and Kv1.3 channels to migration. For ease of comparison with the literature, protein names will occasionally be used if the gene names are not common terms (all gene names are in Tables 2.1 and 2.2). We will focus the discussion on primary microglia because cell lines differ in their molecular profile, activation responses, and ion channel expression (Zhou et al., 1998; Cayabyab et al., 2000; Liu et al., 2013; Butovsky et al., 2014; Das et al., 2016).

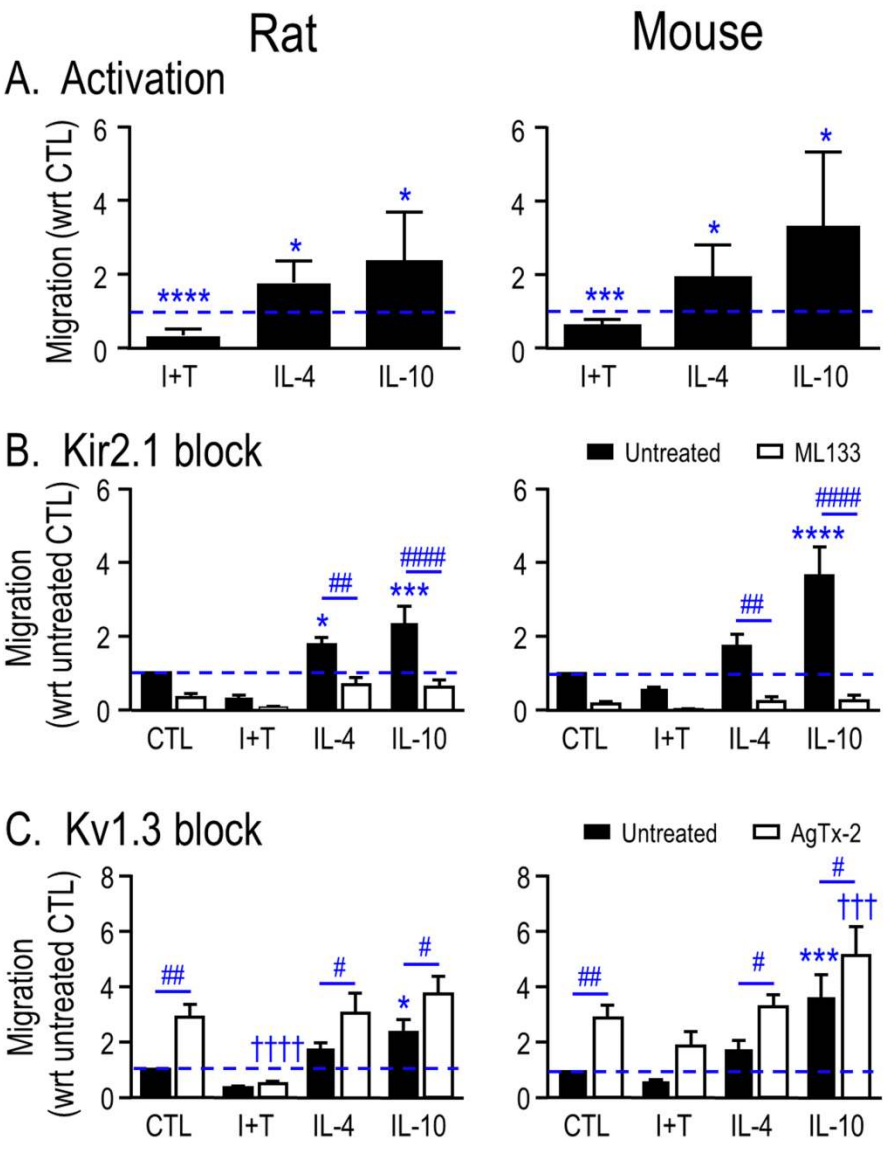
Rat
Mouse
A. Activation
Migration (wrt CTL)
I+T
IL-4
IL-10
B. Kir2.1 block
Untreated
ML133
Migration (wrt untreated CTL)
CTL
C. Kv1.3 block
AgTx-2

Figure 4.10. Kir2.1 and Kv1.3 activity contribute to microglial migration. A. Rat and mouse microglia were unstimulated (CTL) or stimulated for 24 h with IFN-γ and TNF-α (I+T), IL-4 or IL-10. **B.** Microglia with or without 20 μM ML133 to block Kir2.1 channels. **C.** Microglia with or without 5 nM AgTx-2 to block Kv1.3 channels. All results are expressed as fold change normalized to untreated unstimulated cells (indicated by dashed lines). Data are shown as mean ± SEM (n=6–9 individual cultures), and were analyzed by 1-way ANOVA with Dunnett's post-hoc test (activation state) or 2-way ANOVA with Bonferroni's post-hoc test (when channel blockers were used). The comparisons are: * differences between CTL and stimulated cells; † CTL versus activated cells treated with a channel blocker; # effects of a channel blocker within a given activation state. One symbol indicates $p<0.05$, two symbols, $p<0.01$, three symbols, $p<0.001$, four symbols, $p<0.0001$. Transmigration assay was performed and analyzed by Dr. Starlee Lively.

4.4.1 Molecular profiling of activation responses of primary rat and mouse microglia

Most studies of microglial activation have used primary rat or mouse cells. However, very few direct species comparisons have been made and the cell activation state was not determined. A recent *in vitro* study found differences between responses of rat, mouse and human microglia to oxygen glucose deprivation (OGD) but the resulting activation state was not determined (Du et al., 2016). While rat and human microglia were similar, mouse cells differed in cytokine mRNA expression (IL-1α, IL-1β, IL-6, IL-10, and TNF-α) both at baseline and after OGD. In contrast, after OGD, mouse and human levels of several chemokines (CX3CL1, CXCL10, CXCL12, CCL2, CCL3) were unaffected, but they increased in rat microglia. We found one older study that directly compared primary rat and mouse microglia but it was restricted to glutamate secretion in unstimulated cells (Patrizio and Levi, 1994). A small number of *in vivo* studies have directly compared inflammatory responses in rat and mouse CNS but, again, the microglial activation state is not known. After focal cerebral ischemia in mice, induction of pro-inflammatory mediators (IL-1β, iNOS, TNF-α) in the infarcted tissue was lower and more delayed than in rat (Schroeter et al., 2003). In the weeks following intracortical microelectrode implantation, CD68 immunoreactivity declined in the rat but not in the mouse (Potter-Baker et al., 2014). Both species showed similar microglia/macrophages accumulation in the lesion following spinal cord contusion, with maximal infiltration by 7 days (Sroga et al., 2003). However, mice had delayed and/or protracted T lymphocyte and dendritic cell infiltration, and a unique cellular response consisting of clusters of fibrocytes forming a clear fibrous scar.

M(I+T). This pro-inflammatory stimulus evoked several similar gene responses in rat and mouse microglia, although there were quantitative differences. There were increased transcript levels of several well-known pro-inflammatory genes (COX-2, iNOS, IL-6, TNF-α), NOX enzymes (NOX2, NCF1), and some less frequently examined genes (ICE, PYK2). Interestingly, increased PYK2 immunoreactivity was seen in rat microglia *in vivo* after transient middle cerebral artery occlusion or kainate-induced seizures (Tian et al., 2000). Although their activation state was not determined, our results suggest they were in a pro-inflammatory state. Several results are useful when considering the possible continuum of microglial responses to additional or sustained stimuli. The two species showed opposite changes in transcript expression of the innate immune receptor, TLR4, suggesting that they would respond differently to further incoming pro-inflammatory signals. In both species, I+T treatment increased transcript levels of receptors and immunomodulators that promote anti-inflammatory or deactivating signaling cascades and inflammation resolution. We recently found that M(I+T) rat microglia responded to subsequent IL-4 exposure with dampened pro-inflammatory responses (Siddiqui et al., 2016). Similarly, in M(LPS) mouse microglia, the pro-inflammatory responses were dampened by IL-4 treatment (Chhor et al., 2013).

M(IL-4). IL-4 evoked several important species differences in gene expression. We found that two markers commonly used to identify IL-4–mediated alternative activation in mice, FIZZ1 and PPAR-γ (Michelucci et al., 2009; Colton, 2009), were not induced in microglia from Sprague-Dawley rats. CD163 is considered a marker of anti-inflammatory microglia (Colton, 2009), and a marker of perivascular macrophages in the unperturbed brain (Fabriek et al., 2005). We found that IL-4 treatment increased CD163 transcripts in rat microglia but, in mouse, none of the cytokines tested increased it.

MRC1 is often considered an alternative-activation marker. Although it was selectively induced by IL-4 in rat microglia, it was also induced by IL-10 in mouse, as previously reported (Chhor et al., 2013). Thus, molecules used to identify alternative activation in one rodent species are not always generalizable.

M(IL-10). In both rodent species, responses to IL-10 often differed from IL-4. For instance, IL-10 did not reduce transcript expression of pro-inflammatory mediators (NOX2, IL-1β, IFNGR1) or increase anti-inflammatory mediators (CCL22, c-myc, ARG1). Opposite effects were sometimes seen in the two species (FcγRIa, IL-13Rα1, TGFBR2). Surprisingly, M(IL-10) and M(I+T) microglia shared many similarities, but not in induction of pro-inflammatory mediators. Instead, both stimuli induced transcripts of molecules known to modulate inflammatory responses (FcγRIIIa, IL-4Rα IL-13Rα1, SOCS3, TNFRSF1A, TGFBR2, TSPO), but the IL-10 responses were either comparable or lower than I+T responses. Induction of these modulatory genes suggests that self-limiting feedback responses occurred. Similarly, an earlier study of mouse microglia showed that IL-10 increased IL-1RN and SOCS3 mRNA levels and production of IL-6, CXCL1 and CCL2, but generally to a lesser extent than stimulation with LPS, TNF-α or IL-1β (Chhor et al., 2013).

There are important implications of these molecular profiles of microglial inflammatory responses. *(i)* Some molecules routinely used to identify 'activated' microglia/macrophages *in vivo* (CD11b, CD68) were not selectively increased by the pro-inflammatory stimulus, I+T. However, Iba1 was selectively increased in both species. *(ii)* The only genes induced selectively by IL-10 were CD11b and SR-A (rat and mouse), CD68, FcγRIa, TREM2 (rat only), and FcγRIIb (mouse only). CD11b and CD68 are often used as markers of microglial 'activation' *in vivo* (Schlichter et al., 2014;

Korzhevskii and Kirik, 2016), but they differ in temporal and spatial patterns after ischemia in the mouse cortex (Perego et al., 2011). Because CD11b and CD68 are receptors involved in phagocytosis by microglia, they are expected to be important after CNS damage (Noda and Suzumura, 2012; Fu et al., 2016); thus, it is surprising that neither was elevated by I+T (or IL-4) in either species. *(iii)* CX_3CR1 expression was surprisingly malleable and species dependent. This receptor is restricted to microglia in the CNS, where it binds neuron-derived CX_3CL1, and helps maintain microglial quiescence (Wolf et al., 2013). While the CX_3CR1 transcript levels increased slightly after IL-4 treatment only in rat microglia, the most striking change was a decrease following all cytokine treatments in mouse. It is difficult to predict the outcome of these changes. CX_3CR1-null mice are said to display microglial hyper-activation (Wolf et al., 2013) but its role is apparently damage-dependent because CX_3CR1 deletion was beneficial in models of transient ischemia (Denes et al., 2008) and Alzheimer's (Lee et al., 2010) but harmful in Parkinson's and ALS models (Cardona et al., 2006).

4.4.2 Changes in Kir2.1 expression and current in activated rodent microglia

For both Kir and Kv currents, previously published changes with microglial activation have been inconsistent and hint at species differences.

The first reports of Kir2.1 mRNA transcripts in microglia were in the mouse cell lines, BV-2 and C8-B4 (Schilling et al., 2000; Moussaud et al., 2009) and their activation state was not addressed. Recently, we showed that primary rat microglia express Kir2.1 mRNA transcripts (Lam & Schlichter, 2015). This is apparently the first study to show

that microglia from both species express transcripts for several members of the Kir2 family (Kir2.1, Kir2.2, Kir2.3, Kir2.4), and that Kir2.1 transcript expression was much higher and was the only subtype that responded to the activating stimuli.

While the mRNA results suggest that the Kir current in rodent microglia is produced by Kir2.1, numerous patch-clamp studies have not confirmed its identity. It is useful to compare electrophysiological and pharmacological properties of the microglial current with cloned Kir2.1 channels. Like cloned Kir2.1, the microglial current shows fast activation kinetics, Na^+-dependent relaxation at very hyperpolarized potentials, a single channel conductance of 25-30 pS (Kettenmann et al., 1990; Nöremberg et al., 1994; Schilling et al., 2000), and a small outward current above the reversal potential (Newell & Schlichter, 2005; Lam & Schlichter, 2015). There is no selective inhibitor of Kir2.1 channels, and most studies have used the pan-Kir blocker, Ba^{2+}. It is important to note that Ba^{2+} is a poor blocker at depolarized potentials (Lam & Schlichter, 2015), and this will compromise its value in cell function assays that address roles of Kir channels. A better blocker is the Kir2 family-specific blocker, ML133 (20 µM), which is not voltage dependent and blocks most of the Kir current in primary rat microglia within several minutes (Lam & Schlichter, 2015). In the present study, a similar block by 20 µM ML133 was seen in rat (86%) and mouse (95%) microglia. Because ML133 takes time to enter the cell and act on an internal site on the channel (Wang et al., 2011), its efficacy depends on the duration of drug exposure. For mouse microglia, it was recently reported that 20 µM ML133 blocked only ~48% of the Kir current (Wendt et al., 2016) but the exposure time was not stated.

Published responses of the Kir current to microglial activating stimuli have been quite variable. While the Kir current is present in most unstimulated rat and mouse

microglia, effects of pro-inflammatory stimuli in rat microglia range from no change to a small increase (with LPS) or a large increase (with IFN-γ) (Nörenberg et al., 1992 & 1994; Visentin et al., 1995; Draheim et al., 1999). In contrast, in primary mouse microglia, LPS or IFN-γ reduced the Kir2.1 current (Draheim et al., 1999; Prinz et al., 1999; Boucsein et al., 2003). Our direct species comparison showed that M(I+T) decreased the Kir2.1 current in mouse, with no change in rat. For anti-inflammatory activation states, there are even fewer publications. When TGF-β1 or TGF-β2 was used as a deactivating treatment on primary mouse microglia, there was no change in Kir current (Schilling et al., 2000). Here, we found that the Kir2.1 current was reduced by a 30 h stimulation with IL-4 in rat or IL-10 in mouse; changes that were consistent with the Kir2.1 transcript changes. For rat microglia, we previously reported that a shorter treatment (24 h) with IL-4 or IL-10 did not significantly change the current, although the trend was toward a decrease (Lam & Schlichter, 2015).

4.4.3 Changes in Kv1.3 expression and current in activated rodent microglia

Kv1.2, Kv1.3 and Kv1.5 transcripts and protein have been detected in primary rat and mouse microglia (Kotecha & Schlichter, 1999; Khanna et al., 2001; Fordyce et al., 2005; Pannasch et al., 2006; Li et al., 2008). Here, we detected all three channel transcripts in unstimulated rat and mouse microglia but Kv1.5 was very low. Some studies have suggested that elevated Kv1.3 indicates a pro-inflammatory state; e.g., increases in mRNA and channel expression in M(LPS) rat microglia (Fordyce et al., 2005; Liu et al., 2012), and the present increase in Kv1.3 transcript expression only in M(I+T) mouse

microglia. However, for rat microglia, we now show that Kv1.3 expression increased in both M(I+T) and M(IL-4) cells; thus, this channel gene is not a reliable marker of a pro-inflammatory state. Kv1.2 was striking in showing opposite responses to M(I+T): an increase in mouse but a decrease in rat microglia. The only other related studies on Kv transcript expression we found were on mouse cell lines. Kv1.2 mRNA expression increased in M(LPS) BV-2 cells (Li et al., 2008), and Kv1.3 increased after TGF-β1 or TGF-β2 treatment in BV-2 and C8-B4 cells (Schilling et al., 2000; Moussaud et al., 2009).

There is considerable variability in the prevalence of Kv currents reported in primary rodent microglia. For unstimulated microglia, early reports showed an absence in rat (Kettenman et al., 1990 & 1993), presence in a small proportion (<10%) of rat and mouse cells (Draheim et al., 1999; Prinz et al., 1999) or moderate prevalence (30%) in rat cells (Visentin et al., 1995), while several later studies found a Kv current in most to all rat microglia (Korotzer & Cotman, 1992; Kotecha & Schlichter, 1999; Cayabyab et al., 2000; Fordyce et al., 2005; Newell & Schlichter, 2005; Liu et al., 2012). Most studies have not used selective blockers to isolate the Kv1.3 portion of the current. Here, we observed an AgTx-2-sensitive Kv1.3 current in all unstimulated rat microglia, which were predominantly unipolar, and this is consistent with our earlier studies on unstimulated bipolar or amoeboid rat microglia (Schlichter et al., 1996; Kotecha & Schlichter, 1999; Cayabyab et al., 2000). In contrast, despite the similar morphology and molecular profile of unstimulated mouse microglia, the Kv current prevalence was much lower (~56% of cells). A margatoxin (MgTx)-sensitive Kv current was seen in <10% of cultured mouse microglia (Draheim et al., 1999) but that current was not proven to be Kv1.3 because MgTx can block other Kv1-family channels (Bartok et al.,

2014). There is some evidence that the Kv prevalence changes with age in mouse but this has not been examined in rat. In mice, a MgTx- and AgTx-2-sensitive Kv current was seen in 20–60% of postnatal (P5–9) microglia in acutely isolated brain slices (Arnoux et al., 2013). Little or no Kv current was detected in acutely isolated adult mouse brain slices (Schilling & Eder, 2007 & 2015; Arnoux et al., 2013) or microglia isolated from 'control' mouse brain (Chen et al. 2015), but the prevalence increased to 29% in dystrophic microglia from aged mice (Schilling et al., 2015). A further complication is that the Kv prevalence and magnitude increased when mouse hippocampal slices were cultured *ex vivo* (Schilling et al., 2007).

Some variability in the prevalence and amplitude of Kv currents is very likely due to differences in voltage protocols; e.g., using a depolarized holding potential, which is well known to inactivate Kv1.3 (Schlichter et al., 1996; Visentin et al., 1995; Kotecha & Schlichter, 1999) and Kv1.5 channels (Philipson et al., 1993; Kotetcha & Schlichter, 1999). One study that did not detect Kv current in rat microglia used a holding potential of –20 mV (Boucsein et al., 2000). Because Kv1.3 undergoes pronounced cumulative inactivation (Grissmer et al., 1994; Nörenberg et al., 1994; Kotecha & Schlichter, 1999; Cayabyab et al., 2000), the current amplitude can be substantially underestimated if the interval between voltage pulses is too short. Most studies do not state the interpulse interval (Kettenmann et al., 1990; Draheim et al., 1999; Prinz et al., 1999; Boucsein et al., 2000). Additional variability in Kv current might also reflect a different initial activation state, which has rarely been determined. For instance, both Kv1.3 and Kv1.5 currents have been identified in rat and mouse microglia (Kotecha & Schlichter, 1999; Pannasch et al., 2006) but, in rat microglia from hippocampal tissue prints, Kv1.5

produced the current in non-proliferating microglia and was replaced by Kv1.3 as the cells proliferated (Kotecha & Schlichter, 1999).

Both Kv1.3 and Kv1.5 currents have been reported in *ex vivo* rat microglia (Kotecha & Schlichter, 1999) and in M(LPS) mouse microglia (Pannasch et al., 2008). Changes in Kv current with activating stimuli suggest that it is induced or increased in pro-inflammatory states. LPS or IFN-γ increased Kv currents in rat (Nörenberg et al., 1992 & 1994; Visentin et al., 1995; Fordyce et al., 2005) and mouse microglia (Fischer et al., 1995; Draheim et al., 1999; Prinz et al., 1999; Pannasch et al., 2006). Here, we found that the pro-inflammatory M(I+T) state increased the total Kv current and Kv1.3 component in both species. However, for rat microglia, the Kv1.3 increase was not specific to the pro-inflammatory state, as IL-4 also increased the current. Consistent with Kv1.3 mRNA expression, the pro-inflammatory response was more specific in mouse cells, where only I+T increased Kv and Kv1.3 currents. Kv currents were also prevalent in 'activated' microglia in damage models but the specific activation state and channel type were not determined; for instance, in the denervated rat facial nucleus (Boucsein et al., 2000), and in the ischemic cortex (Lyons et al. 2000). MgTx- and AgTx-2-sensitive Kv1.3 currents were found in microglia within the hippocampus of adult mice after status epilepticus but the prevalence and cell activation state were not determined (Menteyne et al., 2009). After LPS injection into the mouse brain, the PAP-1-sensitive Kv1.3 current in acutely isolated adult microglia was 5-fold larger (Chen et al. 2015). The present results show that additional Kv channel types were active in mouse microglia; i.e., less than half the current was blocked by AgTx-2 in unstimulated cells and slightly more than half in M(I+T) cells.

Little is known about Kv currents in anti-inflammatory states. Mouse microglia stimulated with TGF-β1 or TGF-β2 had increased Kv currents that were blocked by kaliotoxin, charybdotoxin or MgTx (Schilling et al., 2000; Moussaud et al., 2009) but the cell activation state was not characterized. In both species, we found that the total Kv and isolated Kv1.3 currents were unchanged in M(IL-4) and M(IL-10) states.

4.4.4 Roles of Kir2.1 and Kv1.3 in microglial migration

For rat microglia, we previously reported that M(LPS) cells migrate less than unstimulated cells, while M(IL-4) and M(IL-10) cells migrate more (Siddiqui et al., 2014; Lively and Schlichter, 2013; Ferreira et al., 2014; Lam & Schlichter, 2015), and that blocking Kir2.1 channels reduced migration in unstimulated, M(IL-4) and M(IL-10) microglia (Lam & Schlichter, 2015). We now report similar changes in migratory capacity with activation state in both species, and that, regardless of the activation state, blocking Kir2.1 inhibited migration while blocking Kv1.3 increased it. In the only directly relevant paper that we found, blocking Kv1.3 with MgTx in rat microglia reduced chemotaxis induced by monocyte chemoattractant protein 1 (CCL2) or ADP but the activation state was not identified (Nutile-McMenemy et al., 2007).

One potential role for Kv and Kir channels is to regulate the membrane potential and subsequent Ca^{2+} signaling, which is involved in cytoskeletal remodeling, adhesion and migration (Ridley et al., 2003; Wei et al., 2012). For rat microglia, we previously showed that Ca^{2+} entry through Ca^{2+} release-activated Ca^{2+} (CRAC) channels is increased with hyperpolarization (Ohana et al., 2009), and that blocking Kir2.1 channels with ML133 reduced CRAC-mediated Ca^{2+} entry and migration (Lam & Schlichter, 2015). Similarly, blocking Kir2.1 in rat microglia with Ba^{2+} prolonged depolarization and

reduced the amplitude of ATP-induced Ca^{2+} transients (Franchini et al., 2004). Blocking Kv1.3 in rat microglia disrupted membrane potential oscillations, showing a role in repolarization after depolarizing events (Newell & Schlichter, 2005). This is apparently the first report of a role for Kv1.3 in microglia migration in the absence of a chemoattractant, and it was surprising that blocking Kv1.3 and Kir2.1 had opposite effects. Further evidence that the two channels do not always play the same functional roles is that Kir2.1 (but not Kv1.3) is involved in myelin phagocytosis and ROS production in activated rat microglia (Siddiqui et al., 2016). One possibility is that the channels have roles other than regulating K^+ flux and membrane potential. For instance, cell migration requires integrins, which regulate adhesion to the extracellular matrix, and there is evidence that integrins and K^+ channels can co-exist in signaling complexes (Arcangeli & Becchetti, 2006). A physical link between Kv1.3 and the β_1 integrin moiety was reported in T lymphocytes and melanoma cells (Levite et al., 2000; Artym & Petty, 2002) but it is not known whether a similar association occurs in microglia. Future studies will be needed to determine the mechanisms by which Kir2.1 and Kv1.3 channels regulate microglia migration.

4.4.5 Broader implications

Studies of disease mechanisms rely on animal models, especially rodents. To fulfill the larger goal of translating such results to humans, it is crucial to understand whether rats and mice respond the same and, if not, which species is a more reliable model. There is considerable debate as to how closely mouse models resemble human responses in inflammatory diseases (Seok et al., 2013; Takao and Miyakawa, 2014). For peripheral immune cells, rat and mouse responses are sometimes assumed to be comparable

(Holsapple et al., 2003). However, very few comparisons of rat and mouse microglia have been published, and our findings illustrate important species differences in molecular activation profiles and K^+ channel activity. Microglial properties are increasingly being investigated in human tissue—often from surgical biopsies from epileptic patients—but their activation state is usually not investigated and they cannot be assumed to be normal, resting cells. Further complications include the potential for strain differences in rodents (Becker, 2016), and genetic polymorphisms and epigenetic changes in humans (Boche et al., 2013). Many potential treatments identified in rodents have failed in human clinical trials. To narrow this translational gap, it is essential to investigate and acknowledge the similarities and differences in immune responses across different species.

4.4.6 Conclusions

While some *in vivo* results suggest that CNS inflammation differs between rats and mice, it is premature to ascribe the differences to microglial responses. The present study contributes considerable comparative data concerning primary rat and mouse microglia, and it highlights species similarities and differences in the inflammatory response following stimulation with pro- and anti-inflammatory cytokines. The search for molecular targets to control microglial activation and specific functions will also require a better understanding of species differences. For instance, Kv1.3 is considered a promising target in autoimmune diseases, such as multiple sclerosis, rheumatoid arthritis, type 1diabetes, and psoriasis (Feske et al., 2015). However, studies are only beginning to directly compare contributions of ion channels in different species. It is intriguing that, despite species differences in the outcome of microglial activation states

on Kir2.1 and Kv1.3 expression and currents, there was no obvious species differences in the channel roles in migration. To determine whether specific microglial K^+ channels can be targeted to modulate neuroinflammation, it will be crucial to undertake species comparisons of other microglia functions using selective inhibitors or cell-targeted channel depletion, and to extend the studies to models of acute CNS injury.

5 Overall Discussion

5.1 Targeting Kv1.3 and Kir2.1 channels to regulate microglial functions

There is a growing interest in targeting Kv1.3 channels to suppress the adaptive immune response in autoimmune diseases, such as multiple sclerosis, rheumatoid arthritis, type 1 diabetes mellitus and psoriasis (Wulff and Zhorov, 2008; Feske et al., 2015). In microglia, not enough was known about Kv1.3 channel expression patterns in resting or in different activation phenotypes to determine whether this channel is an appropriate therapeutic target to modulate the immune response of this cell type following acute CNS damage. Since no specific Kir2.1 channel blockers are available, it has also been difficult to determine whether this channel contributed to microglial functions. In this thesis, I reported for the first time that there are species differences in the expression (mRNA and currents) of Kir2.1 and Kv1.3 channels in rat and mouse microglia under different activation paradigms, defined by the stimulus: M(I+T) to skew to a pro-inflammatory (M1) state; M(IL-4) to skew to the anti-inflammatory, alternative activation (M2a) state; and M(IL-10) to skew to the anti-inflammatory, acquired deactivation (M2c) state. We also reported that both channels play a homeostatic role in cell migration, independent of activation state, but in a reciprocal manner. Additional unpublished data is included as Appendices, which show that Kir2.1 and Kv1.3 channels in both rat and mouse microglia are not necessary for proliferation (Fig. A.2) or NO production (Fig. A.3).

5.1.1 Relevance of Kir2.1 and Kv1.3 expression in microglia *in vitro* to rodent microglia *in situ*

Very little is known about Kir2.1 and Kv1.3 expression in rodent microglia *in situ*, and about whether these channels are regulated under different activation phenotypes. The few studies that examined expression of Kir and Kv currents in activated microglia/macrophages *in situ* from rodent models of CNS damage and disease (Boucsein et al., 2000; Lyons et al., 2000; Menteyne et al., 2009) were based solely on morphology, and pharmacological profiling of these currents was not always done.

We now know that morphology is not an informative method to describe the activation phenotype of microglia, which can exist on a spectrum between pro- (M1) and anti-inflammatory (M2) states. Even *in vitro*, morphology is not a good indicator of microglial activation state, as exemplified in my thesis. Here, we observed dramatic morphological changes following I+T stimulation but not with IL-4 or IL-10 stimulation in both rat and mouse microglia. Nevertheless, gene expression profiles, cellular functions and K^+ channel expression were sometimes different when activation paradigms were compared. In the uninjured adult brain, microglia are highly ramified cells. Following CNS damage, microglia become activated and this is visually identified by a change in morphology from a ramified to hypertrophic cell, as observed in the facial nucleus 48 h and 7 days after facial nerve axotomy (Boucsein et al., 2000) and 48 h in the hippocampus after status epilepticus (Menteyne et al., 2009), or to an amoeboid morphology, as observed 6 h after middle cerebral artery occlusion (Lyons et al., 2000). Since the above-mentioned *in situ* studies did not profile inflammatory mediators (e.g., cytokines) in the damaged brain tissue when characterizing K^+ currents, it is not known

what mediator (e.g. pro- or anti-inflammatory) had activated the microglia and modulated the currents. Thus, there is a need for future studies to use additional methods (i.e. molecular profiling) to identify the activation phenotype (e.g. M1 and multiple M2 states; discussed in §5.2), and correlate it to changes in the expression of K^+ currents.

To examine whether Kir2.1 and Kv1.3 currents are regulated under different microglial activation phenotypes, I used cultured neonatal microglia, which under unstimulated conditions are highly migratory and proliferative (Schlichter et al., 1996; Vincent et al., 2012) and resemble both their postnatal developmental counterpart and the migration and proliferation acquired following CNS injur*y in vivo* (§1.2 and 1.3). Here, I report that the expression of Kir2.1 and Kv1.3 currents in unstimulated rat and mouse neonatal microglia *in vitro* (Chapter 3 and 4) is similar to reports detecting Ba^{2+}-sensitive Kir2.1-like and MgTx-sensitive Kv1.3-like currents in microglia during the developmental period (P5-P9) from both rat and mouse brain slices (Schilling and Eder, 2007; Arnoux et al., 2013). Similarly, hypertrophic and amoeboid rodent microglia acquire Kir and Kv currents following CNS injury (Lyons et al., 2000; Boucsein et al., 2000; Menteyne et al., 2009). In this thesis, I demonstrated that the regulation of Kir2.1and Kv1.3 currents are cytokine and species dependent, which might provide insight into changes in Kir (§5.1.1.1) and Kv (§5.1.1.2) currents observed in activated microglia/macrophages reported *in* situ, even though the activation state and the identity of the currents were not always determined (Boucsein et al., 2000; Lyons et al., 2000; Menteyne et al., 2009).

5.1.1.1 Kir2.1-like current in rodent microglia *in situ*

In situ studies have reported the appearance of a Kir current in adult microglia from acute brain slices obtained from damaged or diseased brain tissue (Boucsein et al., 2000; Lyons et al., 2000; Menteyne et al., 2009). The current resembled Kir2.1 currents recorded from microglia *in vitro*. But the activation state was not identified in these disease models. The Kir2.1-like current was observed in amoeboid microglia within the peri-infarct region 6 h after ischemia in rats (Lyons et al. 2000), and hypertrophic microglia from denervated facial nucleus at 12 h following facial nerve axotomy in rats (Boucsein et al., 2000) and from the hippocampus 48 h after the induction of status epilepticus in mice (Menteyne et al., 2009).

The appearance of a Kir2.1-like current in hypertrophic or ameoboid rat and mouse microglia/macrophages several hours after injury (Lyons et al. 2000; Boucsein et al., 2000; Menteyne et al., 2009), suggests the upregulation of channel expression and activity. Only one study reported that, in rat microglia, stimulation with IFN-γ at 10 ng/mL or 100 ng/mL increased Ba^{2+}-sensitive Kir2.1 current by 33% and 61%, respectively (Visentin et al., 1995). But when IFN-γ was combined with TNF-α, we saw no difference in Kir2.1 channel activity in rat microglia relative to the unstimulated condition. In mouse microglia, inflammatory mediators that upregulate the Kir2.1 current in microglia *in vitro* are not known. Downregulation of Kir current was reported in hypertrophic rat microglia/macrophages *in situ* at day 7 following facial nerve axotomy (Boucsein et al., 2000). In primary rat microglia, Kir2.1 current decreased only in the M(IL-4) state following 30 h but not at 24 h stimulation. We suspect that the additional 6 h was necessary to allow time for changes in channel protein at the cell surface or in

expression of signaling molecules that post-transcriptionally modify the channel; e.g. small GTPases (discussed in §5.1.2.3) that regulate the expression of the channel at the plasma membrane via endocytosis (Jones et al., 2003; Boyer et al., 2009). With the limited transcripts available in M(IL-4) rat microglia and M(I+T) or M(IL-10) mouse microglia, it is possible that synthesis of new Kir2.1 channel protein, and its trafficking to the plasma membrane were insufficient to compete against endocytosis of the channel. If so, this could account for the decreased Kir2.1 current in these activation states. While temporal profiling of Kir current was not examined days after the induction of status epilepticus in mice (Menteyne et al., 2009), we report species differences in the regulation of Kir2.1 channel activity that depends on the activation state of microglia. In mouse microglia, Kir2.1 current decreased in the M(I+T), consistent with previous reports of M1 activated microglia (Draheim et al., 1999; Prinz et al., 1999; Boucsein et al., 2003), and also in the M(IL-10) state. Downregulation of Kir2.1 current was not observed in the M(IL-4) state in mouse microglia, an effect observed in the rat. It is imperative that future studies profile the activation phenotype of microglia, preferably with the use of molecular markers (discussed in §5.2), as changes in the amplitude of the Kir current is an insufficient indicator of microglial activation phenotypes. Also, it will be important that future studies consider the rodent model used to study Kir2.1 channel activity in activated microglia/macrophages *in situ.*

It was not known whether and which Kir channel was expressed in microglia *in situ*, until recently. Following my work using the Kir2 family channel blocker, ML133 (Chapter 3, Lam & Schlichter, 2015), Kettenmann's research group also confirmed ML133-sensitive currents in mouse microglia *in vitro* and then assessed the ML133-sensitive current in adult microglia from acute brain slices (Wendt et al., 2016). ML133

only blocked 12% of the Kir current from microglia *in situ,* which was comparable to a second experiment that used a cocktail of Kir subtype blockers, including ML133, and showed a similar 14% block (Wendt et al., 2016). Notably, the percentage of Kir current sensitive to ML133 or Kir subtype cocktail was less than the 43% blocked by Ba^{2+}. The authors suggested that while the Kir current is predominantly mediated by Kir2.1 channels in microglia *in vitro,* the current in microglia *in situ* is mediated by Kir2.1 channels and an additional Ba^{2+}-sensitive component. However, I think the authors might have underestimated the actual sensitivity of the Kir current to ML133. The authors reported in microglia *in vitro* that only 48% of the inward current blocked by ML133 and 57% blocked by Kir subtype cocktail (Wendt et al., 2016), whereas I observed a near complete block of the Kir current in both rat and mouse microglia (Fig. 3.1 and 4.7B). This is similar to the near complete block of the Kir current in unstimulated primary rat microglia with Ba^{2+} reported by our lab and others (Schlichter et al., 1996; Franchini et al., 2004). While, in the Wendt et al paper, brain slices were incubated with ML133 or Kir subtype cocktail for 2-5 minutes, it is not clear how long cultured cells were exposed to the Kir2 blocker. The incubation time of ML133 is important since steady state block of native (Fig. 3.1E) and cloned Kir2.1 (Wang et al., 2011) channels is time-dependent (~8-10 min). ML133 is membrane permeable and binds to residues on the cytoplasmic side of the inner face of the pore-lining M2 helix, blocking the pore permeation pathway of Kir2.1 (Wang et al., 2011); thus, a longer incubation time is needed. Wendt et al. (2016) was the first study to pharmacologically profile the Kir current using ML133 in adult microglia from acute brain slices, but future studies should be aware of the mode of action of this drug and its time dependent block of Kir2.1 channels.

5.1.1.1.1 Reliability and selectivity of Kir2.1 channel blockers

When I began my PhD, very little was known about Kir2.1 channels in microglia and whether and how they regulate microglial functions. This was likely due to the lack of selective inhibitors for Kir2.1 channels. In Chapter 3, I discussed the limitations of using Ba^{2+} and the possible off-targeted effects, both of which could affect the interpretation of one's finding. In addition to Ba^{2+}, I used ML133 to determine whether two known Kir2.1 channel blockers produced the same effect, thus corroborating the role of Kir2.1 in microglial functions. I reported that both Ba^{2+} and ML133 produced similar effects in rat microglia: slightly increased proliferation in only unstimulated and M(IL-4) states (Fig. 3.3 D), and reduced migration and chemotaxis (with ML133 being more effective) regardless of activation state (Fig. 3.4). While both inhibitors block the inward rectifying current component of Kir2.1, ML133 more effective at blocking the outward Kir2.1 current at depolarized potentials (Fig. 3.1 D) and reducing microglial migration (Fig. 3.4) than Ba^{2+}. Currently, it is not known whether ML133 has off-target effects. ML133 did not affect L-type or N-type calcium channels or several other K^+ channels, including hERG (Wang et al., 2013). While Ba^{2+} could have off-target effects on microglial KCa2.3 and KCa3.1 channels, this is unlikely to account for my results because ML133 showed similar results. Moreover, a contribution from KCa2.3 and KCa3.1 channels is unlikely based on previous findings from the Schlichter lab. KCa2.3 channels do not play a role in microglia migration in unstimulated, M(IL-4) or M(IL-10) state, or in the presence of the chemokine UTP (Ferreira & Schlichter, 2013; Siddiqui et al., 2014). Also, while upregulation of KCa3.1 currents contributed to the enhanced migration in M(IL-4) microglia, blocking this channel did not affect the migration of unstimulated microglia,

which expressed little KCa3.1 current (Ferreira et al., 2014). These findings suggest that the role of KCa3.1 is activation state-dependent. Also, blocking KCa3.1 did not alter cell proliferation in unstimulated or M(IL-4) microglia (Ferreira et al., 2014). Thus, the effects of ML133 observed in this thesis are likely the result of its inhibition of Kir2.1, providing insight into the role of this channel in differentially activated microglia.

5.1.1.2 Kv1.3-like currents in rodent microglia *in situ*

In situ studies have reported the appearance of Kv currents in activated microglia/macrophages from damaged rodent brain tissue: amoeboid microglia as early as 6 h following an ischemic insult in rats (Lyons et al., 2000), and hypertrophic microglia as early as 24 h after facial nerve axotomy in rats (Boucsein et al., 2000) and 48 h after status epilepticus in mice (Menteyne et al., 2009). Of these studies, only Menteyne et al. (2009) showed that the properties of the current resembled homomeric Kv1.3 channels. In hypertrophic hippocampal microglia/macrophages, the biophysical (i.e. voltage-dependent activation, steady-state inactivation, cumulative inactivation) and pharmacological (i.e. blocked by 4-AP, MgTx, and AgTx-2) properties resembled Kv1.3. The presence of Kv currents in activated microglia/macrophages in these injury models is consistent with the upregulation of Kv currents in M1-activated primary rat (Nörenberg et al., 1992 & 1994; Visentin et al., 1995; Fordyce et al., 2005) and mouse microglia (Fischer et al., 1995; Draheim et al., 1999; Prinz et al., 1999; Pannasch et al., 2006). However, my thesis work shows that Kv1.3 expression (mRNA and currents, Fig. 4.6B and 4.8) is also elevated in M2a-activated primary rat (but not mouse) microglia.

It is imperative that future studies define the activation phenotype when characterizing Kv current expression in activated microglia/macrophages, particularly in

the rat model. While targeting Kv1.3 channels in T_{EM} cells is a promising therapeutic approach for autoimmune diseases, the findings in my thesis suggest that targeting Kv1.3 in microglia will depend on the species of the preclinical rodent model. That is, in rats, targeting Kv1.3 could potentially affect both M1 and M2a microglia populations, while in mice only M1 microglia will likely be affected. With respect to Kv1.3 expression, the next question that needs to be addressed in future studies is which rodent model more closely resembles the human condition.

5.1.1.2.1 Standardizing voltage clamp protocols for isolating Kv1.3 currents in microglia *in vitro* and *in situ*

It is becoming apparent from the conflicting literature that there is a need for a standardized voltage protocol for examining Kv1.3 currents in microglia *in vitro* and *in situ* (discussed in Chapter 4, §4.4.3). In particular, the prevalence of an Kv current in unstimulated primary rodent microglia has varied across studies and research groups (Korotzer & Cotman, 1992; Kettenman et al., 1990 & 1993; Visentin et al., 1995; Draheim et al., 1999; Prinz et al., 1999; Kotecha & Schlichter, 1999; Cayabyab et al., 2000; Fordyce et al., 2005; Liu et al., 2012). I think that the variability in these studies can likely be attributed to the voltage protocol (e.g. interpulse interval, holding membrane potential, discussed in Chapter 4).

In this thesis, I developed a voltage step and ramp protocol to isolate Kv1.3 currents in mouse microglia to resolve a technical issue with this preparation. The Schlichter lab routinely used a standardized voltage step protocol to study the Kv1.3 current in rat microglia (Schlichter et al., 1996; Cayabyab et al., 1999; Fordyce et al.,

2005). The voltage protocol used in Fig 4.8 considers voltage-dependent inactivation and cumulative inactivation that is characteristic of Kv1.3; e.g. the holding potential was very negative (–105 mV) to prevent channel inactivation, and a 60 s interpulse interval was used to ensure complete recovery from inactivation (Kotecha & Schlichter, 1999). Thus, when characterizing Kv1.3 currents in rat microglia under different activation states, the experimental protocol I used took about 20 minutes. That is, a 7 min voltage protocol (from –75 to +45 mV at 20 mV intervals) to isolate the total outward current, to perfuse in the Kv1.3 blocker AgTx-2 (for 5 min), and then to reapply the voltage protocol to measure the AgTx-2 insensitive current. Subsequent to data acquisition, AgTx-2 sensitive currents were obtained by subtracting total Kv by AgTx-2 insensitive current traces. Then, the current-voltage (I-V) relationship was graphed to compare against different activation states. I attempted to apply the same protocol to mouse microglia. However, the seal was lost within several minutes of running the experimental protocol for every cell patched. Thus, for mouse microglia, I modified and shortened the voltage protocol (Fig. 4.9): from a holding potential of –105 mV, a single step to +45 mV was applied for 1 s before returning to –105 mV for 60 s, and then a voltage ramp was applied from –75 to +45 mV over 120 ms. It was important to ensure that the duration of the ramp did not induce channel inactivation during the voltage clamp protocol. I found that a 120 ms ramp was optimal, as the peak current amplitude during a +45 mV voltage step was the same as the current amplitude at +45 mV during the ramp (data not shown). Kv1.3 also displays voltage- and time- dependent activation. This is apparent from the current traces obtained from rat microglia in Fig. 4.8, where the time to reach peak amplitude decreases at more depolarized potentials (i.e. > -15 mV). With the ramp component of the voltage protocol, the voltage- and time-dependent activation

was not directly assessed; i.e., when recording Kv1.3 currents in mouse microglia. Thus, it was also important that I found that the measured I-V relations in mouse (n=7) were the same as in rat (n=12) microglia in the unstimulated condition. I compared the slope of the I-V relations of the AgTx-2 sensitive Kv1.3 current between species, and found that the slopes were not significantly different (data not shown). Thus, this modified and shortened voltage protocol, which takes into consideration channel inactivation and cumulative inactivation, could be used in future studies to determine whether Kv1.3 currents are expressed in microglia *in vitro* and *in situ*.

5.1.2 Kir2.1 and Kv1.3 channels have specific functional roles in cytokine-activated microglial functions

In using a pharmacological approach, we examined whether K^+ conductance of Kir2.1 and Kv1.3 channels was necessary for microglial functions. This was independent of the observed changes in their current expression level, which we found was dependent on the activation state of microglia and species; e.g., decreased Kir2.1 currents in M(I+T) and M(IL-10) (mouse) and M(IL-4) (rat), and increased Kv1.3 currents in M(I+T) (both rat and mouse), and M(IL-4) (mouse) microglia. Here we show a role of Kir2.1 and Kv1.3 channels to microglial migration (transmigration, chemotaxis), and recent work from the Schlichter lab has shown a role of Kir2.1 (but not Kv1.3) in myelin phagocytosis (Lam & Schlichter, 2015; Siddiqui et al., 2016; Lam et al., under revision). Like myelin phagocytosis, some microglial functions might not depend on Kv1.3 and /or Kir2.1 channels. Additional unpublished data included in the Appendices, also demonstrate that the conducting role of Kir2.1 and Kv1.3 channels are not necessary for proliferation or

NO production (Fig. A.2 and A.3, p. 183 and 184, respectively). Collectively, these studies suggest that Kir2.1 and Kv1.3 channels have specific roles in microglial functions. But it is not clear whether the same can be said for other microglial functions (e.g. chemokine and cytokine production, respiratory burst, and neurotoxicity, Fig. 5.1), which will need to be investigated in future studies now with a more selective inhibitor for Kir2.1. It still remains unclear how changes in the expression of Kir2.1 and Kv1.3 currents affect different properties of microglial function. For example, future studies can use time lapse imaging of a 2-dimensional scratch wound assay to examine whether activation and species dependent regulation of Kir2.1 and/or Kv1.3 currents correlate to changes in the functional properties of microglial migration (e.g. velocity, cell steering), which could not be addressed using the transmigration assay.

It is interesting that the effect observed in blocking Kir2.1 or Kv1.3 channels was similar in both species for migration, proliferation and NO production. This is particularly important for two reasons: 1) the mechanism that allows Kir2.1 or Kv1.3 channels to modulate microglial migration is conserved between species; and 2) a potential therapeutic advantage in targeting these channels is that a specific microglial function (migration) can be modulated without affecting others (i.e., proliferation, NO production).

5.1.2.1 Kir2.1 and Kv1.3 currents are not required for proliferation of cytokine-activated rodent microglia

In my thesis work, it was important to examine proliferation because, in principle, a reduction or increase in microglial migration or NO production could result from

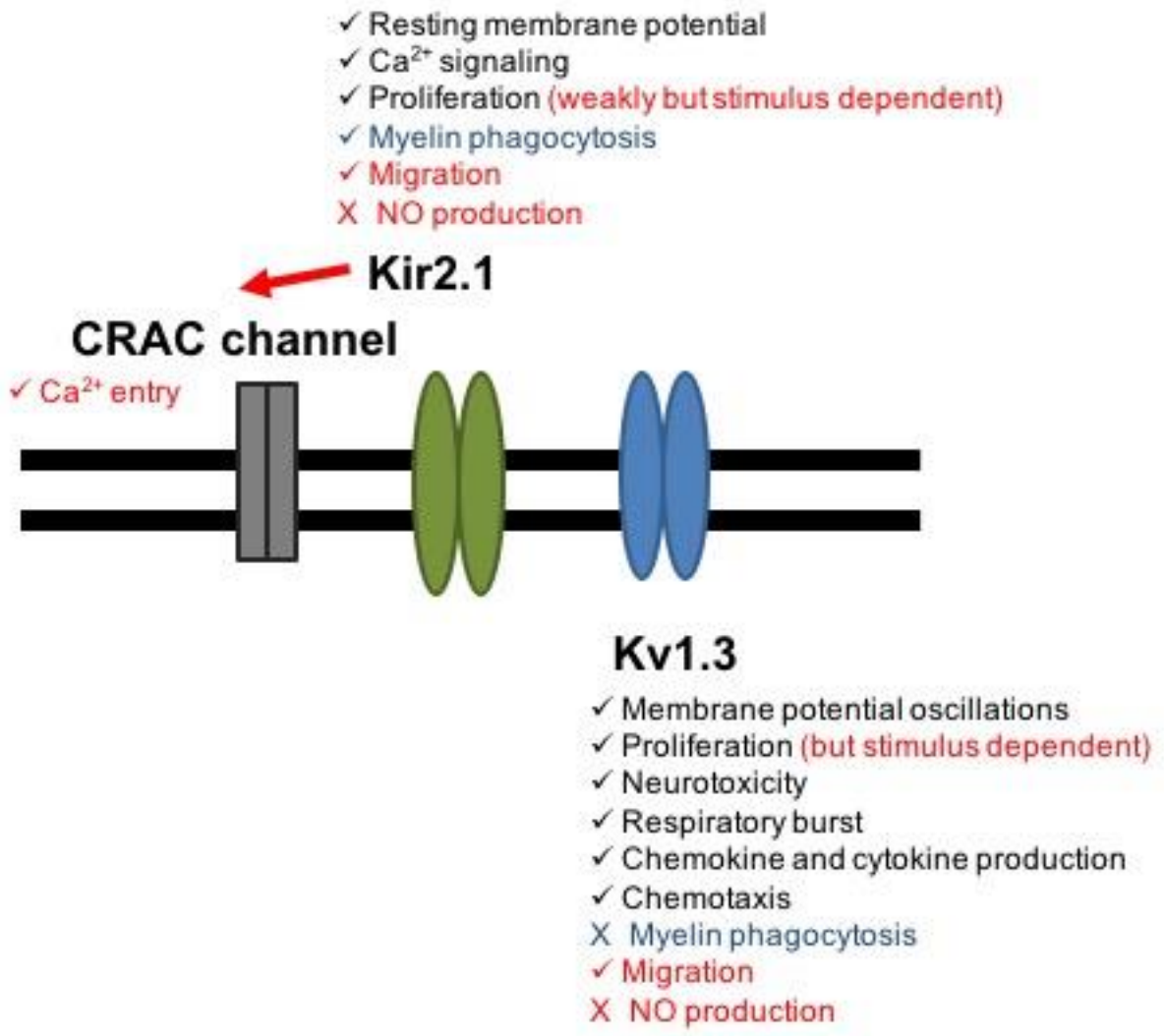

Figure 5.1. Known roles of Kv1.3 and Kir2.1 in microglial functions at the end of my PhD studies. Updated version of Figure 1.3 that lists the known roles of Kir2.1 and Kv1.3 in microglia after my PhD studies (red) and recent findings from the Schlichter lab (blue). In particular, I demonstrated that Kir2.1 channels regulate store-operated Ca^{2+} entry through CRAC channels (red arrow).

changes in cell numbers in response to cytokine stimulation or channel blockers. Neonatal microglia spontaneously proliferate in culture (Schlichter et al., 1996). In Chapter 3, I showed that microglia in a M2a or M2c state, and in the presence of a Kir2.1 channel blocker (Ba^{2+}, ML133) did not dramatically alter their proliferative capacity (as judged by the CyQuant assay). In addition, cell death (as judged by propidium iodide) was minimal (<10%). Thus, changes in total cell numbers did not account for the reduced microglial migration observed in the presence of Kir2.1 blockers. In Chapter 4, we also reported that the proliferative capacity of microglia was not altered in the M1 state, and this was consistent with mouse microglia using the same activation paradigms. This was important since the reduced (by ML133) or enhanced (by AgTx-2) migration observed was not influenced by cell density in unstimulated or stimulated microglia treated with the channel blockers. Similarly, the increase in NO production in M(I+T) microglia from both rat and mouse was not affected by the proliferative capacity of these cells (Fig. A.3).

Not enough is known about Kir2.1 channels in microglial proliferation. Also, it still remains controversial whether Kir2.1 channels contribute to cell proliferation, and it might be cell type specific and/or stimulus dependent. In microglia, my findings suggest that Kir2.1 channel is not essential for proliferation, but blocking the channel weakly increased the proliferative capacity of unstimulated and M2a (but not M2c)-stimulated rat microglia (Fig. 3.3). In mouse microglia, however, blocking Kir2.1 channels did not affect proliferation regardless of the activation state (Fig. A.2). In an earlier study by the Schlichter lab, 1 mM Ba^{2+} increased CSF-1 induced proliferation by 25%, while higher concentrations decreased it with an apparent IC_{50} of 1.5 mM (Schlichter et al. 1996). We now think that the inhibition at 5 and 10 mM Ba^{2+} was an off-target effect, as discussed

in §5.1.1.1.1. Endothelial progenitor cells also had increased proliferation after silencing Kir2.1 with siRNA or blocking it with Ba^{2+} (Jang et al., 2011). However, other studies have shown that blocking or dominant-negative suppression of Kir2.1 either had no effect or reduced proliferation in Schwann cells, mesenchymal stem cells, smooth muscle cells, cardiac c-kit^{+} progenitor cells, and fibroblasts (Sobko et al., 1998; Karkanis et al., 2003; Zhang et al., 2012a & b; Qi et al., 2015; Zhang et al., 2015). Collectively, these studies demonstrate that not enough is known about Kir2.1 in cell proliferation to elucidate a putative mechanism. But it is possible that other channels can compensate for the lack of Kir2.1 channel activity, and still maintain the cell's proliferative capacity (see below).

In microglia, Kv1.3 channels appear to have a role in microglial proliferation, but the results are conflicting. In rat microglia, our lab showed a strong correlation of Kv currents and the proliferative state of cultured rat microglia from hippocampal tissue-prints. Kv1.5 currents is expressed in freshly isolated and short term cultured microglia (0-5 DIC) but switch to Kv1.3 currents with time in culture (> 6 DIC, Kotecha & Schlichter, 1999). AgTx-2 dramatically reduced proliferation of tissue printed microglia at 10 DIC, coincident with the increase in prevalence of a Kv1.3 current and the detection of its protein on the plasma membrane. In contrast, one study used Kv1.3 antisense oligonucleotide approach and showed a modest reduction in Kv1.3 mRNA and currents but increased microglial proliferation in unstimulated and M(LPS)-states (Pannasch et al., 2006). Here, my unpublished data show that blocking Kv1.3 channels with AgTx-2 did not affect proliferation of unstimulated or cytokine-stimulated rat or mouse microglia (Fig. A.2). Similarly, another study by our lab showed that rat microglial proliferation induced by prolonged CSF-1 stimulation (up to 3 weeks) was not affected

by treatment with Kv1.3 blockers, MgTx or charybdotoxin, likely due to the absence of Kv1.3 currents (Schlichter et al., 1996). One *in vivo* study suggested that proliferation and Kv1.3 expression might not be related, which would agree with our unpublished data. That is, proliferation of mouse microglia decreased during development (between P5 and P7) but the incidence of Kv1.3 currents doubled in the population over the same time interval (Arnoux et al., 2013). While there are studies to suggest a role of Kv1.3 channel activity in proliferation (Schlichter et al., 1996; Kotecha & Schlichter, 1999; Pannasch et al., 2006), it is not clear how blocking or reducing K^+ flux modulates this function.

Recent evidence suggests that membrane Kv1.3 channels can regulate cell proliferation not by K^+ flux, but rather through a signaling cascade initiated by phosphorylation of the channel itself (Cidad et al., 2012; Jiménez-Pérez et al., 2016). This might explain the lack of effect of Kv1.3 blockers on microglial proliferation in the above-mentioned *in* vitro studies. The ability of Kv1.3 channels at the plasma membrane to sense the membrane potential of the cell appears to be required for its role in cell proliferation. A poreless Kv1.3 mutant induced proliferation comparable to wildtype channels, but the effect was lost in a voltage-insensitive Kv1.3 mutant or in a poreless Kv1.3 mutant that was unable to localize to the plasma membrane (Cidad et al., 2012). The molecular determinant of Kv1.3 channels' pro-proliferative effect required residues within the intracellular domain of the C-terminus, Tyr-449, Ser-459, and Thr-495 (Jiménez-Pérez et al., 2016; Martinez-Marmol et al., 2016). Mutations to Tyr-449 or Ser-459 abolished the pro-proliferative effect of Kv1.3 (Jiménez-Pérez et al., 2016). However, mutation to Thr-495 maintained the pro-proliferative effect of Kv1.3 channels Jiménez-Pérez et al. (2016). It is interesting, however, that when phosphorylated a

couple of these residues are known to silence Kv1.3 channel activity; either by removing the channel from the plasma membrane or possibly by prolonging the inactivation state the channel. Kv1.3 endocytosis involves ERK1/2-mediated threonine phosphorylation of T495 (Martinez-Marmol et al., 2016). In the case of Thr-495 mutant (Jiménez-Pérez et al., 2016), the inability to phosphorylate this site prevented endocytosis of Kv1.3. Thus, the pro-proliferative effect of Kv1.3 channels was maintained. Kv1.3 currents can be suppressed by tyrosine phosphorylation at any of the six tyrosine sites on the N- and C-terminus (Y111, Y112, 113, Y137, Y449, and Y479), which can be mediated by a non-receptor Src protein tyrosine kinase (PTK) (Holmes et al., 1996; Bowlby et al., 1997; Fadool et al., 1997). It is interesting that C-type inactivation is slowed by Src PTK, or by the mutation of Y449 (Bowlby et al., 1997; Fadool et al., 1997). This unusual response could suggest that tyrosine phosphorylation at sites other than Y449 can prolong the inactivation state of the channel, prevent the ability of the channel to sense membrane potential changes, and possibly abolish the Kv1.3 channel's pro-proliferative effect. But these phenomena have yet to be investigated.

In this thesis work, I detected Kv1.3 currents in all unstimulated and stimulated rat microglia, suggesting that Src PTK did not prevent the function of the channel in these conditions. In mouse microglia, however, the prevalence of Kv currents was much lower in unstimulated (56%), M(IL-4) (42%) or M(IL-10) (56%) states, while it increased (to 92%) in the M(I+T) state. The increase in prevalence of Kv currents in M(I+T) might involve synthesis of new channel protein, as was observed in M(LPS) microglia (Nörenberg et al., 1992) but this was not tested. Alternatively, the prevalence reported for unstimulated, M(IL-4), and M(IL-10) microglia might result from a 50% probability that Src PTK phosphorylated the Kv1.3 channel. There might also be species

differences in the basal level of Src PTK activity and tyrosine phosphorylation. Notably, transcripts levels of *Ptpn6*, which encodes for the protein tyrosine phosphatase, SHP-1, and regulates K^+ currents in a manner opposite to their regulation by Src PTK (Schlichter et al., 2014), were unaffected by the activation state of rat microglia but were differentially regulated in mouse (Fig. 4.5). Whether the prevalence of Kv1.3 currents in microglia from rat and mouse indicates a species difference in the active process of proliferation was not compared in this study. CyQuant is a fluorescent dye that binds to cellular DNA and can be used to determine cell counts within a condition (Jones et al., 2001) but does not indicate whether the cell is actively proliferating. In this thesis, K^+ flux through Kv1.3 channel was not necessary to alter the proliferative capacity of resting or cytokine-activated microglia. However, we cannot rule out the possible effects of a non-conducting Kv1.3 channel protein on proliferative capacity of these cells. Future studies should examine whether Kv1.3 channel protein expression alone and not channel function is required for microglial proliferation under the activation paradigms examined in this thesis.

Other ion channels might compensate and contribute to microglial proliferation under the activation paradigms examined, despite the block of Kir2.1 or Kv1.3 channels. Considering that not all the Kv current in unstimulated and stimulated mouse microglia was blocked by AgTx-2, it is likely that other channels contribute to the AgTx-2-insensitive outward current, such as other members of the Kv1 family. We detected transcripts for Kv1.2 and Kv1.5, and their levels depended on both the activation state and the species (Fig. 4.6). While others have found Kv1.2 and Kv1.5 protein (Fordyce et al., 2005; Kotecha & Schlichter, 1999; Pannasch et al., 2006; Li et al., 2008), it is likely that the remaining current is Kv1.5, because only Kv1.3 and Kv1.5 currents have been

reported in microglia to date (Kotecha & Schlichter, 1999; Pannasch et al., 2006). Like Kv1.3 (see above), Kv1.5 channels are also proposed to contribute to microglial proliferation, but the results are conflicting (Kotecha & Schlichter, 1999; Pannasch et al., 2006). Proliferation was increased in unstimulated and M(LPS) primary mouse microglia treated with either Kv1.3 or Kv1.5 antisense oligonucleotide, or in Kv1.5-null microglia (Pannasch et al., 2006). Proliferation of tissue-printed rat microglia was increased with time in culture. While Kv1.5 currents and protein were detected in microglia 0-5 DIC, blocking the channel with 4-AP had no effect on nonproliferating cells 0 DIC but reduced cell proliferation 5 DIC, an effect opposite to mouse microglia (Pannasch et al., 2006). Since AgTx-2 did not affect cell proliferation at 5 DIC, it suggested that Kv1.5 was acquired to regulate cell proliferation until the switch from Kv1.5 to Kv1.3 expression in tissue-printed microglia greater than 6 DIC, and cell proliferation was reduced by AgTx-2 at 10 DIC. K^+ channel activity and the cell's membrane potential is positively correlated to cell cycle progression (see below). Kir2.1 is prevalent in both rat and mouse microglia, and is required to maintain a very negative resting membrane potential. It is possible that the downregulation of Kir2.1 current in LPS-stimulated mouse microglia (Draheim et al., 1999; Prinz et al., 1999; Boucsein et al., 2003), but not rat microglia (Draheim et al., 1999), was unable to compensate for the loss of Kv1.3 or Kv1.5 channels. Unfortunately, Kir2.1 current expression was not examined in the studies. Thus, while Kv1.5 is a possible candidate to compensate for the loss of Kir2.1 or Kv1.3 currents, its contribution might be species dependent. Another candidate is the swelling-sensitive Cl^- channels, which contribute to the resting membrane potential (Nernst potential ~ –35 mV), volume regulation and proliferation of rat microglia (Schlichter et al., 1996; Newell & Schlichter, 2005; Ducharme et al., 2007). In isotonic

solutions, Cl^- current mediated by swelling-sensitive Cl^- channels is very small, and can easily be mistaken for leak in primary rat microglia. However, blocking the channel is sufficient to depolarize the resting membrane potential (Newell & Schlichter, 2005). In Kv1.3 deficient thymocytes, Cl^- current was upregulated approximately 50 fold, likely to compensate for the loss of Kv1.3 channel expression, with no obvious disruption in cell proliferation (Koni et al., 2003). Thus, it is possible that Cl^- current was upregulated in microglia used for functional assays where the channel blockers were applied for 24 h, and this could compensate for the block of Kir2.1 or Kv1.3 channels.

It is increasingly clear that cell cycle progression is dependent on the membrane potential of the cell. Transition through each check point (i.e. G0/G1, S, G2/M) is positively correlated with changes in K^+ channel activity, and the cell's membrane potential (Pardo et al., 2004; Blackiston et al., 2009; Urrego et al., 2014). Unfortunately, studies detailing the membrane potential during cell cycle are lacking for microglia, but can be extrapolated based on findings from cell lines (Urrego et al., 2014). Kir2.1 or Kv1.3 channel activity, or the lack thereof, might favor particular phases of the cell cycle; e.g. depolarized cells are positively correlated with G0/G1 phase, and hyperpolarized cells are correlated with G1/S and G2/M transition phases (Urrego et al., 2014). In this thesis, cell cycle progression could not be addressed from the CyQuant assay. Thus, the question remains how Kir2.1 activity weakly inhibits proliferation in specific microglial activation phenotypes and not others, which should be addressed in future research examining the role of Kir2.1 in cell cycle progression in microglia.

5.1.2.2 Kir2.1 and Kv1.3 currents do not contribute to NO production in cytokine-activated rodent microglia

To my knowledge, the role of Kir2.1 in NO production in microglia is not known. The role of Kv1.3 in NO production remains unclear and might depend on the activating stimulus based on my findings and the literature. The unpublished data presented in this thesis show elevated NO production in M(I+T) stimulated rat and mouse microglia, which was not affected by either ML133 or AgTx-2 (Fig. A.3). This agrees with an early study from our lab that found blocking Kv1.3 did not affect NO production in M(LPS)-activated rat microglia. Similarly, in mouse microglia, NO production in M(LPS)-activated mouse microglia was not affected by reduced Kv1.3 expression (mRNA and currents) using a Kv1.3 antisense oligonucleotide approach (Pannasch et al., 2006). However, one study found that blocking Kv1.3 reduced both NO and ROS production in HIV-infected rat microglia (Liu et al., 2012), suggesting that other stimuli can recruit Kv1.3 activity for NO production. It is likely that other microglial K^+ channels play a more prominent role in regulating NO production. In mouse microglia, LPS-induced NO production was reduced by either with Kv1.5 antisense oligonucleotide treatment or in Kv1.5-null microglia (Pannasch et al., 2006). Our lab showed that blocking KCa2.3 or KCa3.1 channels reduced both ROS and NO production via attenuated p38 MAPK (but not NF-κB) activation (Kaushal et al., 2007; Schlichter et al., 2010), but this was not affected when blocking Kv1.3 channels (Fordyce et al., 2005). Collectively, there is more evidence to suggest that Kv1.3 is not involved in NO production, but other K^+ channels (e.g. Kv1.5, KCa2.3, or KCa3.1) are more likely to contribute to NO production.

5.1.2.3 Kir2.1 and Kv1.3 currents contribute to the homeostatic role of rodent microglial migration

Migration of primary rat microglia depends on their activation state. M(LPS) microglia migrate less than their unstimulated counterparts, while M(IL-4) and M(IL-10) microglia migrate more (Siddiqui et al., 2014; Lively and Schlichter, 2013; Ferreira et al., 2014; Lam & Schlichter, 2015). We now report that primary mouse microglia respond similarly. I found that blocking either Kir2.1 or Kv1.3 channels affected microglia migration, but in an opposite manner. Blocking Kir2.1 reduced migration of rat microglia in unstimulated, M(IL-4) and M(IL-10) states (Chapter 3), and this was extended to M(I+T) rat and mouse microglia under the same activation paradigms (Chapter 4). These studies are the first to show a direct link between Kir2.1 channel activity and microglia migration. Contrary to Kir2.1, blocking Kv1.3 increased migration, and this was independent of the activation state in both rat and mouse microglia. The role of Kv1.3 in microglial migration remains unclear. Blocking Kv1.3 channels with MgTx reduced MCP-1 or ADP-induced rat microglial chemotaxis (Nutile-McMenemy et al., 2007). However, observations were reported from an *in vivo* study that Kv1.3 blockers (MgTx or AgTx-2) did not prevent microglia migration into the damaged nerve fiber layer 14 days after optic nerve transection in rats (Koeberle & Schlichter, 2010). In other cell types, blocking or knockdown of Kv1.3 generally decreased migration in vascular smooth muscle cells (Cheong et al., 2011), T_{EM} cells (Matheu et al., 2010) and macrophages (Kan et al., 2016). In one study, over-expression of Kv1.3 increased macrophage migration (Kan et al., 2016). It is possible that the differences between our findings and the literature might be cell type or stimulus dependent. Although, the specific

mechanism underlying the role of Kir2.1 and Kv1.3 in microglia migration has not been examined, some insight might be gained from integrin-mediated cell attachment to the extracellular matrix (ECM).

Cell migration requires integrins, transmembrane receptors that regulate cell adhesion to the ECM. Evidence suggests that integrins and K^+ channels are part of a macromolecular signaling complex (Arcangeli & Becchetti, 2006). Kir2.1 and Kv1.3 channel protein is uniformly distributed on the plasma membrane of unipolar microglia (Kotecha & Schlichter, 1999; Muessel et al., 2013), which we have shown are migrating cells (Vincent et al. 2012; Siddiqui et al. 2012; Lively and Schlichter 2013; Ferreira et al. 2014; Siddiqui et al. 2014). Microglia express several different integrin moieties (Milner & Campbell, 2002). A physical link between β_1 integrin and Kv1.3 was reported in T cells and melanoma cells, and blocking Kv1.3 channels not only disassembled that link but also reduced cell adherence (Levite et al., 2000**;** Artym & Petty, 2002). It is not known whether a similar association between integrin and Kv1.3 channels occurs in microglia or whether Kir2.1 channels associate with integrins. However, it is known that regulatory molecules, such as protein tyrosine kinases (PTK), and small Rho GTPases (Rac and Rho), that are downstream of integrin activation, modulate Kv1.3 and Kir2.1 channel activity in microglia (Ridley et al., 2003). Src family PTKs suppressed Kv1.3 currents in rat microglia (Cayabyab et al., 2000). Activated Rac increased the Kir2.1 current in mouse microglia, while activated Rho decreased it (Muessel et al., 2013). Collectively, K^+ channels might contribute to cell migration as a feedback mechanism involved in cell detachment from the ECM. In the case of Kv1.3, one model is that cell adherence activates integrins, induces Src PTK activation, which phosphorylates and

silences Kv1.3 channel activity, and that, in turn, the Kv1.3 channel-integrin complex is disassembled and results in the detachment of the cell from the ECM.

Another possible mechanism is that the channels function to regulate the cell's membrane potential and, thus, the driving force for Ca^{2+} entry. Ca^{2+} is an important signaling molecule involved in actin-myosin based cytoskeletal remodeling, integrin-based adhesion and migration (Ridley et al., 2003; Wei et al., 2012). In rat microglia, there are several candidates that can contribute to Ca^{2+} entry: CRAC channels, TRPM7 channels, ionotropic purinergic receptors (P2X), and the reverse mode of the Na^{+}/Ca^{2+} exchanger (Jiang et al. 2003; Newell et al. 2007; Inoue 2008; Ohana et al. 2009; Siddiqui et al. 2014). Under untreated conditions, in the absence of a depolarizing stimuli (e.g. ATP), we have shown that CRAC channels contribute to the homeostatic role of microglial migration (Siddiqui et al., 2012). Here, I report in rat microglia that blocking Kir2.1 with ML133 reduced the homeostatic function of microglial migration (Lam & Schlichter, 2015), a similar effect when using CRAC channel blockers (Siddiqui et al., 2012). Reduced Ca^{2+} entry through CRAC channels in the presence of ML133, as shown using Ca^{2+} imaging, is a likely mechanism for the suppressive effect of the Kir2.1 blocker on migration. Kir2.1 channels regulate the membrane potential of microglia, and membrane depolarization induced by blocking the channel with Ba^{2+} was associated with reduced ATP-induced Ca^{2+} entry (Chung et al., 1999; Franchini et al., 2004). Ca^{2+} conductance for CRAC channels is dependent on the electrochemical gradient for Ca^{2+} ions: hyperpolarization increases Ca^{2+} influx while depolarization decreases it (Ohana et al., 2009). While reduced Ca^{2+} entry is a likely mechanism to which blocking Kir2.1 with ML133 can affect microglial migration, this was not directly tested when using the transmigration assay. One proposed experiment is to determine whether the

suppressive effect of ML133 of microglial migration can be rescued by elevating intracellular Ca^{2+} concentration either directly with ATP to activate P2X receptors or the Ca^{2+} ionophore, ionomycin, or indirectly by increasing extracellular Ca^{2+} concentration to increase the driving force for Ca^{2+} entry. While CRAC channels primarily contribute to the homeostatic role of microglial migration, Ca^{2+} entry through other Ca^{2+} permeable channels could also be affected by blocking Kir2.1 channels; e.g., TRPM7 contributes to the enhanced migratory capacity of IL-4- or IL-10-stimulated microglia; and P2X receptors are activated by the chemoattract, ATP, during the chemotaxis assay.

It is not clear how blocking Kv1.3 enhanced migration in both rat and mouse microglia, and whether this phenomenon is Ca^{2+} dependent. In rat microglia, Kv1.3 maintains membrane potential oscillations after depolarizing events (Newell & Schlichter, 2005) but the role of Kv1.3 in Ca^{2+} entry in microglia is not known. In T lymphocytes, Kv1.3 channels restore the driving force for Ca^{2+} entry by repolarizing the cell when the channels open in response to depolarization (Chandy et al., 2004; Feske et al., 2015). Future studies should investigate how Kv1.3, membrane potential, and Ca^{2+} entry in microglia affect cell migration.

5.2 Identifying microglial activation *in vivo*, and detecting M1 and M2 activation phenotypes in rodent models of CNS injury

In the mature, uninjured adult brain, microglia are highly ramified cells with several processes that branch. In this form, microglia are presumably in a resting state but are actively surveying their microenvironment through extension and retraction of their processes with little to no cell body displacement (Nimmerjahn et al., 2005; Davalos et a., 2005). Activated microglia *in vivo* are often spatially restricted in and around lesions

in animal models of traumatic brain injury or stroke (Ransohoff and Perry, 2009; Perry, Nicoll and Holmes, 2010). However, several different morphologies of activated microglia have been described (Boche et al., 2013; Ziebell et al., 2015): hyper-ramified and bushy, cells with fewer processes than the 'resting' form, ameboid with no processes, similar to infiltrating macrophages, and elongated (or rod-like). It is it is not known whether these morphological transformations reflect different activation states. In a symposium at the Society for Neuroscience meeting in 2014, Ziebell and Lifshitz reported that cells of these morphologies expressed some but not all cell-surface molecules (Iba1, CD11b, CD68, IB4, MHCII, CD11c, CD45), commonly used to identify activated microglia/macrophages *in vivo* using immunohistochemistry. It is now questioned whether or not these cell-surface molecules are pan-activation markers or whether the expression patterns reflect different activation phenotypes. In Chapter 4, we profiled the gene expression of some of these common activation markers (Iba1, CD11b, CD68 and CX3CR1) in discrete activation states (M(I+T), M(IL-4) and M(IL-10)), and found species- and activation state-dependent regulation of these genes (Table 5.1). For example, in the M(I+T) state, mRNA transcript levels increased for Iba1 (rat and mouse), and decreased for CD11b (mouse), CD68 (rat and mouse) and CX3CR1 (rat and mouse). In the M(IL-4) state, only rat microglia showed downregulation of mRNA transcripts for Iba1, CD11b, and CD68. However, in the M(IL-4) state CX3CR1 mRNA transcripts increased in rat but decreased in mouse microglia. In the M(IL-10) state, mRNA transcripts increased for CD11b (rat and mouse), CD68 (rat) and CX3CR1 (rat). At a transcript level, our findings would argue that Iba1, CD11b, CD68 and CX3CR1 are not good pan-activation markers as their gene expression is regulated by microglial activation phenotypes, and is species-dependent. This agrees with the

Table 5.1. Summary of data in Figure 4.5 on the transcript expression levels of other microglia markers and immunomodulatory molecules.

	Control		I+T		IL-4		IL-10	
	Rat	Mouse	Rat	Mouse	Rat	Mouse	Rat	Mouse
	Microglia markers, immune modulators							
Aif1 (Iba1)	#####	#	↑↑↑↑↑	↑	↓↓↓↓↓	—	—————	—
Nfkbia (IκBα)	####	###	↑↑↑↑↑	↑↑↑	———	↓↓	————	———
Cd68	#####	####	↓↓↓↓↓	↓↓↓↓	↓↓↓↓↓	—————	↑↑↑↑↑	————
Itgam (CD11b)	####	###	————	↓↓↓	↓↓↓	———	↑↑↑↑↑	↑↑↑↑
Cx3cr1	###	###	↓	↓	↑↑↑	↓↓	↓↓	———
Ptpn6 (SHP-1)	###	###	———	↑↑↑↑	———	↓↓↓	———	———
Nr3c1	###	##	↑↑↑↑	↑↑↑	———	——	———	↑↑
Tspo	###	##	↑↑↑↑	↑↑↑↑	———	——	↑↑↑↑	↑↑↑
Tlr2	###	##	———	——	↓↓	↓	———	——
Tlr4	##	##	↓↓	↑↑↑	↑↑↑	↑↑	↑↑↑	↑↑
Socs1	#	#	↑↑↑	↑↑↑↑	↑↑↑	↑↑	—	—
Socs3	#	#	↑↑	↑↑	—	—	↑↑	↑↑

	relative mRNA counts
#	<100
##	101-1000
###	1001-5000
####	5001-10,000
#####	>10,001

The number of symbols (#, arrow, —) indicates the relative mRNA counts for each condition and species. Arrows indicate the directionality of the change in expression levels relative to the unstimulated (control) condition, which were found statistically significant. **"—"** indicates no statistical significance between control and the stimulated condition.

immunohistochemical detection of these proteins in some but not all morphologies adopted by activated microglia/macrophages described by Ziebell and Lifshitz (2014). A pan-activation marker is often relied upon to identify activated microglia/macrophages *in vivo* and when cells are double labeled with a 'classical' molecular marker of the M1 or M2a state to determine the activation phenotype in injured brain tissue. Thus, it is important to consider whether such markers used for immunohistochemistry reliably detect all microglial/macrophages in the injured brain tissue, or whether they underestimate the population size. This might be particularly important when evaluating the temporal profile of microglial activation following CNS injury, where phenotypic shifts from M1 to M2a or vice versa have been observed (discussed below).

In my thesis work, I focused on applying the cytokines, IFN-γ, TNF-α, IL-4 and IL-10, because their protein levels are upregulated in damaged tissues from models of CNS injury, and they could be directing the inflammatory response of microglia. The temporal profile of cytokine levels in the brain following traumatic brain injury (TBI) has been characterized, but not enough is known in rodent models of stroke. Following TBI, protein levels of IFN-γ and TNF-α are upregulated in the damaged tissue as early as 2 h but rapidly decline by 12 or 24 h, respectively, and return to control levels by 7 days post-injury (Harting et al., 2008; Dalgard et al., 2012; Ansari, 2015). IL-4 is detected as early as 4 h and is maintained for up to 24 h before returning to control levels by 7 days post injury, while IL-10 is biphasic and is detected at 4 h and 24 h (Ansari et al., 2015; Dalgard et al., 2012). Levels of IL-10 at 7 days post-injury were not examined. In addition, cytokine levels at weeks to months post-injury are not known, and should be examined in future studies.

Gene expression changes for M1 and M2a markers have been detected in injured brain tissue (Zhao et al., 2007; Lively & Schlichter, 2012; Yang et al., 2016; Wan et al., 2016). Such tissue contains a mixture of cell types (neurons, astrocytes, oligodendrocytes, invading leukocytes); therefore, it does not simply reflect the activation state of microglia/macrophages, as other cell types can express these genes. In recent years, studies are beginning to evaluate the temporal profile of microglial activation *in vivo* following acute CNS injury, such as TBI (Wang et al., 2013; Turtzo et al., 2014; Kumar et al., 2016), ischemia (Hu et al., 2012; Fumagalli et al., 2013; Suenaga et al., 2015), and intracerebral hemorrhage (ICH) (Min et al., 2016). However, there is a need for either a more specific marker or for using a panel of molecular markers to identify the activation phenotype of microglia/macrophages *in vivo.* Immunohistochemistry has also been used to determine the activation phenotype of Iba1- or CX3CR1-positive activated microglia/macrophages by detecting a protein associated with the M1 state (e.g. iNOS; immunoglobulin Fc gamma receptor, CD16/CD32) or M2a state (i.e. Arg1, Ym1, CD206) (Cherry et al., 2014). There is a lack of studies of other activation phenotypes described *in vitro* (e.g. M2c state). In rat and mouse models of TBI, activated microglia/macrophages show a mixed population of M1 and M2a phenotypes in the first 5 days (Hsieh et al., 2013; Wang et al., 2013; Turtzo et al., 2014; Kumar et al., 2016). In particular, isolated Arg1-positive microglia/macrophages from damaged tissue 24 h after injury had increased iNOS mRNA levels (Hsieh et al., 2013). In ischemic and ICH mouse models, a greater population of activated microglia/macrophages were skewed to a M2a phenotype in the first 5 days following injury, and then gradually shifted to a M1 phenotype that peaked at 14 days (Hu et al., 2012; Suenaga et al., 2015; Min et al., 2016). Thus, there is

evidence that the microglial activation state *in vivo* following acute CNS injury is not discrete but can exist on a spectrum between the two extremes. Immunohistochemistry is a useful tool to identify the spatial and temporal progression of activated rodent microglia/macrophages in discrete M1 or M2a states following tissue damage, but the interpretation is limited to the cell's being immunopositive for the one or two protein(s) examined. In fact, gene expression profiling in my thesis and in the study by Hsieh et al. (2013) question the reliability of these M2a markers (discussed below). Thus, there is still the need to identify specific molecular markers for microglial activation phenotypes that are not regulated by other states. But the availability of potential molecular markers to identify microglial activation phenotypes *in vivo* might be limited for rats. That is, there are a lot more commercially available antibodies raised against a particular epitope in mouse but whether it cross-reacts to the same site in rats is often unconfirmed. Moreover, we still do not know how the activation state of microglia affects their effector functions.

In Chapter 4, we report that not all 'classical' molecular markers used to identify a particular activation state in one species can be generalized to another. This will be important for future studies that profile the activation states of microglia/macrophages *in* vivo from rodent models. For instance, we used NanoString Gene Expression assay to evaluate the transcript levels of 58 genes that included pro- and anti-inflammatory mediators and their receptors, neuromodulatory molecules, and K^+ channels, across the different microglial activation phenotypes (M1, M2a, and M2c). We were then able to identify the 'transcript signature' specific to each activation paradigm in both rat and mouse (Table 5.2). For example, the M1 response induced by I+T was similar in both rat and mouse microglia by up-regulating several expected molecules (iNOS, TNF-α,

Table 5.2. Summary of data in Figure 4.2 on the transcript expression levels of pro-inflammatory genes.

	Control		I+T		IL-4		IL-10	
	Rat	Mouse	Rat	Mouse	Rat	Mouse	Rat	Mouse
	Pro-inflammatory mediators							
Il1b	###	#	———	——	↓↓	↓	———	——
Ifngr2	#	###	—	↑↑↑	—	———	—	———
Ptk2b (Pyk-2)	###	##	↑↑↑↑↑	↑↑↑	——	——	———	——
Ptgs2 (COX-2)	#	#	↑↑	↑↑↑↑↑	—	——	—	—
Ifngr1	####	###	————	———	↓↓↓↓	↓↓↓	————	———
Tnfrsf1a	###	##	↑↑↑	↑↑↑	———	——	↑↑↑	↑↑↑
Tnfrsf1b	###	##	↑↑↑	——	↓↓↓	——	↑↑↑	——
Tnf (TNF-α)	##	##	↑↑↑	↑↑↑	↓↓	——	——	——
Casp1 (ICE)	##	##	↑↑↑	↑↑↑↑	——	——	——	——
Nos2 (iNOS)	#	#	↑↑↑↑↑	↑↑↑↑	—	—	—	—
Il6	#	#	↑	↑	—	—	—	—
Ifng	#	#	—	—	—	—	—	—
Il1r1	#	#	—	—	—	—	—	—

	relative mRNA counts
#	<100
##	101-1000
###	1001-5000
####	5001-10,000
#####	>10,001

The number of symbols (#, arrow, —) indicates the relative mRNA counts for each condition and species. Arrows indicate the directionality of the change in expression levels relative to the unstimulated (control) condition, which were found statistically significant. **"—"** indicates no statistical significance between control and the stimulated condition.

Table 5.3 Summary of data in Figures 4.3 and 4.4 on the transcript expression levels of markers associated with alternative (M2a) activation, and anti-inflammatory cytokines and their receptors.

	Control		I+T		IL-4		IL-10	
	Rat	Mouse	Rat	Mouse	Rat	Mouse	Rat	Mouse
	Anti-inflammatory mediators							
Tgfb1	#####	###	↓↓↓↓	———	↑↑↑↑↑	↑↑↑	↑↑↑↑↑	———
Il1rn	###	##	↑↑↑↑↑	↑↑↑	↓↓	↑↑↑	↑↑↑↑↑	——
Retnla (FIZZ1)	#	#	—	—	—	↑↑↑↑↑	—	—
Arg1	#	#	↑	—	↑	↑↑↑↑↑	—	—
Il10rb	###	###	↑↑↑	———	↓↓↓	———	↑↑↑	———
Tgfbr1	###	###	———	↑↑↑	↓↓↓	——	———	——
Tgfbr2	###	###	↑↑↑	↑↑↑	↓↓↓	↓↓	↑↑↑	↑↑↑
Il10ra	##	##	↑↑↑	↑↑↑	———	↓↓	———	——
Ilr4	##	##	↑↑↑	↑↑↑	——	——	↑↑	↑↑↑
Il13ra1	##	##	↑↑↑	↑↑↑	↓↓	↓↓	↑↑	↑↑
Mrc1 (CD206)	###	###	↓	↓↓	↑↑↑↑	↑↑↑	———	↑↑↑
Myc	##	##	↓↓	↓	↑↑↑	↑↑	——	↓↓
Pparg	##	##	↓	—	——	↑↑	——	—
Ccl22	#	#	—	↑↑	↑↑↑	↑↑↑	—	—
Cd163	#	#	—	—	↑↑	—	—	—
Il4	#	#	—	↓	—	—	—	—
Il10	#	#	—	—	—	—	—	—

	relative mRNA counts
#	<100
##	101-1000
###	1001-5000
####	5001-10,000
#####	>10,001

The number of symbols (#, arrow, —) indicates the relative mRNA counts for each condition and species. Arrows indicate the directionality of the change in expression levels relative to the unstimulated (control) condition, which were found statistically significant. "—" indicates no statistical significance between control and the stimulated condition.

COX2, IL-6) as well as some less frequently examined (ICE, PYK2), but the effects were not observed in the M(IL-4) or M(IL-10) state. In contrast, the most striking species differences in gene expression arose when examining common markers of the M2a state induced by IL-4 (Table 5.3). Several hallmark markers were up-regulated by IL-4 (Arg1, CCL22, CD206, Myc) in both species. However, other M2a markers were upregulated by IL-4 but were species dependent: CD163 (rat), PPAR-γ (mouse) and FIZZ1 (mouse). We also report that Arg1 and CD206, which are common markers for the M2a state and used in the above-mentioned in *vivo* studies, were also modulated in the M(I+T) and/ or M(IL-10) state. This questions the interpretation of Arg1- or CD206-positive microglia/macrophages reported in *in vivo* studies, and whether these markers reliably identify cells in the M2a state or rather it also includes a population of cells that are of mixed M1/M2a phenotype as shown by Hsieh et al. (2013). To identify the mixed M1/M2a phenotype in activated microglia/macrophages *in vivo*, the same brain tissue can be triple labelled with molecular markers for both M1 (e.g. iNOS) and M2a (e.g. Arg-1) activation phenotypes and activated microglia/macrophages. This will isolate a population of activated microglia/macrophages that are in the M1 or M2a state only, or M1 and M2a state. Nevertheless, we report that some molecules (Arg1, CD206, CD163, and FIZZ1) used to identify the M2a state in one rodent species cannot be generalized to the other.

5.2.1 Relevance of activation state-dependent functions *in vitro* to *in vivo* observations.

Following CNS injury, microglial responses can evolve over time, and they can acquire a cohort of functions, including migration, proliferation and/or production and secretion of pro- or anti-inflammatory mediators (Lynch, 2009; Kettenmann et al., 2011; Hanisch, 2013). However, whether these functions persist or are modulated under different activation phenotypes *in vivo* remains to be determined. During the course of my PhD studies, the Schlichter lab showed that rat microglial functions *in vitro* are activation state-dependent. Migration and invasion through the ECM were drastically reduced in an M1 state but increased in M2a and M2c states (Lively and Schlichter, 2013; Siddiqui et al., 2014). Myelin phagocytosis was increased in M1 and M2c states but was unaffected in the M2a state (Siddiqui et al., 2016). In this thesis, I reported that the proliferative capacity of microglia was unaffected in M2a or M2c states (Lam & Schlichter, 2015, Chapter 3), and that the activation state dependence of migration in rat is also conserved in mouse microglia (Lam et al., under revision; Chapter 4). In addition, unpublished data from our lab showed that increased NO production is specific to microglia in the M1 state (not M2a or M2c) in both rat and mouse microglia (Fig. A.3). We are beginning to understand that microglial functional responses (e.g. migration and NO production) are regulated differently depending on the activation state of the cell. We will continue to be limited in our interpretation of microglia/macrophages responses *in vivo* until microglial activation states can be readily and reliably differentiated.

Direct evidence of microglial migration immediately following tissue injury has been observed using *in vivo* and *ex vivo* models. Earlier studies reported that neuronal

injury in organotypic hippocampal slices, either due to NMDA-mediated excitotoxicity or the very process of preparing brain tissue slices, induced microglia migration to sites of neuronal degeneration (Heppner et al., 1998; Stence et al., 2001). However, there is evidence that microglial migration might be a delayed process, taking 24 h to a few days to occur. Two seminal studies showed that within the first few minutes following laser-induced or mechanical injury to the cortex, microglia in the immediate vicinity of the injured site project their ramified processes towards the site of injury, with no cell body displacement for at least 10 h (Davalos et al., 2005; Nimmerjahn et al., 2005; Kim & Dustin, 2006). Time-lapse imaging in an ischemic mouse model also reported the same finding; no cell displacement was detected within the first 24 h period following tissue damage (Fumagalli et al., 2012). In a follow up study, ameboid microglia with short ramified processes migrated to the damaged site 1-3 days later following laser-induced parenchymal injury (Kim & Dustin, 2006). Davalos et al. (2005) demonstrated that the initial response of microglia following tissue damage is mediated by ATP, a chemoattractant enhances cell migration *in vitro* (Honda et al., 2001; Lively & Schlichter, 2013). However, the lack of cell migration within 24 h of tissue damage, suggests that other factors are involved to evoke this response. We show that 24 h cytokine stimulation was sufficient to alter the migratory capacity of microglia; i.e., it was enhanced by IL-4 or IL-10, and dampened by I+T. Changes in temporal profiles of these cytokines (within hours) in rodent models of acute CNS injury (discussed §5.2) presents possible candidates that modulate the migratory capacity of microglia in *in vivo* and *ex vivo* preparations.

Evaluating other activated microglial functions *in vivo* remains limited to antibodies available that detect proteins relevant to these functional responses.

However, the information is an over-simplification of the functional attributes, as demonstrated from *in vitro* studies. For instance, iNOS is involved in nitric oxide synthesis, and is commonly used as a M1 marker as described in §5.2. Production of NO is required for formation of peroxynitrite, a neurotoxic molecule released from activated microglia, which contributes to microglia-mediated neurotoxicity (Boje and Arora, 1992; Fordyce et al., 2005). Our unpublished data showed upregulation of iNOS mRNA transcript and NO levels in only the M1 state induced by I+T (but not M2a or M2c state, Fig. A.3). Thus, iNOS is a reliable M1 marker for both rat and mouse microglia. However, an early study by the Schlichter lab demonstrated that NO production might be dependent on the stimulus used to activate microglia into a neurotoxic state. For example, oxygen-glucose-deprived neurons or an mGluRII agonist, used to mimic the release of glutamate from dying neurons, activated primary rat microglial cells, which then became neurotoxic by producing TNF-α but not NO (Kaushal et al., 2008). While the activation state of microglia was not characterized in that study, it suggests the possibility of multiple M1 phenotypes. Thus, while iNOS can be used as a marker for the M1 activation state, it might reflect a subpopulation of activated microglia that are neurotoxic and capable of producing NO, and underestimate the true population of cells that are pro-inflammatory.

5.3 Future studies

5.3.1 Mathematical modeling: interaction between K^+ channels (Kir2.1, Kv1.3), membrane potential and Ca^{2+} entry

There is considerable experimental data from the earlier studies in the Schlichter lab, my thesis, and the literature that suggests a dynamic interaction between Kir2.1 and Kv1.3 channels, the membrane potential, and Ca^{2+} entry in microglia; but collectively this interaction has not been investigated. I had initially proposed this study during my PhD that would combine mathematical modeling with experimental data from my thesis and the literature. Certainly, this study would be a collaborative effort with someone with a mathematics background where we would model the expected inverse relationship between the membrane potential and intracellular Ca^{2+} concentrations. For example, membrane potential oscillations (between –60 mV and –35 mV), over a narrow band of frequencies around 10 Hz, were observed in response to depolarizing current (Newell & Schlichter, 2005). This was consistent with the bi-stable distribution of resting membrane potentials reported in microglia (Nörenberg et al., 1994; Visentin et al., 1995; Chung et al., 1999; Bouscein et al., 2003). In microglia, the membrane potential influences Ca^{2+} entry through store-operated Ca^{2+} channels, primarily mediated by Ca^{2+} release-activated Ca^{2+} (CRAC) channels: hyperpolarization increased Ca^{2+} influx while depolarization decreased it (Ohana et al., 2009). Interestingly a similar oscillation frequency in intracellular Ca^{2+} levels (~10 Hz) was observed in T cells when interacting with antigen-presenting cells, a reported observation by M. Davis mentioned by Newell and Schlichter (2005).

With this model, we can incorporate the biophysical properties of Kir2.1 and Kv1.3 channels to examine how K^+ flux mediated by Kir2.1 or Kv1.3 channels affect membrane potential oscillations and the subsequent change in intracellular Ca^{2+} levels. Studies have demonstrated that Kir2.1 and Kv1.3 channels regulate the membrane potential of microglia. Kir2.1 channels are important for keeping the resting membrane potential very negative, while Kv1.3 channels are important for repolarization and membrane potential oscillations (Chung et al., 1998 &1999; Franchini et al., 2004; Newell & Schlichter, 2005). While it is not known whether Kv1.3 influences Ca^{2+} entry in microglia, we now know that blocking Kir2.1 with ML133 channels reduced Ca^{2+} entry through CRAC channels (Lam & Schlichter, 2015), which is consistent with reduced ATP-induced Ca^{2+} entry observed in rat microglia by blocking Kir current with Ba^{2+} and prolonging membrane depolarization (Franchini et al., 2004).

In developing such a model, we can evaluate whether and how Kir2.1 and Kv1.3 channel activity affect membrane potential and intracellular Ca^{2+} oscillations (i.e. frequency, period, amplitude). This might provide insight into Ca^{2+} dependent microglial functions, like migration. Here, we demonstrated that both Kir2.1 and Kv1.3 channels contribute to the homeostatic function of migration, but in an antagonistic manner, in both rat and mouse microglia regardless of activation state. This is interesting since I demonstrated that Kir2.1 and Kv1.3 currents are regulated depending on the cytokine stimulus and rodent species (Chapter 4). Ideally, we can perturb the model by changing K^+ conductance, similar to current amplitudes I reported from cytokine-activated microglia, and address whether there is a threshold for K^+ conductance to alter membrane potential oscillations and subsequent intracellular Ca^{2+} oscillations. Likewise, we can also address whether and how the directionality of K^+ flux affects this model. For

instance, in §5.1.1.1.1 I discussed the limitations of using Ba^{2+} in cell-based assays because it blocks Kir2.1 in a voltage dependent manner (weak at depolarized potentials). Thus, I also used ML133, which I showed was voltage-independent, to strengthen the role of Kir2.1 channels in cellular functions. Both Ba^{2+} and ML133 reduced microglial migration and chemotaxis regardless of activation state (Chapter 3), but ML133 was more effective. The question remains whether the small K^+ current (~60 pA, Fig. 3.1) of Kir2.1 is capable of influencing membrane potential oscillations and subsequently intracellular Ca^{2+} oscillations. Secondly, we demonstrated that blocking Kv1.3 channels enhanced microglial migration, suggesting that K^+ efflux is required for this function. With additional experimental data on the role of Kv1.3 on Ca^{2+} entry, we could then determine whether this enhancement is Ca^{2+} signaling dependent, and in using the model we can propose the 'how'.

5.3.2 Translating rodent models to human

With recent advances in molecular technology, large-scale screening and expression studies have evaluated whether genes are evolutionarily conserved across species. Inter-species transcriptome analysis revealed baseline tissue-specific expression of orthologous genes that were highly conserved across species (i.e. human, mouse, rat) (Tsaparas et al., 2006; Zheng-Bradley et al., 2010; Prasad et al., 2013). But the closely related rodents, mouse and rat, exhibited a higher expression of these genes relative to humans (Prasad et al., 2013). Despite this global similarity between species, there is still some debate as to whether rodent models mimic human inflammatory diseases (Seok et al., 2013; Takao and Miyakawa, 2015). Seok et al. (2013) reported that blood samples from patients with inflammatory diseases (e.g. trauma, burn and endotoxemia)

exhibited similar gene expression patterns between the human inflammatory diseases, but fewer correlations to the corresponding mouse models. The authors concluded that mouse models poorly mimic the human condition. However, Takao et al. (2015) reanalyzed the data set and challenged the interpretation, reporting that cohorts of genes that changed in both the human condition and mouse model were highly correlated, and thus mouse models greatly mimic their counterpart human diseases. However, it is important to consider the cell type(s) used when examining the genomic response in the mouse models compared to their counterpart human condition (Seok et al., 2013; Takao and Miyakawa, 2015). In particular, circulating neutrophils are far more abundant in human than mouse (Mestas et al., 2004). Of note, the transcriptome studies by Seok et al. (2013) and Takao and Miyakawa (2015), only compared the genomic response between mouse models and the human conditions, and yet provoked the scientific community to the discuss whether rodent models, in general, should be used to investigate human diseases for translational research (Cauwels et al., 2013; de Souza, 2013; Drake, 2013; Osterburg et al., 2013; Warren et al., 2015; Shay et al., 2015). This debate also implicated rat models despite no comparisons being made to the human condition.

5.3.2.1 Microglial immune response in rodents versus humans

My thesis work is apparently the first to report that the choice of rodent species can affect molecular and functional responses of microglia to activating stimuli, and possibly the outcome in preclinical models. The question remains, then, whether these rodent models are a good predictor of humans when studying microglia physiology. There are only a couple of studies that directly compare inter-species immune responses of

microglia *in vitro*, particularly gene expression profiles and NO production. Recently, inter-species differences were assessed in primary cultures of neurons, astrocytes and microglia from mice, rats and humans. It examined gene expression, levels of chemokines (CX3CL1, CXCL12, CCL2, CCL3, and CXCL10) and cytokines (IL-1α, IL-1 β, IL-6, IL-10, and TNF-α) before and after oxygen-glucose deprivation (OGD) and reoxygenation (Du et al., 2016). In general, differences in baseline levels of chemokines and cytokines between human and rodent species were detected. Following OGD and reoxygenation, primary cultures from rats upregulated all chemokines and cytokines, mouse microglia showed smaller mixed changes and humans showed stronger mixed responses. Of interest to the work reported in this thesis, cytokine expression changes following OGD and reoxygenation in microglia were comparable between rats and humans (i.e. upregulation of IL-1α, IL-1β, IL-6 and TNF-α), while mouse showed negligible but mixed gene expression changes (i.e. upregulation of IL-1β and downregulation of IL-10 and TNF-α, but not IL-1α and IL-6). Only the downregulation of IL-10 in microglia following OGD and reoxygenation in mice was similar to the human response. Species differences in reactive oxygen species (i.e. superoxide anion and NO) production were reported in microglia (Colton et al., 1996). Human microglia produced more superoxide anion following phagocytosis of opsonized zymosan than rat microglia. Unfortunately, mouse microglia were not examined. Also, while basal NO levels were detected in both human and mouse microglia, only mouse microglia increased NO following stimulation with pro-inflammatory mediators (LPS, TNF-α, IL-1β). While the authors did not examine NO production in rat microglia, the findings in my thesis demonstrate that both rat and mouse microglia increase NO production in the M(I+T) state. It is possible that human microglia might regulate their functions in a

manner different from rat or mouse, but this will need to be investigated by future studies.

Not enough is known about species differences *in vivo* using studies that compare rat and mouse models of CNS injury. The neuroimmune response following CNS injury might be tissue-, cell type-, or injury model-specific. Following spinal cord injury, the time course of microglial activation (as judged by CD68 immunoreactivity) was similar in both rat and mouse, but it was evident that T-lymphocyte and dendritic cell infiltration varied between these species (Sroga et al., 2003). Following intracortical microelectrode implantation, species differences were apparent in CD68 immunoreactivity in rats versus mouse. CD68 immunoreactivity declined between 2 and 16 weeks in the rat model but no change was seen in the mouse model (Potter-Baker et al. 2014). Sroga et al. (2003) and Potter-Baker et al. (2014) did not examine whether inflammatory mediators that condition the cellular environment and thus could affect cellular responses were different between species. Rat and mouse species differences were reported in mRNA expression of pro-inflammatory mediators (iNOS, TNF- α, IL-1β) from the injured tissue *in vivo* following focal brain ischemia (Schroeter et al., 2003). Strong gene expression changes were observed in rat; e.g. TNF-α peaked at 4 h, while iNOS and IL-1β peaked at 16 h following ischemic injury. However, in mouse, the gene expression changes were weaker and delayed: both TNF-α and IL1-β peaked at 24 h and iNOS at peaked at 14 day. Immunoreactivity for iNOS was strongly expressed in cells (cell type not identified) surrounding the infarct as early as 1 day following ischemic injury in rats; however, iNOS immunoreactivity in mouse was low but detectable at day 14. Studies that phenotyped activated microglia/macrophages following ischemic injury reported a transient M2a phenotype that gradually shifted to a M1 phenotype (as judged

by iNOS immunoreactivity, described in §5.2), but this was only examined in mice (Hu et al., 2012; Suenaga et al., 2015). It is possible that the immune response of activated microglia/macrophages following ischemic injury is delayed in mice, which might not be the case in rats (Schroeter et al., 2003). Thus, it will be important that future studies elucidate and compare whether microglia responses (i.e. molecular and function profiles) are conserved or different between rodent species, and whether they compare to human microglia *in vitro* and *in vivo*.

5.3.2.2 Expression of Kir2.1 and Kv1.3 channels in human microglia

Very little is known about expression of Kv1.3 channels in human microglia and nothing is known about Kir2.1 channels. Kv1.3 channels have been detected in activated microglia/macrophages from post-mortem human tissue from ischemic infarcts (Chen et al., 2015) and Alzheimer's disease (Rangaraju et al., 2015). Like rodent microglia, K^+ currents were seen in human microglia isolated from fetal human tissue (McLarnon et al., 1997 & 2002; Franciosi et al., 2002). Human microglia expressed Cs^+-sensitive inward K^+ currents but no outward K^+ currents were observed 1-2 days post-plating. However, 5-7 days post-plating, an outward K^+ current was seen, which displayed C-type inactivation and sensitivity to 4-AP (McLarnon et al., 1997). In subsequent studies, the authors reported upregulation of 4-AP- and TEA-sensitive K^+ currents in all cells (n=5) stimulated with IFN-γ but its presence in only a low proportion of cells (14/41) following stimulation with TNF-α (McLarnon et al., 2001 & 2002), similar to rodent microglia (Nörenberg et al., 1992 & 1994; Visentin et al., 1995; Fordyce et al., 2005;

Draheim et al., 1999; Prinz et al., 1999; Pannasch et al., 2006). While no specific Kv blockers were used to identify the channel(s) involved, the authors noticed that the inactivation of outward K^+ current in human microglia stimulated IFN-γ was different from TNF-α stimulation; e.g. Kv1.3-like following IFN-γ stimulation and Kv1.5-like following TNF-α stimulation. It is possible that the expression of Kv1 subtypes in human microglia is stimulus dependent, but pharmacological profiling of the currents will need to be done in future studies. In rodent microglia, Kv1.3 channels are predominantly expressed and regulated under different activation states, but it is not clear whether this is also the case in humans. Interestingly, the inward K^+ current was not affected by either IFN-γ or TNF-α stimulation, which is similar to my observations in rat (but not mouse) microglia. With a more selective, and commercially available inhibitor for Kir2.1 (ML133) and Kv1.3 (e.g. AgTx-2, PAP-1), future studies can now elucidate whether Kir2.1 and Kv1.3 channels are expressed in human microglia, and whether these channels are feasible drug targets in microglia, as demonstrated in rodents.

5.4 Conclusion

Potassium channels are potential drug targets for regulating microglial functions during CNS inflammation. When I began my thesis work, not enough was known about K^+ channel expression and contributions to microglia functions, and whether and if they are modulated under different activation phenotypes *in vitro* and *in vivo*. In my thesis work, I highlighted similarities and differences in the inflammatory response, migration capacity, and K^+ channel activity in rat and mouse microglia following stimulation with pro- and anti-inflammatory cytokines. The findings have provided valuable information about discrete microglial activation states *in vitro* that are relevant to neuroinflammation *in*

vivo, and might provide insight for identifying microglial activation states in future *in vivo* studies. Moreover, I report that despite species differences in Kir2.1 and Kv1.3 expression and currents in the activation paradigms examined, Kir2.1 and Kv1.3 currents were required for microglial migration (but not for proliferation or NO production), and interestingly the two channels regulate this function in a reciprocal manner. In particular, I demonstrated that Kir2.1 channel activity regulates store-operated Ca^{2+} entry through CRAC channels, and two Ca^{2+} dependent functions (migration and proliferation). With a more specific blocker for Kir2.1, future studies can now elucidate roles for Kir2.1 channels in other microglial responses. Moreover, it is important that future studies be aware that the microglial responses *in vitro* (e.g. gene expression, channel activity, function) and, by extension, the inflammatory response from preclinical models might not be generalizable from one species to another.

References

Ansari, M. A. (2015). Temporal profile of M1 and M2 responses in the hippocampus following early 24h of neurotrauma. *J. Neurol. Sci.* 357, 41-49.

Arcangeli, A., and Becchetti, A. (2006). Complex functional interaction between integrin receptors and ion channels. *Trends Cell. Biol.* 16, 631-9.

Armstrong, C.M., Swenson, R.P., Jr., and Taylor, S.R. (1982). Block of squid axon K channels by internally and externally applied barium ions. *J. Gen. Physiol.* 80, 663-682.

Armstrong, C.M., and Taylor, S.R. (1980). Interaction of barium ions with potassium channels in squid giant axons. *Biophys. J.* 30, 473-488.

Arnoux, I., Hoshiko, M., Mandavy, L., Avignone, E., Yamamoto, N., and Audinat, E. (2013). Adaptive phenotype of microglial cells during the normal postnatal development of the somatosensory "Barrel" cortex. *Glia.* 61, 1582-94.

Artym, V.V., and Petty, H.R. (2002). Molecular proximity of Kv1.3 voltage-gated potassium channels and β_1-integrins on the plasma membrane of melanoma cells: effects of cell adherence and channel blockers. *J. Gen. Physiol.* 120, 29-37.

Barcia, C., Ros, C. M., Annese, V., Gomez, A., Ros-Bernal, F., Aguado-Yera, D., et al. (2011). IFN-gamma signaling, with the synergistic contribution of TNF-alpha, mediates cell specific microglial and astroglial activation in experimental models of Parkinson's disease. *Cell Death Dis.* 2, e142.

Baronas, V.A., and Kurata, H.T. (2014). Inward rectifiers and their regulation by endogenous polyamines. *Front. Physiol.* 5, 325.

Bartok, A., Toth, A., Somodi, S., Szanto, T.G., Hajdu, P., Panyi, G., and Varga, Z. (2014). Margatoxin is a non-selective inhibitor of human Kv1.3 K^+ channels. *Toxicon*. 87, 6-16.

Becchetti, A., Pillozzi, S., Morini, R., Nesti, E., and Arcangeli, A. (2010). New insights into the regulation of ion channels by integrins. *Int. Rev. Cell. Mol. Biol.* 279, 135-190.

Beck, A., Penner, R., and Fleig, A. (2008). Lipopolysaccharide-induced down-regulation of Ca^{2+} release-activated Ca^{2+} currents (I CRAC) but not Ca^{2+}-activated TRPM4-like currents (I CAN) in cultured mouse microglial cells. *J. Physiol.* 586, 427-439.

Becker, K.J. (2016). Strain-related differences in the immune response: relevance to human stroke. *Transl. Stroke Res*. 7, 303-12.

Benjamini, Y., and Yekutieli, D. (2001). The control of the false discovery rate in multiple testing under dependency. *Ann. Stat.* 29, 1165-88.

Blackiston, D.J., McLaughlin, K.A., and Levin, M. (2009). Bioelectric controls of cell proliferation: ion channels, membrane voltage and the cell cycle. *Cell Cycle* 8, 3527-3536.

Blais, V., and Rivest, S. (2004). Effects of TNF-alpha and IFN-gamma on nitric oxide-induced neurotoxicity in the mouse brain. *J. Immunol.* 172, 7043-7052.

Boche, D., Perry, V.H., and Nicoll, J.A. (2013). Review: activation patterns of microglia and their identification in the human brain. Neuropathol. Appl. Neurobiol. 39, 3-18.

Boje, K. M., and Arora, P. K. (1992). Microglial-produced nitric oxide and reactive nitrogen oxides mediate neuronal cell death. Brain Res. 587, 250-256.

Borowiec, A.S., Bidaux, G., Pigat, N., Goffin, V., Bernichtein, S., and Capiod, T. (2014). Calcium channels, external calcium concentration and cell proliferation. *Eur. J. Pharmacol.* 739, 19-25.

Boucsein, C., Kettenmann, H., and Nolte, C. (2000). Electrophysiological properties of microglial cells in normal and pathologic rat brain slices. *Eur. J. Neurosci.* 12, 2049-2058.

Boucsein, C., Zacharias, R., Farber, K., Pavlovic, S., Hanisch, U.K., and Kettenmann, H. (2003). Purinergic receptors on microglial cells: functional expression in acute brain slices and modulation of microglial activation in vitro. *Eur. J. Neurosci.* 17, 2267-2276.

Bowlby, M.R., Fadool, D.A., Holmes, T.C., and Levitan, I.B. (1997). Modulation of the Kv1.3 potassium channel by receptor tyrosine kinases. *J. Gen. Physiol*. 110, 601-610.

Boyer, S.B., Slesinger, P.A., and Jones, S.V. (2009). Regulation of Kir2.1 channels by the Rho-GTPases, Rac1. *J. Cell. Physiol.* 218, 385-393.

Brockhaus, J., Ilschner, S., Banati, R.B., and Kettenmann, H. (1993). Membrane properties of ameboid microglial cells in the corpus callosum slice from early postnatal mice. *J. Neurosci.* 13, 4412-4421.

Bryant, C.E., and Monie, T.P. (2012). Mice, men and the relatives: cross-species studies underpin innate immunity. *Open Biol.* 2, 120015.

Butovsky, O., Jedrychowski, M.P., Moore, C.S., Cialic, R., Lanser, A.J., Gabriely, G., Koeglsperger, T., Dake, B., Wu, P.M., Doykan, C.E., et al. (2014). Identification of a unique TGF-beta-dependent molecular and functional signature in microglia. *Nat. Neurosci.* 17, 131-143.

Cahalan, M. D., and Chandy, K. G. (2009). The functional network of ion channels in T lymphocytes. *Immunol. Rev.* 231, 59-87.

Cao, Y.J., and Houamed, K.M. (1999). Activation of recombinant human SK4 channels by metal cations. *FEBS Lett.* 446, 137-141.

Capiod, T. (2011). Cell proliferation, calcium influx and calcium channels. *Biochimie.* 93, 2075-2079.

Cardona, A.E., Pioro, E.P., Sasse, M.E., Kostenko, V., Cardona, S.M., Dijkstra, I.M., Huang, D., Kidd, G., Dombrowski, S., Dutta, R., et al. (2006). Control of microglial neurotoxicity by the fractalkine receptor. *Nat. Neurosci*. 9, 917-24.

Cauwels, A., Vandendriessche, B., and Brouckaert, P. (2013). Of mice, men, and inflammation. *Proc. Natl. Acad. Sci. U. S. A.* 110, E3150.

Cayabyab, F.S., Khanna, R., Jones, O.T., and Schlichter, L.C. (2000). Suppression of the rat microglia Kv1.3 current by src-family tyrosine kinases and oxygen/glucose deprivation. *Eur. J. Neurosci.* 12, 1949-60.

Chan, W. Y., Kohsaka, S., and Rezaie, P. (2007). The origin and cell lineage of microglia: new concepts. *Brain Res. Rev.* 53, 344-354.

Chandy, K. G., Wulff, H., Beeton, C., Pennington, M., Gutman, G. A., and Cahalan, M. D. (2004). K^+ channels as targets for specific immunomodulation. Trends Pharmacol. Sci. 25, 280-289.

Chao, C. C., Hu, S., Molitor, T. W., Shaskan, E. G., and Peterson, P. K. (1992). Activated microglia mediate neuronal cell injury via a nitric oxide mechanism. *J. Immunol.* 149, 2736-2741.

Charolidi, N., Schilling, T., and Eder, C. (2015). Microglial Kv1.3 Channels and P2Y12 Receptors Differentially Regulate Cytokine and Chemokine Release from Brain Slices of Young Adult and Aged Mice*. PLoS One*. 10, e0128463.

Chen, Y.J., Nguyen, H.M., Maezawa, I., Grössinger, E.M., Garing, A.L., Köhler, R., Jin, L.W., and Wulff, H. (2015). The potassium channel KCa3.1 constitutes a pharmacological target for neuroinflammation associated with ischemia/reperfusion stroke. *J. Cereb. Blood Flow Metab*. doi: 10.1177/0271678X15611434

Cherry, J.D., Olschowka, J.A., and O'Banion, M.K. (2014). Neuroinflammation and M2 microglia: the good, the bad, and the inflamed. *J. Neuroinflammation.* 11, 98.

Chhor, V., Le Charpentier, T., Lebon, S., Ore, M.V., Celador, I.L., Josserand, J., Degos, V., Jacotot, E., Hagberg, H., Savman, K., et al. (2013). Characterization of phenotype markers and neuronotoxic potential of polarised primary microglia in vitro. Brain Behav *Immun.* 32, 70-85.

Chung, S., Joe, E., Soh, H., Lee, M. Y., and Bang, H. W. (1998). Delayed rectifier potassium currents induced in activated rat microglia set the resting membrane potential. *Neurosci. Lett*. 242, 73-76.

Chung, S., Jung, W., and Lee, M.Y. (1999). Inward and outward rectifying potassium currents set membrane potentials in activated rat microglia. *Neurosci. Lett.* 262, 121-124.

Chung, I., and Schlichter, L.C. (1997a). Native Kv1.3 Channels are upregulated by protein kinase C. *J. Membr. Biol*. 156, 73-85.

Chung, I., and Schlichter, L.C. (1997b) Regulation of native Kv1.3 channels by cAMP-dependent protein phosphorylation. *Am. J. Physiol*. 273, C622-33.

Cidad, P., Jimenez-Perez, L., Garcia-Arribas, D., Miguel-Velado, E., Tajada, S., Ruiz-McDavitt, C., et al. (2012). Kv1.3 channels can modulate cell proliferation during phenotypic switch by an ion-flux independent mechanism. *Arterioscler. Thromb. Vasc. Biol.* 32, 1299-1307.

Coetzee, W.A., Amarillo, Y., Chiu, J., Chow, A., Lau, D., McCormack, T., Morena, H. et al. (1999). Molecular diversity of K^+ channels. *Ann. N.Y. Acad. Sci*.1, 233-285.

Colton, C., Wilt, S., Gilbert, D., Chernyshev, O., Snell, J., and Dubois-Dalcq, M. (1996). Species differences in the generation of reactive oxygen species by microglia. *Mol. Chem. Neuropathol.* 28, 15-20.

Colton, C.A. (2009). Heterogeneity of microglial activation in the innate immune response in the brain. *J. Neuroimmune Pharmacol.* 4, 399-418.

Crain, J. M., Nikodemova, M., and Watters, J. J. (2013). Microglia express distinct M1 and M2 phenotypic markers in the postnatal and adult central nervous system in male and female mice. *J. Neurosci. Res*. 91, 1143-1151.

Cunningham, C. (2013). Microglia and neurodegeneration: the role of systemic inflammation. *Glia*. 61, 71-90.

Czeh, M., Gressens, P., and Kaindl, A.M. (2011). The yin and yang of microglia. *Dev. Neurosci.* 33, 199-209.

Das, A., Kim, S.H., Arifuzzaman, S., Yoon, T., Chai, J.C., Lee, Y.S., Park, K.S., Jung, K.H., and Chai, Y.G. (2016). Transcriptome sequencing reveals that LPS-triggered transcriptional responses in established microglia BV2 cell lines are poorly representative of primary microglia. *J. Neuroinflammation*. 13, 182.

Dalgard, C. L., Cole, J. T., Kean, W. S., Lucky, J. J., Sukumar, G., McMullen, D. C., et al. (2012). The cytokine temporal profile in rat cortex after controlled cortical impact. *Front. Mol. Neurosci*. 5, 6.

Dassau, L., Conti, L.R., Radeke, C.M., Ptacek, L.J., and Vandenberg, C.A. (2011) Kir2.6 regulates the surface expression of Kir2.x inward rectifier potassium channels. *J. Biol. Chem.* 286, 9526-41.

Davalos, D., Grutzendler, J., Yang, G., Kim, J.V., Zuo, Y., Jung, S., Littman, D.R., Dustin, M.L., and Gan, W.B. (2005). ATP mediates rapid microglial response to local brain injury in vivo. *Nat. Neurosci.* 8, 752-758.

de Boer, T. P., Houtman, M. J., Compier, M., and van der Heyden, M. A. (2010). The mammalian K(IR)2.x inward rectifier ion channel family: expression pattern and pathophysiology. *Acta. Physiol. (Oxf).* 199, 243-256.

De Simoni, A., Allen, N.J., and Atwell D. (2008). Charge compensation for NADPH oxidase activity in microglia in rat brain slices does not involve a proton current. *Eur. J. Neurosci*. 28, 1146-1156.

de Souza, N. (2013). Model organisms: Mouse models challenged. *Nat. Methods*. 10, 288.

Dénes, A., Ferenczi, S., Halász, J., Környei, Z., and Kovács, K.J. (2008). Role of CX3CR1 (fractalkine receptor) in brain damage and inflammation induced by focal cerebral ischemia in mouse. *J. Cereb. Blood Flow Metab*. 28, 1707-21.

Derler, I., Madl, J., Schutz, G., and Romanin, C. (2012). Structure, regulation and biophysics of I(CRAC), STIM/Orai1. *Adv. Exp. Med. Biol.* 740, 383-410.

Dheen, S. T., Jun, Y., Yan, Z., Tay, S. S., and Ling, E. A. (2005). Retinoic acid inhibits expression of TNF-alpha and iNOS in activated rat microglia. *Glia*. 50, 21-31.

Draheim, H.J., Prinz, M., Weber, J.R., Weiser, T., Kettenmann, H., and Hanisch, U.K. (1999). Induction of potassium channels in mouse brain microglia: cells acquire responsiveness to pneumococcal cell wall components during late development. *Neuroscience* 89, 1379-1390.

Drake, A. C. (2013). Of mice and men: what rodent models don't tell us. *Cell. Mol. Immunol.* 10, 284-285.

Du, Y., Deng, W., Wang, Z., Ning, M., Zhang, W., Zhou, Y., Lo, E.H., and Xing, C. (2016). Differential subnetwork of chemokines/cytokines in human, mouse, and rat brain cells after oxygen-glucose deprivation. *J. Cereb. Blood. Flow. Metab.* pii: 0271678X16656199. [Epub ahead of print]

Ducharme, G., Newell, E.W., Pinto, C., and Schlichter, L.C. (2007). Small-conductance Cl^- channels contribute to volume regulation and phagocytosis in microglia. *Eur. J. Neurosci.* 26, 2119-2130.

Eder, C. (2005). Regulation of microglial behavior by ion channel activity. *J. Neurosci. Res.* 81, 314-321.

Fabriek, B.O., Dijkstra, C.D., and van den Berg, T.K. (2005). The macrophage scavenger receptor CD163. *Immunobiology.* 210, 153-60.

Fadool, D.,A., Holmes, T.C., Berman, K., Dagan, D., Levitan, I.B. (1997). Tyrosine phosphorylation modulates current amplitude and kinetics of a neuronal voltage-gated potassium channel. *J. Neurophysiol.* 78, 1563-1573.

Farber, K., and Kettenmann, H. (2006). Purinergic signaling and microglia. *Pflugers Arch.* 452, 615-621.

Ferreira, R., Lively, S., and Schlichter, L.C. (2014). IL-4 type 1 receptor signaling up-regulates KCNN4 expression, and increases the KCa3.1 current and its contribution to migration of alternative-activated microglia. *Front. Cell. Neurosci.* 8, 183.

Ferreira, R., and Schlichter, L.C. (2013). Selective activation of KCa3.1 and CRAC channels by P2Y2 receptors promotes Ca^{2+} signaling, store refilling and migration of rat microglial cells. *PLoS One* 8, e62345.

Feske, S., Wulff, H., and Skolnik, E.Y. (2015). Ion channels in innate and adaptive immunity. *Annu. Rev. Immunol*. 33, 291-353.

Fischer, H.G., Eder, C., Hadding, U., and Heinemann, U. (1995). Cytokine-dependent K^+ channel profile of microglia at immunologically defined functional states. *Neuroscience*. 64, 183-91.

Fordyce, C. B., Jagasia, R., Zhu, X., and Schlichter, L. C. (2005). Microglia Kv1.3 channels contribute to their ability to kill neurons. J Neurosci, 25(31), 7139-7149.

Franciosi, S., Choi, H. B., Kim, S. U., and McLarnon, J. G. (2002). Interferon-gamma acutely induces calcium influx in human microglia. *J. Neurosci. Res.*, 69, 607-613.

Franchini, L., Levi, G., and Visentin, S. (2004). Inwardly rectifying K^+ channels influence Ca^{2+} entry due to nucleotide receptor activation in microglia. *Cell Calcium* 35, 449-459.

Franco, R., and Fernandez-Suarez, D. (2015). Alternatively activated microglia and macrophages in the central nervous system. *Prog. Neurobiol*. 131, 65-86.

Fu, R., Shen, Q., Xu, P., Luo, J.J., and Tang, Y. (2014). Phagocytosis of microglia in the central nervous system diseases. *Mol. Neurobiol*. 49, 1422-34.

Fumagalli, S., Perego, C., Ortolano, F., and De Simoni, M. G. (2013). CX3CR1 deficiency induces an early protective inflammatory environment in ischemic mice. *Glia.* 61, 827-842.

Fürst, O., Mondou, B., and D'Avanzo, N. (2014). Phosphoinositide regulation of inward rectifier potassium (Kir) channels. *Front. Physiol.* 4, 404.

Garcia, M.L., Garcia-Calvo, M., Hidalgo, P., Lee, A., and MacKinnon, R. (1994). Purification and characterization of three inhibitors of voltage-dependent K^+

channels from Leiurus quinquestriatus var. hebraeus venom. *Biochemistry.* 33, 6834-9.

Geiss, G.K., Bumgarner, R.E., Birditt, B., Dahl, T., Dowidar, N., Dunaway, D.L., Fell, H.P., Ferree, S., George, R.D., Grogan, T., et al. (2008). Direct multiplexed measurement of gene expression with color-coded probe pairs. *Nat. Biotechnol*. 26, 317-25.

Ginhoux, F., Lim, S., Hoeffel, G., Low, D., and Huber, T. (2013). Origin and differentiation of microglia. *Front. Cell. Neurosci*. 7, 45.

Grissmer, S., Nguyen, A.N., Aiyar, J., Hanson, D.C., Mather, R.J., Gutman, G.A., Karmilowicz, M.J., Auperin, D.D., and Chandy, K.G. (1994). Pharmacological characterization of five cloned voltage-gated K^+ channels, types Kv1.1, 1.2, 1.3, 1.5, and 3.1, stably expressed in mammalian cell lines. *Mol. Pharmacol.* 45, 1227-34.

Gutman, G. A., Chandy, K. G., Grissmer, S., Lazdunski, M., McKinnon, D., Pardo, L. A, et al. (2005). International Union of Pharmacology. LIII. Nomenclature and molecular relationships of voltage-gated potassium channels. *Pharmacol. Rev*. 57, 473-508.

Harting, M. T., Jimenez, F., Adams, S. D., Mercer, D. W., and Cox, C. S., Jr. (2008). Acute, regional inflammatory response after traumatic brain injury: Implications for cellular therapy. *Surgery*. 144, 803-813.

Hanisch, U.K., and Kettenmann, H. (2007). Microglia: active sensor and versatile effector cells in the normal and pathologic brain. *Nat. Neurosci.* 10, 1387-1394.

Hanisch U.K. (2013). Functional diversity of microglia - how heterogeneous are they to begin with? *Front. Cell. Neurosci.* 7, 65-83.

Hao, C., Guilbert, L. J., and Fedoroff, S. (1990). Production of colony-stimulating factor-1 (CSF-1) by mouse astroglia in vitro. *J. Neurosci. Res*. 27, 314-323.

Hashimoto, D., Chow, A., Noizat, C., Teo, P., Beasley, M.B., Leboeuf, M., et al. (2013). Tissue-resident macrophages self-maintain locally throughout adult life with minimal contribution from circulating monocytes. *Immunity*. 38, 792-804.

Heppner, F. L., Skutella, T., Hailer, N. P., Haas, D., and Nitsch, R. (1998). Activated microglial cells migrate towards sites of excitotoxic neuronal injury inside organotypic hippocampal slice cultures. *Eur. J. Neurosci*. 10, 3284-3290.

Hibino, H., Inanobe, A., Furutani, K., Murakami, S., Findlay, I., and Kurachi, Y. (2010). Inwardly rectifying potassium channels: their structure, function, and physiological roles. *Physiol. Rev.* 90, 291-366.

Hilgemann, D.W., Feng, S., and Nasuhoglu, C. (2001). The complex and intriguing lives of PIP2 with ion channels and transporters. *Sci STKE* 2001, re19.

Holsapple, M.P., West, L.J., and Landreth, K.S. (2003). Species comparison of anatomical and functional immune system development. *Birth Defects Res. B. Dev. Reprod. Toxicol*. 68, 321-34.

Holmes, T. C., Fadool, D. A., and Levitan, I. B. (1996). Tyrosine phosphorylation of the Kv1.3 potassium channel. *J. Neurosci.*, 16, 1581-1590.

Honda, S., Sasaki, Y., Ohsawa, K., Imai, Y., Nakamura, Y., Inoue, K., and Kohsaka, S. (2001). Extracellular ATP or ADP induce chemotaxis of cultured microglia through Gi/o-coupled P2Y receptors. *J. Neurosci*. 21, 1975-1982.

Hu, X., Li, P., Guo, Y., Wang, H., Leak, R. K., Chen, S., et al. (2012). Microglia/macrophage polarization dynamics reveal novel mechanism of injury expansion after focal cerebral ischemia. *Stroke*. 43, 3063-3070.

Iannaccone, P.M., and Jacob, H.J. (2009). Rats! *Dis. Model. Mech*. 2, 206-10.

Inoue, K. (2008). Purinergic systems in microglia. *Cell. Mol. Life Sci.* 65, 3074-3080.

Jang, S.S., Park, J., Hur, S.W., Hong, Y.H., Hur, J., Chae, J.H., Kim, S.K., Kim, J., Kim, H.S., and Kim, S.J. (2011). Endothelial progenitor cells functionally express inward rectifier potassium channels. *Am. J. Physiol. Cell. Physiol.* 301, C150-161.

Jiang, X., Newell, E.W., and Schlichter, L.C. (2003). Regulation of a TRPM7-like current in rat brain microglia. *J. Biol. Chem.* 278, 42867-42876.

Jimenez-Perez, L., Cidad, P., Alvarez-Miguel, I., Santos-Hipolito, A., Torres-Merino, R., Alonso, E., et al. (2016). Molecular Determinants of Kv1.3 Potassium Channels-induced Proliferation. *J. Biol. Chem*. 291, 3569-3580.

Joiner, W.J., Wang, L.Y., Tang, M.D., and Kaczmarek, L.K. (1997). hSK4, a member of a novel subfamily of calcium-activated potassium channels. *Proc. Natl. Acad. Sci. U. S. A.* 94, 11013-11018.

Jones, S.V. (2003). Role of the small GTPase Rho in modulation of the inward rectifying potassium channel Kir2.1. *Mol. Pharmacol.* 64: 987-993.

Jones, L. J., Gray, M., Yue, S. T., Haugland, R. P., and Singer, V. L. (2001). Sensitive determination of cell number using the CyQUANT cell proliferation assay. *J. Immunol. Methods.* 254, 85-98.

Kan, X. H., Gao, H. Q., Ma, Z. Y., Liu, L., Ling, M. Y., and Wang, Y. Y. (2016). Kv1.3 potassium channel mediates macrophage migration in atherosclerosis by regulating ERK activity. *Arch. Biochem. Biophys*. 591, 150-156.

Karkanis, T., Li, S., Pickering, J.G., and Sims, S.M. (2003). Plasticity of KIR channels in human smooth muscle cells from internal thoracic artery. *Am. J. Physiol. Heart Circ. Physiol.* 284, H2325-2334.

Kaushal, V., Koeberle, P.D., Wang, Y., and Schlichter, L.C. (2007). The Ca^{2+}-activated K^+ channel KCNN4/KCa3.1 contributes to microglia activation and nitric oxide-dependent neurodegeneration. *J. Neurosci.* 27, 234-244.

Kaushal, V., and Schlichter, L. C. (2008). Mechanisms of microglia-mediated neurotoxicity in a new model of the stroke penumbra. *J. Neurosci.* 28, 2221-2230.

Kawaharada, K., Kawamata, M., and Ochiya, T. (2015). Rat embryonic stem cells create new era in development of genetically manipulated rat models. *World J. Stem Cells*. 7, 1054-63.

Kettenmann, H., Hoppe, D., Gottmann, K., Banati, R., and Kreutzberg, G. (1990). Cultured microglial cells have a distinct pattern of membrane channels different from peritoneal macrophages. *J. Neurosci. Res*. 26, 278-87.

Kettenmann, H., Banati, R., and Walz, W. (1993). Electrophysiological behavior of microglia. *Glia* 7, 93-101.

Kettenmann, H., Hanisch, U.K., Noda, M., and Verkhratsky, A. (2011). Physiology of microglia. *Physiol. Rev.* 91, 461-553.

Khanna, R., Roy, L., Zhu, X., and Schlichter, L.C. (2001). K^+ channels and the microglial respiratory burst. *Am. J. Physiol. Cell. Physiol*. 280, C796-806.

Kierdorf, K., Erny, D., Goldmann, T., Sander, V., Schulz, C., Perdiguero, E. G., et al. (2013). Microglia emerge from erythromyeloid precursors via Pu.1- and Irf8-dependent pathways. *Nat. Neurosci*. 16, 273-280.

Kim, J. V., & Dustin, M. L. (2006). Innate response to focal necrotic injury inside the blood-brain barrier. J *Immunol*. 177, 5269-5277.

Koeberle, P. D., and Schlichter, L. C. (2010). Targeting K(V) channels rescues retinal ganglion cells in vivo directly and by reducing inflammation. *Channels (Austin).* 4, 337-346.

Kong, G. Y., Peng, Z. C., Costanzo, C., Kristensson, K., and Bentivoglio, M. (2000). Inducible nitric oxide synthase expression elicited in the mouse brain by inflammatory mediators circulating in the cerebrospinal fluid. *Brain Res.* 878, 105-118.

Korzhevskii, D.E., and Kirik, O.V. 2016. Brain microglia and microglial markers. *Neurosci. Behav. Physiol.* 46, 284-90.

Kotecha, S.A., and Schlichter, L.C. (1999). A Kv1.5 to Kv1.3 switch in endogenous hippocampal microglia and a role in proliferation. *J. Neurosci.* 19, 10680-93.

Korotzer, A.R., and Cotman, C.W. (1992). Voltage-gated currents expressed by rat microglia in culture. *Glia.* 6, 81-8.

Kubo, Y., Baldwin, T.J., Jan, Y.N., and Jan, L.Y. (1993). Primary structure and functional expression of a mouse inward rectifier potassium channel. *Nature* 362, 127-133.

Kumar, A., Barrett, J. P., Alvarez-Croda, D. M., Stoica, B. A., Faden, A. I., and Loane, D. J. (2016). NOX2 drives M1-like microglial/macrophage activation and neurodegeneration following experimental traumatic brain injury. *Brain Behav. Immun.*

Lam, D., and Schlichter, L.C. (2015). Expression and contributions of the Kir2.1 inward-rectifier K^+ channel to proliferation, migration and chemotaxis of microglia in unstimulated and anti-inflammatory states. *Front. Cell. Neurosci.* 9, 185.

Lam, D., Lively, S., and Schlichter, L.C. (under revision). A rat versus mouse comparison of microglia in different activation states: Molecular profiles, K^+ channels and migration. *J. Neuroinflammation.*

Lawson, L. J., Perry, V. H., and Gordon, S. (1992). Turnover of resident microglia in the normal adult mouse brain. *Neuroscience*. 48, 405-415.

Lee, S., Varvel, N.H., Konerth, M.E., Xu, G., Cardona, A.E., Ransohoff, R.M., and Lamb, B.T. 2010.CX3CR1 deficiency alters microglial activation and reduces beta-amyloid deposition in two Alzheimer's disease mouse models. *Am. J. Pathol*. 177, 2549-62.

Levite, M., Cahalon, L., Peretz, A., Hershkoviz, R., Sobko, A., Ariel, A., Desai, R., Attali, B., and Lider, O. (2000). Extracellular K^+ and opening of voltage-gated potassium channels activate T cell integrin function: physical and functional association between Kv1.3 channels and beta1 integrins. *J. Exp. Med.* 191, 1167-76.

Li, F., Lu, J., Wu, C.Y., Kaur, C., Sivakumar, V., Sun, J., Li, S., and Ling, E.A. (2008). Expression of Kv1.2 in microglia and its putative roles in modulating production of proinflammatory cytokines and reactive oxygen species. *J. Neurochem*. 106, 2093-2105.

Lieb, K., Engels, S., and Fiebich, B. L. (2003). Inhibition of LPS-induced iNOS and NO synthesis in primary rat microglial cells. *Neurochem. Int.* 42, 131-137.

Linder, S., and Wiesner, C. (2015). Tools of the trade: podosomes as multipurpose organelles of monocytic cells. *Cell. Mol. Life Sci*. 72, 121-35.

Liu, B.S., Ferreira, R., Lively, S., and Schlichter, L.C. (2013). Microglial SK3 and SK4 currents and activation state are modulated by the neuroprotective drug, riluzole. *J. Neuroimmune Pharmacol.* 8, 227-37.

Liu, J., Xu, C., Chen, L., Xu, P., and Xiong, H. (2012). Involvement of Kv1.3 and p38 MAPK signaling in HIV-1 glycoprotein 120-induced microglia neurotoxicity. *Cell Death Dis*. 3, e254.

Lively, S., and Schlichter, L.C. (2013). The microglial activation state regulates migration and roles of matrix-dissolving enzymes for invasion. *J. Neuroinflammation* 10, 75.

Lively, S., and Schlichter, L. C. (2012). Age-related comparisons of evolution of the inflammatory response after intracerebral hemorrhage in rats. *Transl. Stroke Res.* 3, 132-146.

Lively, S., and Schlichter, L. C. (manuscript in preparation). Two classical activation conditions, LPS and IFN-γ and TNF-α, elicits differential responses in primary rat microglia.

Lu, Z. (2004). Mechanism of rectification in inward-rectifier K^+ channels. *Annu. Rev. Physiol.* 66, 103-129.

Lynch MA. (2009). The multifaceted profile of activated microglia. Mol Neurobiol . 40, 139-156.

Lyons, S.A., Pastor, A., Ohlemeyer, C., Kann, O., Wiegand, F., Prass, K., Knapp, F., Kettenmann, H., and Dirnagl, U. (2000). Distinct physiologic properties of microglia and blood-borne cells in rat brain slices after permanent middle cerebral artery occlusion. *J. Cereb. Blood Flow Metab.* 20, 1537-1549.

Masia, R., Krause, D.S., and Yellen, G. (2015). The inward rectifier potassium channel Kir2.1 is expressed in mouse neutrophils from bone marrow and liver. *Am. J. Physiol. Cell Physiol.* 308, C264-276.

Martínez-Mármol, R., Comes, N., Styrczewska, K., Pérez- Verdaguer, M., Vicente, R, Pujadas, L., et al. Unconventional EGF-induced ERK1/2-mediated Kv1.3 endocytosis. Cell Mol. Life Sci. *73*, 1515–1528.

McLarnon, J. G., Franciosi, S., Wang, X., Bae, J. H., Choi, H. B., and Kim, S. U. (2001). Acute actions of tumor necrosis factor-alpha on intracellular Ca^{2+} and K^{+} currents in human microglia. *Neuroscience*. 104, 1175-1184.

McLarnon, J. G., Xu, R., Lee, Y. B., and Kim, S. U. (1997). Ion channels of human microglia in culture. *Neuroscience*. 78, 1217-1228.

Menteyne, A., Levavasseur, F., Audinat, E., and Avignone, E. (2009). Predominant functional expression of Kv1.3 by activated microglia of the hippocampus after Status epilepticus. *PloS one.* 4, e6770.

Mestas, J., and Hughes, C.C.W. (2004). Of mice and not men: differences between mouse and human immunology. *J. Immunol.* 172, 2731-2738.

Michaelis, M., Nieswandt, B., Stegner, D., Eilers, J., and Kraft, R. (2015). STIM1, STIM2, and Orai1 regulate store-operated calcium entry and purinergic activation of microglia. *Glia* 63, 652-663.

Michell-Robinson, M.A., Touil, H., Healy, L.M., Owen, D.R., Durafourt, B.A., Bar-Or, A., Antel, J.P., and Moore, C.S. (2015). Roles of microglia in brain development, tissue maintenance and repair. *Brain.* 138, 1138-59.

Michelucci, A., Heurtaux, T., Grandbarbe, L., Morga, E., and Heuschling, P. (2009). Characterization of the microglial phenotype under specific pro-inflammatory and anti-inflammatory conditions: Effects of oligomeric and fibrillar amyloid-beta. *J. Neuroimmunol.* 210, 3-12.

Milner, R., and Campbell, I. L. (2002). The integrin family of cell adhesion molecules has multiple functions within the CNS. *J. Neurosci. Res.* 69, 286-291.

Min, H., Jang, Y. H., Cho, I. H., Yu, S. W., and Lee, S. J. (2016). Alternatively activated brain-infiltrating macrophages facilitate recovery from collagenase-induced intracerebral hemorrhage. *Mol. Brain.* 9, 42.

Möller, T. (2002). Calcium signaling in microglial cells. Glia, 40(2), 184-194.

Moore, K. W., de Waal Malefyt, R., Coffman, R. L., and O'Garra, A. (2001). Interleukin-10 and the interleukin-10 receptor. *Annu. Rev. Immunol*. 19, 683-765.

Moussaud, S., Lamodiere, E., Savage, C., and Draheim, H.J. (2009). Characterisation of K^+ currents in the C8-B4 microglial cell line and their regulation by microglia activating stimuli. *Cell Physiol. Biochem.* 24, 141-152.

Muessel, M.J., Harry, G.J., Armstrong, D.L., and Storey, N.M. (2013). SDF-1alpha and LPA modulate microglia potassium channels through rho gtpases to regulate cell morphology. *Glia* 61, 1620-1628.

Murray, P.J., Allen, J.E., Biswas, S.K., Fisher, E.A., Gilroy, D.W., Goerdt, S., Gordon, S., Hamilton, J.A., Ivashkiv, L.B., Lawrence, T., et al. (2014). Macrophage activation and polarization: nomenclature and experimental guidelines. *Immunity.* 41, 14-20.

Nayak, D., Roth, T.L., and McGavern, D.B. (2014). Microglia development and function. *Ann. Rev. Immunol.* 32, 367-402.

Newell, E.W., and Schlichter, L.C. (2005). Integration of K^+ and Cl^- currents regulate steady-state and dynamic membrane potentials in cultured rat microglia. *J Physiol.* 567, 869-890.

Newell, E.W., Stanley, E.F., and Schlichter, L.C. (2007). Reversed Na^+/Ca^{2+} exchange contributes to Ca^{2+} influx and respiratory burst in microglia. *Channels (Austin)* 1, 366-376.

Nikodemova, M., Kimyon, R. S., De, I., Small, A. L., Collier, L. S., and Watters, J. J. (2015). Microglial numbers attain adult levels after undergoing a rapid decrease in cell number in the third postnatal week. *J. Neuroimmunol*. 278, 280-288.

Nimmerjahn, A., Kirchhoff, F., and Helmchen, F. (2005). Resting microglial cells are highly dynamic surveillants of brain parenchyma in vivo. *Science*. 308, 1314-1318.

Nguyen, D., and Xu, T. (2008). The expanding role of mouse genetics for understanding human biology and disease. *Dis. Model. Mech.* 1, 56-66.

Noda, M., and Suzumura, A. (2012). Sweepers in the CNS: Microglial migration and phagocytosis in the alzheimer disease pathogenesis. *Int. J. Alzheimers. Dis*. 2012, 891087.

Nörenberg, W., Gebicke-Haerter, P.J., and Illes, P. (1992). Inflammatory stimuli induce a new K^+ outward current in cultured rat microglia. *Neurosci. Lett* 147, 171-174.

Nörenberg, W., Gebicke-Haerter, P.J., and Illes, P. (1994). Voltage-dependent potassium channels in activated rat microglia. *J. Physiol.* 475, 15-32.

Nutile-McMenemy, N., Elfenbein, A., and Deleo, J.A. (2007). Minocycline decreases in vitro microglial motility, beta1-integrin, and Kv1.3 channel expression. *J. Neurochem*. 103, 2035-46.

Ohana, L., Newell, E.W., Stanley, E.F., and Schlichter, L.C. (2009). The Ca^{2+} release-activated Ca^{2+} current (I(CRAC)) mediates store-operated Ca^{2+} entry in rat microglia. *Channels (Austin)* 3, 129-139.

Olmos, G., and Lladó, J. (2014). Tumor necrosis factor alpha: a link between neuroinflammation and excitotoxicity. *Mediators Inflamm.* 2014, 861231.

Parekh, A. B., and Putney, J. W., Jr. (2005). Store-operated calcium channels. *Physiol. Rev.* 85, 757-810.

Pannasch, U., Farber, K., Nolte, C., Blonski, M., Yan Chiu, S., Messing, A., and Kettenmann H. (2006). The potassium channels Kv1.5 and Kv1.3 modulate distinct functions of microglia. *Mol. Cell. Neurosci.* 33,401-11.

Pardo, L.A. (2004). Voltage-gated potassium channels in cell proliferation. *Physiology (Bethesda)* 19, 285-292.

Patrizio, M., and Levi, G. (1994). Glutamate production by cultured microglia: differences between rat and mouse, enhancement by lipopolysaccharide and lack effect of HIV coat protein gp120 and depolarizing agents. *Neurosci. Lett.* 178, 184-9.

Perego, C., Fumagalli, S., and De Simoni, M.G. (2011). Temporal pattern of expression and colocalization of microglia/macrophage phenotype markers following brain ischemic injury in mice. *J. Neuroinflammation*. 8, 174.

Perego, C., Fumagalli, S., and De Simoni, M. G. (2013). Three-dimensional confocal analysis of microglia/macrophage markers of polarization in experimental brain injury. *J. Vis. Exp.*

Perry, V. H., Nicoll, J. A., and Holmes, C. (2010). Microglia in neurodegenerative disease. *Nat. Rev. Neurol*. 6, 193-201.

Philipson, L.H., Malayev, A., Kuznetsov, A., Chang, C., and Nelson, D.J. (1993). Functional and biochemical characterization of the human potassium channel Kv1.5 with a transplanted carboxyl-terminal epitope in stable mammalian cell lines. *Biochim. Biophys. Acta*. 1153, 111-21.

Pocock, J.M., and Kettenmann, H. (2007). Neurotransmitter receptors on microglia. *Trends Neurosci.* 30, 527-35.

Potter-Baker, K.A., Ravikumar, M., Burke, A.A., Meador, W.D., Householder, K.T., Buck, A.C., Sunil, S., Stewart, W.G., Anna, J.P., Tomaszewski, W.H., and Capadona, J.R. (2014). A comparison of neuroinflammation to implanted microelectrodes in rat and mouse models. *Biomaterials*. 35, 5637-46.

Prasad, A., Kumar, S. S., Dessimoz, C., Bleuler, S., Laule, O., Hruz, T., et al. (2013). Global regulatory architecture of human, mouse and rat tissue transcriptomes. *BMC Genomics*. 14, 716.

Pratt, B.M., and McPherson, J.M. (1997). TGF-beta in the central nervous system: potential roles in ischemic injury and neurodegenerative diseases. *Cytokine Growth Factor Rev.* 8, 267-292.

Prinz, M., Kann, O., Draheim, H.J., Schumann, R.R., Kettenmann, H., Weber, J.R., and Hanisch, U.K. (1999). Microglial activation by components of gram-positive and -negative bacteria: distinct and common routes to the induction of ion channels and cytokines. *J. Neuropathol. Exp. Neurol.* 58, 1078-1089.

Qi, X.Y., Huang, H., Ordog, B., Luo, X., Naud, P., Sun, Y., Wu, C.T., Dawson, K., Tadevosyan, A., Chen, Y., Harada, M., Dobrev, D., and Nattel, S. (2015). Fibroblast inward-rectifier potassium current upregulation in profibrillatory atrial remodeling. *Circ. Res.* 116, 836-845.

Ransohoff, R. M., and Perry, V. H. (2009). Microglial physiology: unique stimuli, specialized responses. *Annu. Rev. Immunol.* 27, 119-145.

Richardson, A., Hao, C., and Fedoroff, S. (1993). Microglia progenitor cells: a subpopulation in cultures of mouse neopallial astroglia. *Glia*. 7, 25-33.

Ridley, A.J., Schwartz, M.A., Burridge, K., Firtel, R.A., Ginsberg, M.H., Borisy, G., Parsons, J.T., and Horwitz, A.R. (2003). Cell migration: integrating signals from front to back. *Science*. 302, 1704-9.

Russo, M. V., and McGavern, D. B. (2015). Immune Surveillance of the CNS following Infection and Injury. *Trends Immunol*. 36, 637-650.

Ryan, D.P., da Silva, M.R., Soong, T.W., Fontaine, B., Donaldson, M.R., Kung, A.W., Jongjaroenprasert, W., Liang, M.C., Khoo, D.H., Cheah, J.S., et al. (2010). Mutations in potassium channel Kir2.6 cause susceptibility to thyrotoxic hypokalemic periodic paralysis. *Cell.* 140, 88-98

Schilling, T., and Eder, C. (2007). Ion channel expression in resting and activated microglia of hippocampal slices from juvenile mice. *Brain Res.* 1186, 21-28.

Schilling, T., and Eder, C. (2015). Microglial K^+ channel expression in young adult and aged mice. *Glia* 63, 664-672.

Schilling, T., Quandt, F.N., Cherny, V.V., Zhou, W., Heinemann, U., Decoursey, T.E., and Eder, C. (2000). Upregulation of Kv1.3 K^+ channels in microglia deactivated by TGF-beta. *Am. J. Physiol. Cell Physiol.* 279, C1123-1134.

Schlichter, L.C., Hutchings, S., and Lively, S. (2014). Inflammation and white matter injury in animal models of ischemic stroke. In Baltan S, Carmichael ST, Matute C, Xi G, Zhang JH editors. White matter injury in stroke and CNS disease. p.461-504.

Schlichter, L.C., Jiang, J., Wang, J., Newell, E.W., Tsui, F.W.L., and Lam, D. (2014). Regulation of hERG and hEAG channels by Src and by SHP-1 tyrosine phosphatase via an ITIM region in the cyclic nucleotide binding domain. *PLos One*. 9. e90024.

Schlichter, L.C., Kaushal, V., Moxon-Emre, I., Sivagnanam, V., and Vincent, C. (2010). The Ca^{2+} activated SK3 channel is expressed in microglia in the rat striatum and contributes to microglia-mediated neurotoxicity in vitro. *J. Neuroinflammation* 7, 4.

Schlichter, L.C., Sakellaropoulos, G., Ballyk, B., Pennefather, P.S., and Phipps, D.J. (1996). Properties of K^+ and Cl^- channels and their involvement in proliferation of rat microglial cells. *Glia* 17, 225-236.

Schneider, W. M., Chevillotte, M. D., and Rice, C. M. (2014). Interferon-stimulated genes: a complex web of host defenses. *Annu. Rev. Immunol.* 32, 513-545.

Schroeter, M., Küry, P., and Jander, S. (2003). Inflammatory gene expression in focal cortical brain ischemia: differences between rats and mice. *Brain Res. Mol. Brain Res.* 117, 1-7.

Schulz, C., Gomez Perdiguero, E., Chorro, L., Szabo-Rogers, H., Cagnard, N., Kierdorf, K., et al. (2012). A lineage of myeloid cells independent of Myb and hematopoietic stem cells. *Science.* 336, 86-90.

Schwab, A., Hanley, P., Fabian, A., and Stock, C. (2008). Potassium channels keep mobile cells on the go. *Physiology (Bethesda)*. 23, 212-220.

Schwab, A., Nechyporuk-Zloy, V., Fabian, A., and Stock, C. (2007). Cells move when ions and water flow. *Pflugers Arch.* 453, 421-432.

Schwaller, B. (2010). Cytosolic Ca^{2+} buffers. *Cold Spring Harb. Perspect. Biol.* 2, a004051

Seok, J., Warren, H.S., Cuenca, A.G., Mindrinos, M.N., Baker, H.V., Xu, W., Richards, D.R., McDonald-Smith, G.P., Gao, H., Hennessy, L., et al. (2013). Genomic responses in mouse models poorly mimic human inflammatory diseases. Proc. Natl. Acad. Sci. U.S.A. 110, 3507-12.

Shay, T., Lederer, J. A., and Benoist, C. (2015). Genomic responses to inflammation in mouse models mimic humans: we concur, apples to oranges comparisons won't do. *Proc. Natl. Acad. Sci. U. S. A.* 112, E346.

Shim, A.H., Tirado-Lee, L., and Prakriya, M. (2015). Structural and functional mechanisms of CRAC channel regulation. *J. Mol. Biol.* 427, 77-93.

Sieger, D., and Peri, F. (2008). Animal models for studying microglia: the first, the popular, and the new. *Glia.* 61, 3-9.

Siddiqui, T., Lively, S., Ferreira, R., Wong, R., and Schlichter, L.C. (2014). Expression and contributions of TRPM7 and KCa2.3/SK3 channels to the increased migration and invasion of microglia in anti-inflammatory activation states. *PLoS One* 9, e106087.

Siddiqui, T.A., Lively, S., and Schlichter, L.C. (2016). Complex molecular and functional outcomes of single versus sequential cytokine stimulation of rat microglia. *J. Neuroinflammation*. 13, 66.

Siddiqui, T.A., Lively, S., Vincent, C., and Schlichter, L.C. (2012). Regulation of podosome formation, microglial migration and invasion by Ca^{2+}-signaling molecules expressed in podosomes. *J. Neuroinflammation* 9, 250.

Sivagnanam, V., Zhu, X., and Schlichter, L.C. (2010). Dominance of E. coli phagocytosis over LPS in the inflammatory response of microglia. *J. Neuroimmunol*. 227, 111-9.

Skaper, S. D. (2011). Ion channels on microglia: therapeutic targets for neuroprotection. *CNS Neurol. Disord. Drug. Targets.* 10, 44-56.

Sobko, A., Peretz, A., Shirihai, O., Etkin, S., Cherepanova, V., Dagan, D., and Attali, B. (1998). Heteromultimeric delayed-rectifier K^+ channels in schwann cells: developmental expression and role in cell proliferation. *J. Neurosci.* 18, 10398-10408.

Soh, H., and Park, C.S. (2001). Inwardly rectifying current-voltage relationship of small-conductance Ca^{2+}-activated K^+ channels rendered by intracellular divalent cation blockade. *Biophys. J.* 80, 2207-2215.

Sroga, J.M., Jones, T.B., Kigerl, K.A., McGaughy, V.M., and Popovich, P.G. (2003). Rats and mice exhibit distinct inflammatory reactions after spinal cord injury. *J. Comp. Neurol*. 462, 223-40.

Stanley, E. R., and Chitu, V. (2014). CSF-1 receptor signaling in myeloid cells. *Cold Spring Harb. Perspect. Biol. 6*.

Stebbing, M. J., Cottee, J. M., and Rana, I. (2015). The Role of Ion Channels in Microglial Activation and Proliferation - A Complex Interplay between Ligand-Gated Ion Channels, K^+ Channels, and Intracellular Ca(2.). *Front. Immunol*. 6, 497.

Stence, N., Waite, M., and Dailey, M. E. (2001). Dynamics of microglial activation: a confocal time-lapse analysis in hippocampal slices. *Glia*. 33, 256-266.

Suenaga, J., Hu, X., Pu, H., Shi, Y., Hassan, S. H., Xu, M., et al. (2015). White matter injury and microglia/macrophage polarization are strongly linked with age-related long-term deficits in neurological function after stroke. *Exp. Neurol*. 272, 109-119.

Suzumura, A., Sawada, M., Yamamoto, H., and Marunouchi, T. (1993). Transforming growth factor-beta suppresses activation and proliferation of microglia in vitro. *J. Immunol.* 151, 2150-2158.

Takao, K., and Miyakawa, T. (2015). Genomic responses in mouse models greatly mimic human inflammatory diseases. Proc. Natl. Acad. Sci. U.S.A. 112, 1167-72.

Tang, Y., and Le, W. (2016). Differential Roles of M1 and M2 Microglia in Neurodegenerative Diseases. *Mol.* Neurobiol. 53, 1181–1194.

Tay, T. L., Savage, J., Hui, C. W., Bisht, K., and Tremblay, M. E. (2016). Microglia across the lifespan: from origin to function in brain development, plasticity and cognition. *J. Physiol*. doi:10.1113/JP272134

Thomas, A.C., and Mattila, J.T. (2014). "Of mice and men": arginine metabolism in macrophages. *Front. Immunol.* 5, 479.

Tian, D., Litvak, V., and Lev, S. (2000). Cerebral ischemia and seizures induce tyrosine phosphorylation of PYK2 in neurons and microglial cells. *J. Neurosci.* 20, 6478-87.

Tozaki-Saitoh, H., Tsuda, M., M., and Inoue, K. (2012). P2Y receptors in microglia and neuroinflammation. *WIREs Membr. Transp. Signal.* 1, 493-201.

Tsaparas, P., Marino-Ramirez, L., Bodenreider, O., Koonin, E. V., and Jordan, I. K. (2006). Global similarity and local divergence in human and mouse gene co-expression networks. *BMC Evol. Biol.* 6, 70.

Turtzo, L. C., Lescher, J., Janes, L., Dean, D. D., Budde, M. D., and Frank, J. A. (2014). Macrophagic and microglial responses after focal traumatic brain injury in the female rat*. J. Neuroinflammation*. 11, 82.

Urrego, D., Tomczak, A.P., Zahed, F., Stuhmer, W., and Pardo, L.A. (2014). Potassium channels in cell cycle and cell proliferation. *Philos. Trans. R. Soc. Lond. B. Biol. Sci.* 369, 20130094.

Van Dyken, S. J., and Locksley, R. M. (2013). Interleukin-4- and interleukin-13-mediated alternatively activated macrophages: roles in homeostasis and disease. *Annu. Rev. Immunol.* 31, 317-343.

Vincent, C., Siddiqui, T.A., and Schlichter, L.C. (2012). Podosomes in migrating microglia: components and matrix degradation. *J. Neuroinflammation* 9, 190.

Visentin, S., Agresti, C., Patrizio, M., and Levi, G. (1995). Ion channels in rat microglia and their different sensitivity to lipopolysaccharide and interferon-gamma. *J. Neurosci. Res.* 42, 439-451.

Walz, W., Ilschner, S., Ohlemeyer, C., Banati, R., and Kettenmann, H. (1993). Extracellular ATP activates a cation conductance and a K^+ conductance in cultured microglial cells from mouse brain. *J. Neurosci.* 13, 4403-4411.

Wan, S., Cheng, Y., Jin, H., Guo, D., Hua, Y., Keep, R. F., and Xi, G. (2016). Microglia activation and polarization after intracerebral hemorrhage in mice: the role of protease-activated receptor-1. *Transl. Stroke Res.*

Wang, G., Zhang, J., Hu, X., Zhang, L., Mao, L., Jiang, X., et al. (2013). Microglia/macrophage polarization dynamics in white matter after traumatic brain injury*. J. Cereb. Blood Flow Metab*. 33, 1864-1874.

Wang, H.R., Wu, M., Yu, H., Long, S., Stevens, A., Engers, D.W., Sackin, H., Daniels, J.S., Dawson, E.S., Hopkins, C.R., Lindsley, C.W., Li, M., and McManus, O.B. (2011). Selective inhibition of the K(ir)2 family of inward rectifier potassium channels by a small molecule probe: the discovery, SAR, and pharmacological characterization of ML133. *ACS Chem. Biol.* 6, 845-856.

Warren, H. S., Tompkins, R. G., Moldawer, L. L., Seok, J., Xu, W., Mindrinos, M. N.,et al. (2015). Mice are not men. *Proc. Natl. Acad. Sci. U. S. A*. 112, E345.

Wei, C., Wang, X., Zheng, M., and Cheng, H. (2012). Calcium gradients underlying cell migration. *Curr. Opin. Cell. Biol*. 24, 254-61.

Wendt, S., Wogram, E., Korvers, L., and Kettenmann, H. (2016). Experimental cortical spreading depression induces NMDA receptor dependent potassium currents in microglia. *J. Neurosci.* 36, 6165-74.

Wolf, Y., Yona, S., Kim, K.W., and Jung, S. (2013). Microglia, seen from the CX3CR1 angle. *Front. Cell. Neurosci.* 7, 26.

Wong, R., and Schlichter, L.C. (2014). PKA reduces the rat and human KCa3.1 current, CaM binding, and Ca^{2+} signaling, which requires Ser332/334 in the CaM-binding C terminus. *J. Neurosci.* 34, 13371-13383.

Wulff, H., and Christophersen, P. (2015). Recent developments in ion channel pharmacology. *Channels (Austin)*. 9, 335.

Wulff, H., and Zhorov, B. S. (2008). K^+ channel modulators for the treatment of neurological disorders and autoimmune diseases. *Chem. Rev*. 108, 1744-1773.

Xie, Z., Wei, M., Morgan, T. E., Fabrizio, P., Han, D., Finch, C. E., and Longo, V. D. (2002). Peroxynitrite mediates neurotoxicity of amyloid beta-peptide1-42- and lipopolysaccharide-activated microglia. *J. Neurosci.* 22, 3484-3492.

Yang, J., Ding, S., Huang, W., Hu, J., Huang, S., Zhang, Y., and Zhuge, Q. (2016). Interleukin-4 Ameliorates the Functional Recovery of Intracerebral Hemorrhage Through the Alternative Activation of Microglia/Macrophage. *Front. Neurosci.* 10, 61.

Yellen, G. (2002). The voltage-gated potassium channels and their relatives. *Nature.* 419, 35-42.

Zhang, Y. Y., Li, G., Che, H., Sun, H. Y., Xiao, G. S., Wang, Y., and Li, G. R. (2015). Effects of BKCa and Kir2.1 Channels on Cell Cycling Progression and Migration in Human Cardiac c-kit+ Progenitor Cells. *PLoS One*. 10, e0138581.

Zhang, J., Chan, Y.C., Ho, J.C., Siu, C.W., Lian, Q., and Tse, H.F. (2012a). Regulation of cell proliferation of human induced pluripotent stem cell-derived mesenchymal stem cells via ether-a-go-go 1 (hEAG1) potassium channel. *Am. J. Physiol. Cell. Physiol.* 303, C115-125.

Zhang, X.H., Zhang, Y.Y., Sun, H.Y., Jin, M.W., and Li, G.R. (2012b). Functional ion channels and cell proliferation in 3T3-L1 preadipocytes. *J. Cell. Physiol.* 227, 1972-1979.

Zhao, X., Zhang, Y., Strong, R., Zhang, J., Grotta, J. C., and Aronowski, J. (2007). Distinct patterns of intracerebral hemorrhage-induced alterations in NF-kappaB subunit, iNOS, and COX-2 expression. J. Neurochem. 101, 652-663.

Zheng-Bradley, X., Rung, J., Parkinson, H., and Brazma, A. (2010). Large scale comparison of global gene expression patterns in human and mouse. *Genome Biol*. 11, R124.

Ziebell, J.M., and Lifschitz, J. (2014). Morphology alone does not define microglial phenotype. (abstract). In: Proceedings of the Society for Neuroscience Meeting. Washington, DC. Nov 15-19, 383.06

Ziebell, J. M., Adelson, P. D., and Lifshitz, J. (2015). Microglia: dismantling and rebuilding circuits after acute neurological injury. Metab. Brain. Dis. 30, 393-400.

Zhou, W., Cayabyab, F.S., Pennefather, P.S., Schlichter, L.C., and DeCoursey, T.E. (1998). HERG-like K^+ channels in microglia. *J. Gen. Physiol*. 111, 781-94.

Zusso, M., Methot, L., Lo, R., Greenhalgh, A. D., David, S., and Stifani, S. (2012). Regulation of postnatal forebrain amoeboid microglial cell proliferation and development by the transcription factor Runx1. *J. Neurosci.* 32, 11285-11298.

Appendices

A.1. Comparing transcript expression levels of NOX enzymes, and phagocytosis and purinergic receptors in primary rat and mouse microglia.

	Rat				Mouse			
Gene	CTL	I+T	IL-4	IL-10	CTL	I+T	IL-4	IL-10
Ncf1	8165 ± 2199	49163 ± 8222 ****	4720 ± 639 **	7636 ± 1820	903 ± 78	3746 ± 577 ****	892 ± 173	1231 ± 293
Nox1	17 ± 6	10 ± 4	7 ± 4	16 ± 8	18 ± 4	18 ± 15	56 ± 30 *	13 ± 6
Cybb (Nox2)	3409 ± 575	6470 ± 582 ****	1803 ± 246 ****	4944 ± 852 ***	7403 ± 1851	25788 ± 4876 ****	3264 ± 1362 ***	5142 ± 1059
Nox4	4 ± 1	9 ± 3	4 ± 1	6 ± 2	13 ± 4	13 ± 2	12 ± 5	7± 2
Fcgr1a	6142 ± 2064	2484 ± 177 ****	3134 ± 307 ***	9098 ±2884 *	1273 ±183	8363 ± 2665 ****	604 ± 461 **	3023 ± 592 *
Fcgr2b	5579 ± 1291	3999 ± 1859	22354 ± 3645 ****	19936 ± 9082 ****	2920 ± 513	2228 ± 262	2865 ± 1145	11450 ± 2754 ****
Fcgr3a	7946 ± 4435	29902 ± 3854 ****	2552 ± 557 ***	16873 ± 6539 **	3680 ± 935	8991 ± 333 ****	3725 ± 850	7078 ± 1742 **
Trem2	6233 ± 938	268 ± 98 ****	2986 ± 695 ****	7762 ± 1296 *	206 ± 10	34 ± 13 ****	225 ± 35	163 ± 17 *
Msr1 (SR-A)	6720 ± 1325	709 ± 148 ****	2036 ± 272 ***	8511 ± 1873 *	3115 ± 497	2880 ± 625	2422 ± 822	6026 ± 1430 **
P2rx7	185 ± 45	241 ± 126	325 ± 83	277 ± 91	219 ± 29	194 ± 29	192 ± 33	251 ± 52
P2ry2	72 ± 13	292 ± 96 ****	145 ± 35 **	179 ± 73 ***	63 ± 14	73 ± 26	82 ± 26	79 ± 7
P2ry12	432 ± 49	154 ± 30 ****	783 ± 132 ****	410 ± 95	136 ± 58	124 ± 26	58 ± 12 **	204 ± 78

Transcript levels of several phagocytic receptors, and NOX enzymes (NADPH oxidases) that are involved in myelin phagocytosis and consequent production of reactive oxygen species (ROS) (Siddiqui et al., 2016) and purinergic receptors known to modulate phagocytosis, ROS production, cytokine secretion, and migration of microglia (Pocock and Kettenmann, 2007). Data are expressed as mean relative mRNA counts ± S.D for 4–6 individual cultures per treatment. Asterisk colors indicate increased (green) or decreased (red) gene expression relative to unstimulated microglia (CTL). One symbol indicates $p<0.05$; two symbols, $p<0.01$; three symbols, $p<0.001$; four symbols, $p<0.0001$. NanoString data was analyzed by Dr. Starlee Lively.

A.2. Inhibition of Kir2.1 or Kv1.3 channels did not dramatically affect proliferation in cytokine-activated microglia.

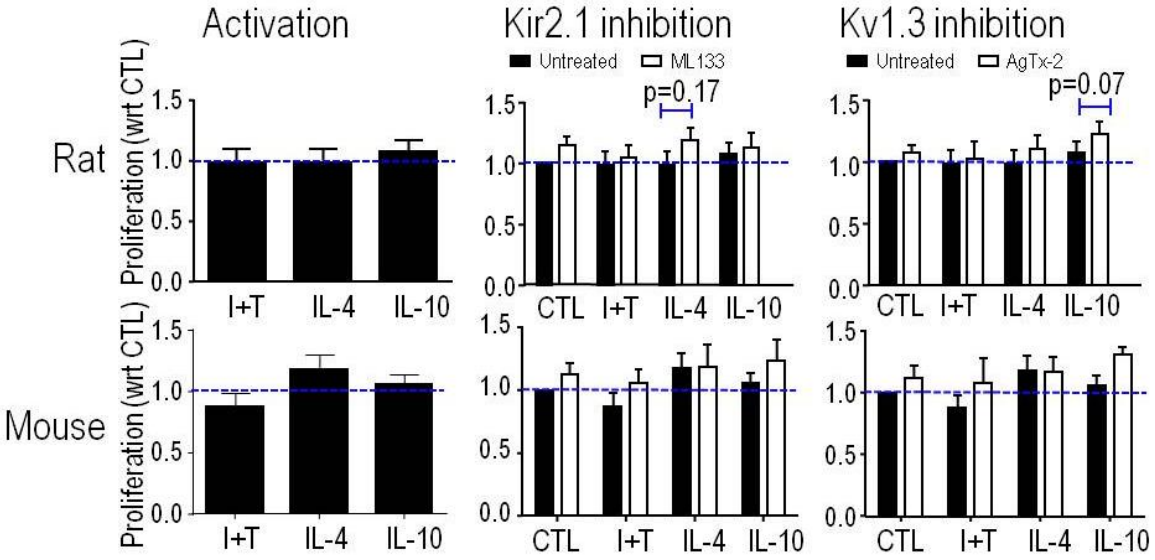

Proliferative capacity of rat and mouse microglia that were unstimulated (CTL) or stimulated for 24 h with IFN-γ and TNF-α (I+T), IL-4 or IL-10 (left column). Microglia with or without 20 μM ML133 to block Kir2.1 channels (middle column). Microglia with or without 5 nM AgTx-2 to block Kv1.3 channels (right column). All results are expressed as fold change normalized to untreated unstimulated cells (indicated by dashed lines). Data are shown as mean ± SEM (n=3 individual cultures), and were analyzed by one-way ANOVA with Dunnett's post-hoc test (activation state) or two-way ANOVA with Bonferroni's post-hoc test (when channel blockers were used). The comparisons are: * differences between CTL and stimulated cells; † CTL versus activated cells treated with a channel blocker; # effects of a channel blocker within a given activation state. One symbol indicates $p<0.05$, two symbols, $p<0.01$, three symbols, $p<0.001$, four symbols, $p<0.0001$.

A.3. Inhibition of Kir2.1 or Kv1.3 channels did not affect NO production in cytokine-activated microglia.

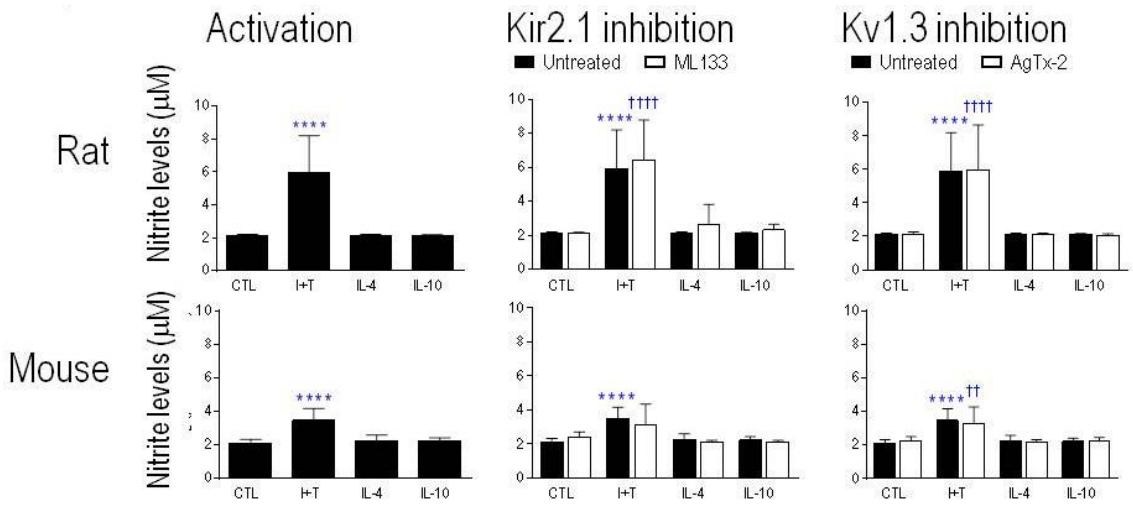

Nitrite levels mean ± SEM (n=6–9 individual cultures) in rat and mouse microglia that were unstimulated (CTL) or stimulated for 24 h with IFN-γ and TNF-α (I+T), IL-4 or IL-10 (left column). Microglia with or without 20 μM ML133 to block Kir2.1 channels (middle column). Microglia with or without 5 nM AgTx-2 to block Kv1.3 channels (right column). Data was analyzed by one-way ANOVA with Dunnett's post-hoc test (activation state) or two-way ANOVA with Bonferroni's post-hoc test (when channel blockers were used). The comparisons are: * differences between CTL and stimulated cells; † CTL versus activated cells treated with a channel blocker. Two symbols indicate $p<0.01$, four symbols, $p<0.0001$. Griess assay was performed and analyzed by Dr. Starlee Lively.